2016-01-01

Modeling Of Piezoelectric Traveling Wave Rotary Ultrasonic Motors With The Finite Volume Method

Ivan Arturo Renteria Marquez
University of Texas at El Paso, iarenteria@miners.utep.edu

MODELING OF PIEZOELECTRIC TRAVELING WAVE ROTARY ULTRASONIC MOTORS WITH THE FINITE VOLUME METHOD.

IVAN ARTURO RENTERIA MARQUEZ

Doctoral Program in Electrical and Computer Engineering

APPROVED:

Valentin Bolborici, Ph.D., Chair

Thompson Sarkodie-Gyan, Ph.D.

Louis Everett, Ph.D.

Scott Starks, Ph.D.

Charles Ambler, Ph.D.
Interim Dean of the Graduate School

Dedication

This work is dedicated to my family

MODELING OF PIEZOELECTRIC TRAVELING WAVE ROTARY ULTRASONIC MOTORS WITH THE FINITE VOLUME METHOD

by

IVAN ARTURO RENTERIA MARQUEZ, MS EE

DISSERTATION

Presented to the Faculty of the Graduate School of

The University of Texas at El Paso

in Partial Fulfillment

of the Requirements

for the Degree of

DOCTOR OF PHILOSOPHY

Department of Electrical and Computer Engineering

THE UNIVERSITY OF TEXAS AT EL PASO

May 2016

Acknowledgements

I would like to thank my dissertation adviser Dr. Valentin Bolborici for all his support, both scientific and financial. Without his help this work would not be possible.

I thank to Drs. Thomson Sarkodie-Gyan and Louis Everett for their support and useful suggestions.

I would like to specially thank Drs. Joseph Pierluissi and Miguel Velez-Reyes for their suggestions and financial support.

Abstract

In 1983 Toshiiku Sashida developed a new motor concept called Piezoelectric Traveling Wave Rotary Ultrasonic Motor (PTRUSM). The advantages of these motors include high torque at low speed, absence of a generated magnetic field, and high potential for miniaturization. Unfortunately PTRUSMs have some disadvantages that limit the areas of applications for these types of motors. The disadvantages are a short operating life (about 1000 hours), small output power, and the need of a complex motor controller.

On one hand, these motors have been used in satellites, mobile phones, photocopiers, robotic arms, telescopes, automobiles, and camera autofocusing. On the other hand, the use of the PTRUSM is still limited in its applications because of the previously mentioned disadvantages of these motors.

Modeling of the PTRUSM is a current challenge because the existing models of the motor are just focused in describing the behavior of certain parts of the motor, or the models have several assumptions that degrade the accuracy of these models. There is no accurate complete model of the PTRUSM capable of being implemented in a model-based control strategy to operate these motors.

This dissertation presents a complete and accurate mathematical model of the PTRUSM. The motivation of this work was the need of a complete and accurate model of the motor capable of being used as the backbone of a model-based control strategy.

A 2D model of the motor is presented. The PTRUSM stator is modeled using a finite volume discretization. Two models of the PTRUSM stator were proposed: a static and a dynamic one. A simple model of the rotor with the capability of being coupled with the stator model was developed as well.

The stator and rotor models are coupled to model the stator-rotor contact interface of the motor. Two algorithms were prosed to model the contact between stator and rotor. These algorithms provide the

contact zone width, height, the normal force distribution, and the breaking and driving contact zones; these parameters define the horizontal rotor velocity.

The torque-speed characteristic of the USR60 is calculated with the proposed model. The results of the model are compared versus the real torque-speed of the motor. It was observed that this novel model accurately reflects the most important characteristic of the PTRUSM.

Table of Contents

List of Tables

List of Figures

Nomenclature

Acronyms

PTRUSM	Piezoelectric traveling wave rotary ultrasonic motor
USR60	Piezoelectric traveling wave rotary ultrasonic motor manufactured by Shinsei
FEM	Finite Element Method
MRI	Magnetic resonance imaging
FVM	Finite Volume Method
DC	Direct current
NASTRAN	Commercial finite element software
3D	Three-dimension
JNIKE3D	Commercial finite element software
PID	Proportional, integrand and derivative
2D	Two dimensional
PBC	Periodic boundary conditions

Notations

A,B	Phases of the ultrasonic motor
F_N	Pre-compressive force
L	External load
V_{rotor}	Linear rotor velocity
Ω	Traveling wave direction
E_z	Electric field in the z direction
d	Piezoelectric material thickness
F_{bx}	Body force applied in the x direction
F_{bz}	Body forces applied in the z direction

ΔV	Volume of the control volume of interest
P	Center of the current control volume
E	Center of the East control volume
RE	Center of the Rear-East control volume
R	Center of the Rear control volume
RW	Center of the Rear-West control volume
W	Center of the West control volume
FW	Center of the Front-West control volume
FE	Center of the Front-East control volume
y_v	Stator width
$\Delta x, \Delta z$	External dimensions of the control volume
ΔA	Area of the control volume of interest
u_p, w_p	Displacements in the x and z directions in the control volume of interest
u_E, w_E	Displacements in the x and z directions in the *East* control volume
u_W, w_W	Displacements in the x and z directions in the *West* control volume
u_F, w_F	Displacements in the x and z directions in the *Front* control volume
u_R, w_R	Displacements in the x and z directions in the *Rear* control volume
u_{FE},w_{FE}	Displacements in the x, and z directions in the *Front-East* control volume
u_{FW},w_{FW}	Displacements in the x, and z directions in the *Front-West* control volume
u_{RE},w_{RE}	Displacements in the x, and z directions in the *Rear-East* control volume
u_{RW},w_{RW}	Displacements in the x, and z directions in the *Rear-West* control volume
m_P	Mass of the current control volume
F_{xP}	Force of the current control volume applied in the x direction
F_{zP}	Force of the current control volume applied in the z direction
F_x	Normal force applied on the boundary normal in the x direction
F_z	Normal force applied on the boundary normal in the z direction
u_I, w_I	Displacements in the x and z directions in the piezo-metal interface

F_{kx}	Spring foundation force applied in the x direction
k_x, k_z	Spring constants of the spring foundation in the x and z directions.
g	Gap between the stator and contact layer
k_n	Imaginary spring stiffness rotor and contact layer
n	Number of stator control volumes in contact with the rotor
Z_i	Vector that contains the vertical displacement of each stator control volume involved in contact
Z_{RVD}	Vertical displacement of the rigid body
F_{Fi}	Vector that contains the friction force of each control volume involved in contact
V_{si}	Vector that contains the stator horizontal velocities
V_R	Rotor horizontal velocity
μ_k	Dynamic coefficient of friction
F_{NT}	Total normal force

Variables and constants

φ	Time phase shift between input voltage phases
ω	Angular frequency
t	Time
k	Wave number
λ	Wavelength
x,y,z	Cartesian system of coordinates
V	Voltage
σ_x	Normal stress applied in the x direction
σ_z	Normal stress applied in the z direction

τ_{zx}	Shear strain applied in the zx plane
ε_x	Normal strain applied in the x direction
ε_z	Normal strain applied in the z direction
γ_{zx}	Shear strain applied in the zx plane
Y	Young's modulus
v	Poisson's ratio
ρ	Mass density
∇	Vector differential operator
c_K	Damping parameter proportional to the stiffness matrix
c_M	Damping parameter proportional to the mass matrix
γ	Constant of the Newmark method
β	Constant of the Newmark method
Δt	Increment of time

Matrices, vectors and tensors

σ	Stress tensor
c	Elasticity matrix
ε	Strain vector
e	Electromechanical coupling matrix
D	Charge density displacement vector
ϵ	Permittivity matrix
u_T	Displacement vector
F_b	Body force vector
A	Matrix that contains the coefficients of the current control volume and the internal adjacent control volumes

B	Matrix that contains the coefficients of the boundary control volumes adjacent to the current control volume
X	Vector that contains the average displacements at the center of the control volumes
U	Vector that contains the average u and w displacements at the boundary faces of the boundary control volumes
F_P	Vector that contains the concentrated forces applied at the center of the control volumes
F_E	Vector that contains the forces produced by the electric field at the control volumes boundaries
F_M	Vector that contains the mechanical forces at the control volumes boundaries.
C	Matrix that contains the coefficients of the internal displacements of the boundary equation
D	Matrix that contains the coefficients of the boundary displacements of the boundary equation
K	Global stiffness matrix
F_T	Vector that contains all the forces applied in the PTRUSM stator
M	Matrix that contains the masses of the control volumes forming the PTRUSM stator
C	Matrix that contains the viscous damping coefficients of the PTRUSM stator
$\ddot{X}$	Vector that contains the acceleration of the control volumes forming the PTRUSM stator
$\dot{X}$	Vector that contains the velocity of the control volumes forming the PTRUSM stator
F	Vector that contains the time dependent forces applied in the continuum

Chapter 1: Introduction

Electromagnetic motors were the best choice for most of the actuating requirements in engineering and science. Engineers and researchers have put a lot of effort into their design and optimization. Nevertheless, in recent years, many new actuator and motor requirements have appeared. They include: a compact size, a high torque at a low speed, a light weight, low noise, self-breaking, and the capability to operate in strong magnetic fields. All of these requirements are difficult to achieve with electromagnetic motors due to their principle of operation and structure. In order to provide a high torque at low speed, electromagnetic motors use a gear reduction unit. This increases the actuator size and mass because of the power transmission mechanism. Electromagnetic motors need an external break to stop the shaft when are not energized. This adds extra weight, size, and cost. Another disadvantage is that electromagnetic motors cannot operate in strong magnetic fields, as they interfere with their principle of operation.

In 1983 Toshiiku Sashida developed a new motor concept called Piezoelectric Traveling Wave Rotary Ultrasonic Motor (PTRUSM). Fig. 1.1 shows a picture of the PTRUSM USR60. The principle of operation is based on a stator ring that induces vibration in the ultrasonic range produced by the inverse piezoelectric effect [1]. The term "ultrasonic" is added to these motors because the stator produces frequencies in the ultrasonic range of 25 to 70 kHz.

The advantages of the PTRUSM, as shown in [1-4], include:

- High torque at low speed.
- Small inertia.
- High holding torque.
- Stable operating speed in microseconds.
- High potential for miniaturization.

Figure 1.1: Shinsei Motor USR60

- Absence of a generated magnetic field.
- Able to operate in a strong magnetic field.
- Low noise.

Unfortunately, the PTRUSMs have some disadvantages [1-4] that limit the areas of applications for these types of motors. The disadvantages of these motors are:

- Short operating life (about 1000 hours).
- Small output power.
- Requires a complex motor controller.

PTRUSMs are actuators with a completely different principle of operation when compared to conventional electromagnetic motors. Since their invention, these motors have been used in a wide range of applications. On one hand, [2] reports that these motors have been used in satellites, mobile phones, photocopiers, robotic arms, telescopes, automobiles, and camera autofocusing. PTRUSMs are used for low torque and low speed applications, where size minimization and weight reduction are required. Other important applications of PTRUSMs are in environments with strong magnetic fields, such as

MRI equipment. On the other hand, the PTRUSM has a limited usage in its applications because of the previously mentioned disadvantages of these motors.

1.1 Literature review

Modeling of PTRUSMs is a challenge that is still not properly reached. During the last two decades, researchers have been trying to model these motors using different methods. All of these models neglect important characteristics of the motor or the models are just focused in describing the behavior of certain parts of the motor.

One can classify the models of the motor as models of the PTRUSM stator and models of the stator-rotor contact interface. A brief literature review regarding the most representative PTRUSM models and control strategies developed so far is presented in the next subsections.

1.1.1 Modeling of the ultrasonic motor stator

The PTRUSM inventor in collaboration with an expert in conventional electric motors wrote a book [1] with the goal of introducing researchers and engineers the concept, design, and modeling of the PTRUSM. These authors model the PTRUSM stator with an equivalent circuit. The circuit is composed of capacitors, inductors, and resistors. In this model, the capacitance, inductance and resistance represent the stator stiffness, mass, and losses respectively. A method to define the capacitance of the equivalent circuit that represents the stiffness of the stator was provided, but the authors reported that by using this capacitance value the output of the model does not approximate the output of the real motor. Thus, it is necessary to use the trial and error method to determine different capacitance values that allow more accurate results. The advantage of this model is that it is simple. The disadvantage of this model is that the parameters of the equivalent circuit need to be determined empirically.

In [5] and [6] an equivalent mechanical model of the PTRUSM stator is presented. The equivalent system is composed of basic mechanical elements like springs, dampers, and masses. The

output of the model is the amplitude of the stator traveling wave. The traveling wave generated on the stator surface is assumed to be the superposition of a sine and cosine waveforms. The advantages of the model are the clear relationship of the equivalent mechanical model components with respect to the PTRUSM stator, and the low computational effort required to calculate the amplitude of the stator traveling wave and the surface velocity. The disadvantages include lack of accuracy due the assumed sinusoidal shape of the stator traveling wave. In addition, the model does not include a procedure to model the amplitude and shape of the stator traveling wave when subject to the stator-rotor contact forces. Besides that, the authors proposed to do a separate model of the stator using the Finite Element Method (FEM) to define the parameters of the stator model. Nevertheless, the authors did not provide an explanation or procedure to calculate these parameters.

Hagood [7] proposes a stator model based on the modified Hamilton's Principle for general electromechanical systems. Because the PTRUSM stator is a thin plate, the electric field was assumed to be only in the vertical direction. The stator was simplified using plane stress approximation, and the traveling wave generated on the stator surface is assumed to be the superposition of a sine and cosine waveforms. The advantages of this model are that it is simple and a transient response can be obtained with it. Nevertheless, this model just provides the amplitude of the stator traveling wave. That means the stator model has one degree of freedom. Because the PTRUSM stator-rotor contact interface is a surface, the amplitude of the stator traveling wave provided by this model does not provide enough information to develop an accurate model of the stator-rotor contact interface.

A stator model developed to obtain the eigenfrequency of the PTRUSM stator is presented in [8]. The model was derived using Hamilton's principle. The electric field applied in the piezoelectric ceramics was modeled with a linear function. In order to simplify the problem, the stator was modeled as a 2D body using plane stress approximation. The Ritz method was proposed to find an approximated solution of the dynamic equation. The advantage of this model is that the influence of the stator teeth is

considered in the eigenfrequency analysis. The disadvantage of this model is that the frequency provided by this model is not the optimal frequency to power the motor because the pre-compressive force, output load, the stator bridge and temperature effect were not considered in the model. The eigenfrequency of the PTRUSM stator is lower than the one provided by this model because compressive forces decrease it. The stator stiffness changes under the action of a compressive load. Galef's formula [12] describes the relationship between the eigenfrequency of beams and the axial loads applied to them. Besides that, the increase of temperature in the stator and rotor during motor operation changes the eigenfrequency of the stator. That means the eigenfrequency analysis of the PTRUSM is a temperature dependent problem.

References [9,10] present a novel numerical strategy to model thin piezoelectric-metal beams using the Finite Volume Method (FVM). The system of equations was developed with the goal of computing the PTRUSM stator free body eigenfrequency [11]. The method was tested versus commercial FEM, and it was found that the solution reach convergence with less degrees of freedom using FVM than with commercial FEM. The advantages of this numerical model are that accurately provides the stator free body eigenfrequency, and that the computational effort is lower than the computational effort required with a similar model using FEM. The disadvantage is that like in [8] the pre-compressive force, output load, the stator bridge and temperature effect were not considered in the model.

Rodriguez [13] presents a summary of existing stator models. The PTRUSM stator models are classified as either numerical models using techniques like finite element and finite difference, or analytical models. Numerical models are able to describe complex stator geometries, like annular plates and stators with teeth on top of it. The disadvantage of using a numerical method to describe the stator is its complexity and the amount of demanded computational effort. Numerical methods are commonly used for design purposes. The advantages of analytical models include their simplicity and their low

computational effort. Proposed analytical models of the stator are inaccurate because these models have lots of simplifications and assumptions.

1.1.2 Modeling of the ultrasonic motor contact

The equivalent circuit used in [1] to model the stator was extended to model the stator-rotor contact as well. A direct current (DC) voltage and an inductor were added to the circuit to model the motor applied pre-force and the mass of the assembly. A network with Zener diodes in series with resistors was added to model the output load. The advantage of this model is that it is simple. However, a method to calculate the breakdown voltage of the Zener diodes and the resistances values was not defined. The major problem with this method is that the parameters of the circuit need to be determined empirically.

In [5], a simple model of the stator-rotor contact interface is presented. The rotor (metal) was modeled as a rigid body, and the contact layer was modeled as a linear spring. The rotor was considered to be vertically fixed, and reactions from the rotor to the stator were neglected. The overlap between stator and rotor was used to calculate the normal force distribution. The advantage of this model is the low computational effort required to obtain the output torque of the motor. The drawback of this model is that it is very inaccurate due to the assumptions and simplifications used. The author reported in [14] that the stator-rotor contact model is not sufficiently accurate to develop a model-based control strategy of the PTRUSM.

In order to model the contact, Hagood [7] assumes that the stator is rigid (the shape of the stator is independent of the contact forces), and the rotor (metal) is modeled as a linear spring. The vertical displacement of the rotor was included in the model. The overlap between the stator and rotor is used to calculate the normal force distribution. The advantage of this model is that a transient response can be obtained with it. Nevertheless, the author did not provide a comparison between the torque-speed characteristic of the real motor versus the torque-speed characteristic obtained with the proposed model.

A simulation of the amplitude of the traveling wave when the motor is subjected to different loads was provided, but it was observed that the amplitude of the traveling wave obtained with this simulation is independent of the external load. This result is incorrect because the amplitude of the stator traveling wave decreases when the external load of the motor increases. According to these results, one can conclude that the model does not reflect the real PTRUSM behavior.

The problem of modeling the stator-rotor contact mechanism is treated by Schmidt in [15]. The stator was modeled as a Bernoulli-Euler beam, the rotor was assumed to be rigid, and the contact layer attached to the rotor was modeled as a viscoelastic layer. Coulomb friction law was used to model the tangential forces on the contact interface. A contact algorithm was developed to solve this non-linear problem, (refer to [16]). The advantage of this model is that it considers the non-linearity of the stator-rotor contact zone because the system of equations is solved with iterations. The main drawback of the proposed method is the simplified stator model used as part of the contact model. The force produced in the stator by the inverse piezoelectric effect was modeled with a distributed force applied on the beam. However, a method to calculate the distributed force as a function of the electric field was not provided.

Sattel [4, 17] presents a planar contact model under the plane stress assumption. The problem is solved in four steps. First, the contact layer displacements are analytically obtained, and then, the displacements of the contact layer are expressed as a function of the stator and rotor displacements. The second step consists in generating a Fourier-series expansion of the stator and rotor displacement. In order to obtain the normal and tangential forces, it was assumed that the normal forces are independent of the tangential forces. Because of this assumption, the third step consists of calculating the normal forces. In the final step, the tangential forces are calculated using the obtained normal forces in the previous step. A contact algorithm was developed to solve the system of equations, (refer to [4]). The advantage of this model is that considers the non-linearity of the stator-rotor contact zone. The drawback of this model is the lack of an accurate stator model. Like in [15], the stator was modeled as a Bernoulli-

Euler beam and the force produced in the stator by the inverse piezoelectric effect was modeled with a distributed force applied to the beam. Besides that, the model simulation results presented in [17] were no compared versus measurements of the motor.

A FEM contact model was proposed in [18]. First, one tooth of the stator was modeled using the commercial finite element software NASTRAN. The model was used to compute the stator eigenfrequency. In order to model the stator-rotor contact interface, a FEM model was proposed as well. The model is composed of a 3D rotor in contact with a 3D tooth (model of the stator). The model was generated and solved using the commercial finite element software JNIKE3D. The software solved the contact problem using the penalty method. The advantage is that the contact between stator and rotor is solved in 3D. This allows one to obtain an accurate distribution of the stator-rotor contact zone forces. The disadvantages of this PTRUSM model are that the model of the stator is inaccurate because a model of the stator piezoelectric material was not included, and the computational effort required to solve the 3D contact model is very high. Besides that, the problem was solved using commercial software. Because of that, the implemented system of equations and algorithms are unavailable.

Other similar contact models can be found in [19-25]. It is important to mention that there is no model to calculate the optimal normal pre-compressive force applied to the contact interface between stator and rotor.

1.1.3 Ultrasonic motor control techniques

The PTRUSM has a strong non-linear behavior due to the contact between stator and rotor. When supplied with a fixed voltage and frequency, the output speed of the motor varies in time because the temperature of the stator and rotor increases. Besides that, the motor has a dead-zone. It is well known that the speed of the motor jumps from zero to a certain speed value depending on the motor model when the amplitude of the stator traveling wave is gradually increase from zero to a certain

height, (see section 2.2.4). These characteristics make it difficult to develop proper control strategies of the PTRUSM.

Since the invention of these motors, researchers have proposed different control techniques. These control strategies are mainly based on empirical data. One can find in the literature several control strategies that propose the use of fuzzy logic techniques to control the speed and position of the motor. A brief review of the most representative control strategies is presented in this section.

In [26, 27] a speed-position control strategy of the ultrasonic motor is presented. The strategy is based on fuzzy logic concepts. The speed of the motor is controlled through amplitude modulation of the driving voltages. On one hand, the control strategy was tested using a step load, reporting a good agreement. On the other hand, the control strategy was not properly tested. The authors only tested the control strategy using a specific load at a specific speed. Unfortunately, the authors did not provide enough information about the obtained fuzzy reasoning rules. The advantage of this control strategy is that the effect of the motor external load was considered in the control strategy. The main drawback of this control strategy is that one needs to perform experiments every time one changes the motor.

Cha [28] observed that the increase of temperature of the PTRUSM when operated for a long time produces a decrease of its resonant frequency, input current, and output speed. This author proposed a fuzzy controller to overcome this problem. The speed of the motor was controlled using frequency modulation of the driving voltages. This strategy was tested at different temperatures. The advantage of this control strategy is that the effect of the temperature was considered. Nevertheless, the effect of the driving load was not considered into the model and test.

Most recently, the problem of controlling the speed of the PTRUSM when subjected to a temperature increase is treated in [29]. These authors pointed out that it is difficult to control the speed of the PTRUSM because the heat generated by friction changes the tangential forces produced in the stator-rotor contact interface. A PID (proportional, integral, derivative) control strategy was proposed

here. An equation that approximates the torque-speed characteristic of the PTRUSM using curve fitting was used to develop the control strategy. Amplitude modulation of the driving voltages was used to control the motor output velocity. The advantage of this model is that the motor can be operated at its maximum efficiency because the speed of the motor was controlled using amplitude modulation of the driving voltages. The disadvantage of this control strategy is that only the unloaded motor case situation is considered.

In [30] a speed control strategy of the PTRUSM using a fuzzy neural network was proposed. The control strategy is based on a PI (proportional, integral) control with auto-tuning. The auto-tuning is based on fuzzy logic using a neural network. The speed of the motor was controlled using frequency modulation of the driving voltages. The advantage of this model is that the control rules are self-adapted with the auto-tuning controller. The disadvantage is that the fuzzy rules were obtained only for the unloaded motor case. The author reported that when the driving load is high, the rules are not valid.

Bal in [31] implements a speed controller of the PTRUSM. Frequency modulation technique is used to control the speed of the motor. The speed controller is tested with a variety of loads. The advantage of this control strategy is that one can control the motor speed with different loads. The disadvantage is that the temperature effect was no considered in the control strategy.

In [32] a neural network is used to compensate the nonlinearities of the PTRUSM. The author used amplitude modulation of the driving voltages. The reason of using amplitude modulation instead of frequency modulation was to avoid the pull-out phenomenon, (refer to [33]). If the driving frequency applied to the motor is decreased below the motor resonant frequency, the stator traveling wave decays abruptly. If the driving frequency is now increased to the eigenfrequency value, the rotor starts rotating abruptly (refer to [34]); this characteristic is the pull-out phenomenon. In addition, a hysteresis loop is observed when varying the driving frequency as described in this paragraph. The advantage of this control strategy is that it is not susceptible to the pull-out phenomenon and hysteresis effect. The

disadvantage is that one needs to do experiments to obtain the neural network each time a new motor is used.

Mass [34] implemented a model of the stator to develop a model-based control strategy of the PTRUSM. A simple analytical model of the stator was developed to be implemented in the control strategy. Nevertheless, the author pointed out that the existing models of the stator-rotor contact interface are not sufficiently accurate to be implemented in a model-based control strategy. The author used the neural network presented in [32] to model the stator-rotor contact interface. Amplitude modulation of the driving voltages was used to control the amplitude of the stator traveling wave. The advantages of this control strategy are that the motor can be operated at or below the resonant frequency, and it allows one to operate the motor with a wide range of speeds. The main drawback when using a neural network is that one needs to do time consuming experiments to obtain the neural network of every new motor model.

In [35] a fuzzy neural network was proposed to develop a speed control strategy of the PTRUSM. The author of this recent publication pointed out the lack of a proper mathematical model of the PTRUSM. Frequency and phase modulation of the driving voltages were used to control the speed of the motor. The proposed control strategy was tested for the unloaded motor. The results show a good agreement with respect to the experimental measurement. In addition, the control strategy was tested with a small load, reporting a good agreement as well. The advantage of this control strategy is that it allows one to operate the motor with a wide range of speeds because frequency and phase modulation are used together to operate the motor. The drawback is that this control strategy is susceptible to the pull-out phenomenon and hysteresis effect. In addition, one needs to consider that the strategy was not tested under the action of variable and high loads, and the temperature effect is not considered in the control strategy.

Senjyu proposes in [36] an equation to model the rotor speed of the ultrasonic motor. The torque-speed characteristic of the PTRUSM was approximated using curve fitting. The author proposes to use this equation to develop a speed control strategy of the motor. Frequency and phase modulation of the driving voltages were proposed to control the motor speed. The advantage of this model is the low computational effort required to compute the velocity of the rotor. The disadvantage of this model is that this equation is just valid for a specific motor model. In addition, this model is unable to consider important parameters of the motor like pre-compressive force, geometry of the stator, coefficient of friction, driving voltage, and temperature effects.

Besides speed control strategies, one can find in the literature control strategies to control the position of the rotor shaft. So far, only fuzzy control strategies were proposed to control the position of the rotor shaft, (refer to [37-38]).

1.2 Motivation

PTRUSMs are actuators with a completely different principle of operation when compared to conventional electromagnetic motors. Because of this new principle of operation, one needs to develop new mathematical models and new control strategies to operate these motors.

Modeling of the PTRUSM is a current challenge because the models of the motor discussed in the literature review are just focused in describing the behavior of certain parts of the motor, or the models have several assumptions that degrade the accuracy of these models. Most of the analytical models proposed so far are not accurate enough to be implemented in real applications. Because of that, these complete analytical models were never implemented in model-based control strategies.

The most robust model one can find in the literature of the PTRUSM stator-rotor contact is [17]. In this publication, the PTRUSM stator-rotor contact problem is treated in more detail than in other existing publications. On one hand, one algorithm was proposed to model this high non-linear problem providing a more realistic model of the stator-rotor contact interface. On the other hand, due to the

complexity of the stator-rotor contact, the stator was modeled as a simple Bernoulli-Euler beam. A mechanical force was applied to the beam to simulate the deformation of the stator, but this did not reflect the real behavior of the stator because the forces generated by the stator piezoelectric ceramics were not calculated. It is important to specify that the inputs of this contact model are a mechanical force and the velocity of the rotor and the output of the model is the output torque; these characteristics make it difficult to use this model in a model-based control strategy to operate these motors. So far, there is no model of the stator-rotor contact interface with the capability of being implemented in a model-based control strategy to operate the PTRUSM.

The lack of a complete and accurate model of the PTRUSM makes it difficult to develop model-based control strategies to operate these motors. As mentioned in the literature review, most of the PTRUSM control techniques proposed so far are based on neural networks, fuzzy control techniques and empirical equations (curve fitting). In order to develop an efficient control strategy for the PTRUSM able of being used with different motors without the need of time consuming experiments, one needs to develop first a complete and accurate mathematical model of the PTRUSM.

The three ways to control the output velocity of the PTRUSM are frequency, amplitude and phase modulation of the driving voltages [35]. Frequency modulation has the big disadvantage of being susceptible of the pull-out phenomenon and hysteresis effect [32]. Besides that, frequency and phase modulation of the driving voltages are inefficient control techniques. The reason is that the highest efficiency of the motor is reached when a perfect traveling wave is generated in the stator [38]. A perfect traveling wave is achieved when the PTRUSM is excited with equal amplitude of the driving voltages with a phase shift of 90 degrees in space and time between phases [5]. Because of that, a control strategy using amplitude modulation of the driving voltages is the best choice to efficiently operate the PTRUSM.

This dissertation is focused on developing of a complete and accurate mathematical model of the PTRUSM. The reason for developing a model of the PTRUSM is to provide an accurate model able of being used to develop a model-based control strategy for it. This model could be used in a control strategy that implements amplitude modulation of the driving voltages. Amplitude modulation of the driving voltages is proposed for two reasons: the first reason is to avoid the pull-out phenomenon and hysteresis effect, and the second reason is to operate the motor at its maximum efficiency.

1.3 Dissertation objectives

The objective of this dissertation is to develop a complete and accurate mathematical model of the PTRUSM. Because the model of the PTRUSM could be used in a control strategy using amplitude modulation of the driving voltages, the amplitude of the stator traveling wave model needs to be controlled by the amplitude of the driving voltages, and the output of the model needs to be the rotor velocity.

An accurate and complete model of the PTRUSM able of being used in a model-based control strategy needs to contain a model of the stator, rotor, and the stator-rotor contact interface. Therefore, the objectives of this dissertation are to accurately model the stator, rotor and the stator-rotor contact interface of the PTRUSM. The objectives of this dissertation are explained in detail below.

1. **Model of the stator.** The first objective is to develop an accurate model of the PTRUSM stator. The amplitude of the stator traveling wave needs to be controlled using the amplitude of the input voltages. A 2D stator model needs to be developed using the 3D system of equations that models a piezoelectric-metal cantilever beam, (refer to [9, 10]). This stator model includes:

- The computation of the forces generated by the action of the driving voltages. The deformation produced in the stator piezoelectric material should be modeled in detail.

- The computation of the reaction forces produced by the bridge supporting the stator. The PTRUSM is attached to the motor case by a bridge. Because of that the reaction forces produced in the bridge need to be considered in the model.
- The computation of the stator displacements. The model needs to accurately calculate the displacements produced in the stator under the action of an applied voltage and the action of external forces.
- The computation of the stator velocities. The stator model needs to accurately calculate the motion of the stator traveling wave.

2. Model of the rotor. In order to develop a complete model of the motor, the model of the rotor should be able of being coupled with the stator model. This rotor model includes:

- The computation of the vertical displacement of the whole structure (rotor). The model needs to include one degree of freedom that corresponds to the vertical displacement of the rotor.
- The computation of the vertical deformation of the rotor. The vertical deformation of the rotor when in contact with the stator needs to be computed because it determines the contact forces produced in the stator-rotor contact interface.

3. **Model of the stator-rotor contact interface.** It is important to mention that this model represents the complete model of the PTRUSM. The stator and rotor models need to be coupled to develop a model of the stator-rotor contact interface. Besides the input of the stator model (voltage), the inputs of the stator-rotor contact model need to be the normal pre-compressive force and the external load. This model needs to include:

- The computation of the contact zone height and length. In order to accurately model the contact between stator and rotor, an algorithm should be developed to determine the penetration of the rotor. After the penetration of the rotor is calculated, one can determine the contact zone height and length.

- The computation of the normal forces produced over the stator-rotor contact interface. The normal force distribution needs to be calculated as a function of the penetration of the rotor.
- The computation of the tangential forces produced over the stator-rotor contact interface. The tangential force distribution needs to be calculated as a function of the normal force distribution.
- The computation of the rotor horizontal velocity. The output of the complete PTRUSM model is the rotor velocity.

1.4 Dissertation outline

This dissertation contains 6 chapters and two appendixes.

In Chapter 2 one can find an introduction to PTRUSMs; the construction and principle of operation of these motors is presented in this chapter. The chapter concludes with an introduction to the PTRUSM model that is presented in the following chapters.

Chapter 3 deals with the static modeling of the PTRUSM stator. The stator model presented in this chapter was discretized with the FVM and is supported with a spring foundation that models the stator bridge. This chapter concludes with a simulation of one wavelength of the USR60 stator, this model is used to calculate the displacements of the stator under the action of a DC voltage.

The static stator model obtained in Chapter 3 was used to develop a dynamic model of the PTRUSM stator. The dynamic stator model is presented in Chapter 4. The time domain analysis of the stator allows one to model in detail its motion. This chapter concludes with a simulation of three wavelengths of the USR60 stator. In this simulation the stator surface velocities and the elliptical motion of the stator were calculated.

Chapter 5 contains the stator-rotor contact model of the PTRUSM. First, a rotor model able of being coupled with the stator model is presented. After that, two algorithms used to model the normal and tangential contact between stator and rotor are presented. At the end of this chapter one can find a

comparison of the torque-speed characteristic of the motor versus the torque-speed characteristic obtained with the complete model of the PTRUSM.

Chapter 6 presents the conclusions of this dissertation. In this chapter one can find the conclusions, contributions and the future work.

Appendix A presents the derivation of a 2D system of equations that describe a piezoelectric-metal beam. The system of equations presented in this appendix is composed of static equations. One can use this system of equations to model the equilibrium of a piezoelectric-metal beam when subjected to a DC voltage.

Appendix B presents the material properties of copper and lead zirconate titanat.

Chapter 2: Introduction to ultrasonic motors

PTRUSMs are defined as actuators that use the inverse piezoelectric effect of a piezoelectric ring to transform electrical energy into mechanical vibrations in the ultrasonic range. The vibrations are rectified through the stator-rotor contact mechanism to generate movement.

2.1 Construction

Nowadays one can find several commercial PTRUSMs designs. These designs have differences, but all of them are composed of a stator, a rotor, and a case. The most common PTRUSM used as a reference in publications is the Shinsei ultrasonic motor USR60, (refer to Fig. 2.1). This is considered the most representative for these motors because it was the first traveling wave rotary ultrasonic motor in the market. A description of each motor component is presented next.

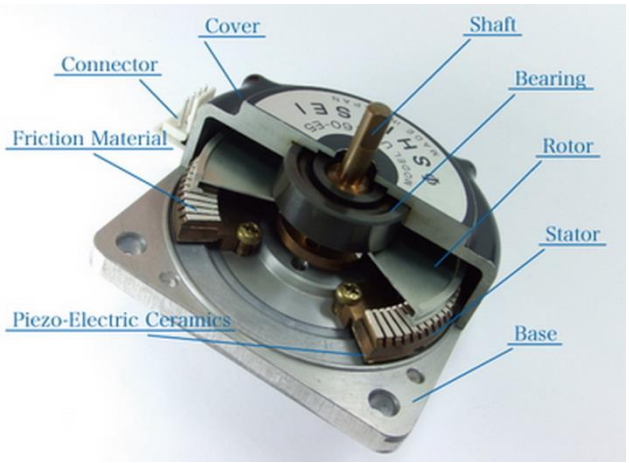

Figure 2.1: Internal components of Shinsei Motor USR60 (refer to www.shinsei-motor.com)

2.1.1 The stator

The stator of a PTRUSM is composed of two bonded rings mounted on a case, (refer to Fig. 2.2). The upper ring is made of metal, and teeth are machined on top of it. A piezoelectric ring is bonded on the bottom of the metallic one. The piezoelectric ring is the actuator of the motor. It generates mechanical vibrations in the composite ring.

2.1.2 The rotor

The rotor of a PTRUSM is a metallic disc with variable thickness, as shown in Fig. 2.3. The edge of the disc is thicker than the rest of it. The edge is the only part of the rotor that is in contact with the stator. In order to improve the wear properties of the contact zone, the rotor bottom edge is covered with a friction resistant material. The PTRUSM contact layer is a composite material. It is composed of a matrix, reinforced filler and a friction regulator (refer to [2]). One of the matrix materials used to manufacture the contact layer is epoxy resin. The shaft of the PTRUSM is mounted on the center of the disc.

Figure 2.2: USR60 stator

2.1.3 The case

The case of the motor is composed of two parts. The upper part of the case contains the bearing that allows the rotor shaft to rotate and the spring that provides the compressive force between the rotor and the stator, (refer to Fig. 2.4).

Figure 2.3: USR60 rotor

Figure 2.4: USR60 case

2.2 Principle of operation

The operating principle of the PTRUSM is based on two energy conversion processes. The two processes used to generate the output torque are briefly discussed next.

2.2.1 The traveling wave

PTRUSMs use the inverse piezoelectric effect to generate movement. Piezoelectric ceramics exposed to an electric field mechanically deform their original geometry. The deformation is proportional to the applied electric field and can be an expansion or contraction. The expansion or contraction depends on the electric field direction and the polarization of the piezoelectric material. If a positive voltage is applied to the stator in the direction of polarization, the sections with positive polarization will suffer an expansion, while the sections with negative polarization will suffer a contraction, as shown in Fig. 2.5 a. The opposite effect happens when a negative voltage is applied to the stator. The sections with positive polarization will suffer a contraction, while the sections with negative polarization will suffer an expansion, as shown in Fig. 2.5 b.

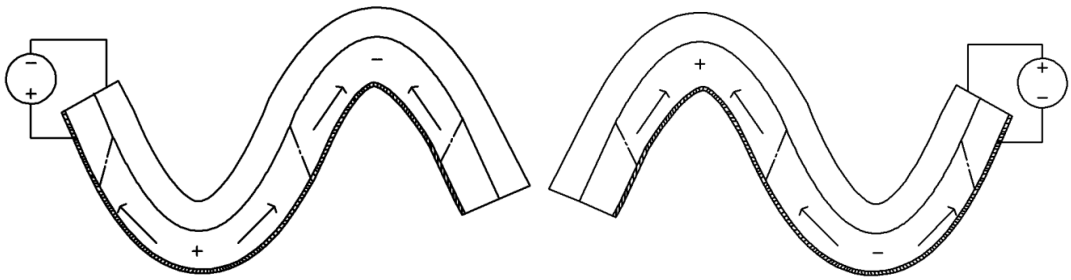

Figure 2.5: Stator deformation under an applied voltage (inverse piezoelectric effect)

The piezoceramic ring is divided into two semicircular sectors labeled phase A and phase B. Each phase is formed by piezoceramic elements with an alternate polarization plus (+) and minus (-), as shown in Fig. 2.6. In the case of Fig. 2.6 each phase is composed of four wavelengths. This is the case of the USR60. Phases A and B are used as vibrators to generate two standing waves. The standing waves have a space phase shift of a quarter of wavelength and the excitation voltages have a time phase shift represented with the symbol φ. The excitation voltages are mathematically represented by $Asin(\omega t)$ and $Acos(\omega t)$, where ω is the angular electrical frequency.

If phase A is supplied with a sinusoidal voltage $A\sin(\omega t)$, a standing wave is generated in the stator. Similarly, if phase B is supplied with a sinusoidal voltage of the form $Acos(\omega t)$, a standing wave is generated in the stator with a time phase shift φ with respect to phase A.

The superposition of both standing waves produces a traveling wave in the stator. According to [1], the mathematical expression describing the superposition of the two standing waves is:

$$A\sin(\omega t)\sin(kx) + Acos(\omega t)\cos(kx) = Acos(kx - \omega t) \qquad 2.1$$

$$k = \frac{2\pi}{\lambda}$$

In equation (2.1) ω, t, k, x and λ are the angular frequency of the traveling wave, time, the wave number, horizontal coordinate, and the wavelength, respectively.

It is desired for optimal operation to generate a perfect traveling wave on the stator surface at resonance [39]. In order to achieve a perfect traveling wave, three conditions are required: first, both stator phases must be excited with sinusoidal voltages with a phase shift of 90 degrees in time. Second, a space phase shift of one quarter of wavelength between the phases must exist. The last condition is to have the same voltage amplitude for both excitation signals.

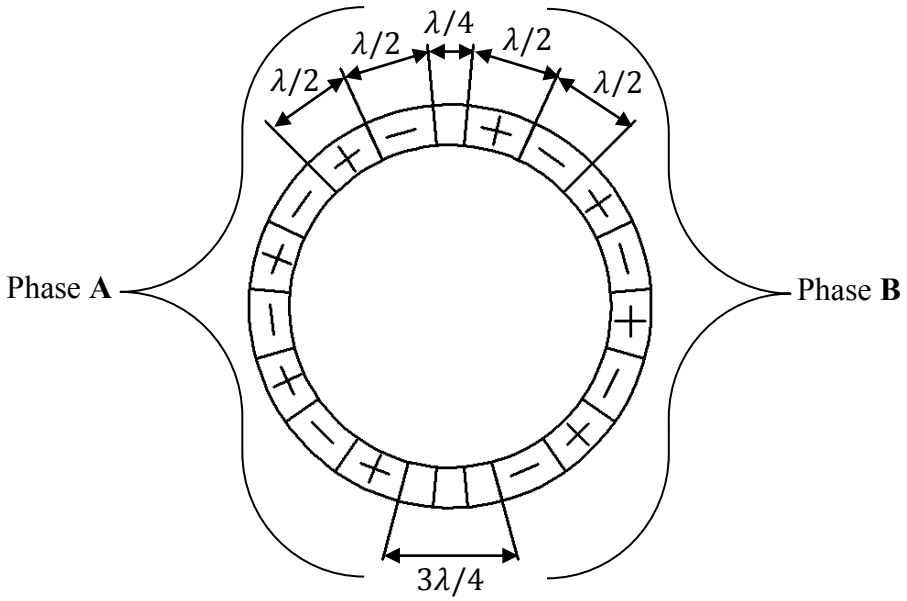

Figure 2.6: Electrode arrangement of the piezoelectric ring

2.2.3 The stator-rotor contact mechanism

When the traveling wave is excited in the stator, an elliptical motion at the surface of the stator wave crest is produced. The micro-motion along the horizontal axis is the one responsible for driving the rotor. In order to use the micro-motion produced in the stator surface, it is required to rectify the movement. The micro-motion is converted in unidirectional macro-motion through the stator-rotor contact mechanism. Fig. 2.7 shows a planar drawing of the stator-rotor contact mechanism.

In order to improve the contact characteristics of the stator-rotor contact mechanism, a layer made of a material with good friction wearing properties is bonded to the rotor. In some cases the contact layer is bonded to the stator instead.

The contact mechanism is composed of the stator with the rotor on top of it. During the motor assembly process, a spring is added between the case and the rotor. The spring is compresed, adding a normal force that presses the rotor against the stator. This force is labelled pre-compressive force F_N.

During motor operation, the contact force is distributed over the stator traveling wave crest in contact with the rotor. The total force can be decomposed into normal and tangential forces. The normal force is opposing the pre-compressive force and the tangential force is the one responsible for moving the rotor. Because of that, the contact interface will determine the output characteristics of the motor. According to [1], the rotor will move one micrometer per cycle of the elliptical motion. Nevertheless, it can reach a speed of 2 cm/s when operating at a frequency of 20 kHz.

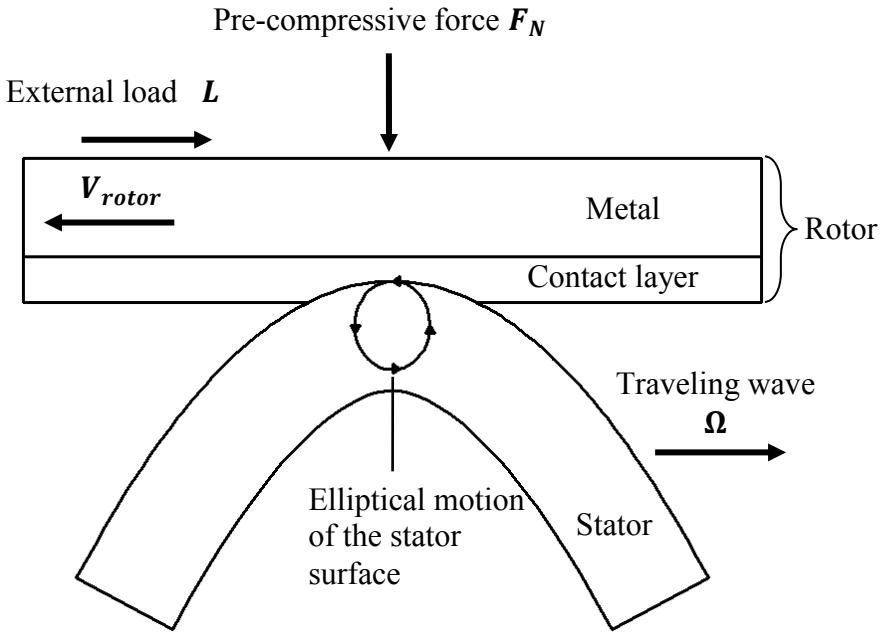

Figure 2.7: Stator-rotor contact mechanism

2.2.4 Ultrasonic motor Torque-Speed characteristic

The torque-speed characteristic of the motor USR60 is shown in Fig. 2.8. From this graph one can see that the maximum speed is 150 rpm at no load. The motor can drive loads up to 1.0 Nm. The graph shows as well that the motor is not able to gradually increase the output speed from zero. According to [3], this phenomenon happens because when a traveling wave with small amplitude is

generated in the stator surface, the contact layer has a horizontal displacement that stop the rotor movement. Table 2.1 shows a summary with the most important characteristics of the USR60.

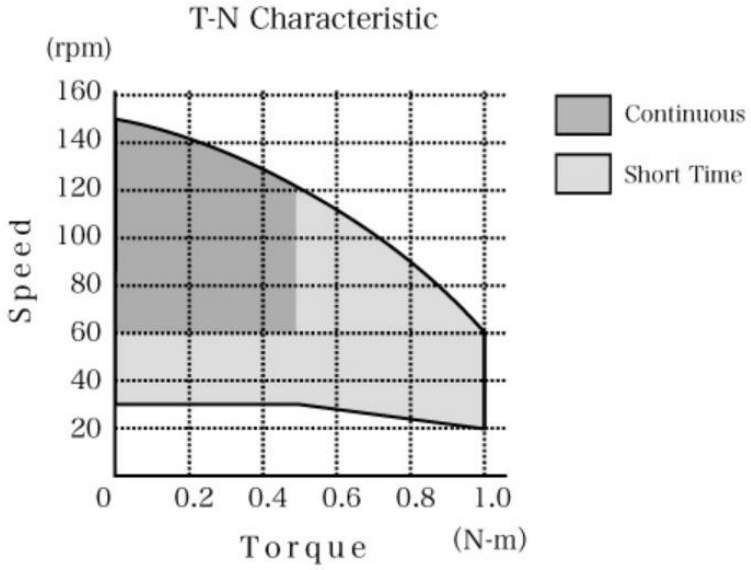

Figure 2.8: Torque-speed characteristic of USR60 (refer to www.shinsei-motor.com)

Table 2.1: USR60 characteristics

USR60	
Drive frequency	40 [kHz] to 45[kHz]
Drive voltage	130 [Vrms]
Rated output	5.0 [W]
Maximum output	10.0 [W]
Rated speed	100 [RPM]
Maximum speed	150 [RPM]
Rated torque	0.5 [N.m]
Maximum torque	1.0 [N.m]
Holding torque	1.0 [N.m]
Response	Less than 1[ms]
Direction of rotation	CW, CCW
Operational temperature range	-10 [^{o}C] to +55[^{o}C]
Endurance time	1,000 [Hours]
Weight	190 g

2.3 Introduction to the PTRUSM model

The SHINSEI USR60 is taken as the reference motor in this work. The stator-rotor contact mechanism is a high non-linear problem that demands to be mathematically described with inequalities. Because of the complexity of the problem, it is required to introduce certain valid simplifications.

As explained in [40], when the PTRUSM is operating in steady-state, the contact between stator and rotor occurs in a surface with a small thickness. When a traveling wave is excited in the stator, it forms an angle with respect to the horizontal. As shown in Fig. 2.9, the stator bridge bends at an angle between the stator and contact layer surfaces. The normal forces at the stator-rotor contact mechanism produce the bridge deformation. Because of that, the width of the contact surface is very small. Experimental results showing the wear of the contact layer of the SHINSEI USR60 are presented in [40]. Due to that fact, a two dimensional (2D) model of the motor is appropriated. Therefore, the contact between stator and rotor will be modeled as a line of contact. A cross-sectional view of the stator-rotor contact mechanism when operating at steady-state is shown in Fig. 2.9.

In order to model the contact, a moving reference coordinate system on top of the stator traveling wave is introduced, (refer to Fig. 2.10). This simplifies the steady-state modeling, because one can reduce a time dependent problem into a time independent problem [4]. Therefore, time independency motivates the use of a static model. Nevertheless, it is still required to model the stator surface velocities.

Two stator models are developed to model the whole PTRUSM. The first one is a static model, and the second one is a dynamic model. The details of the models are explained in the following chapters.

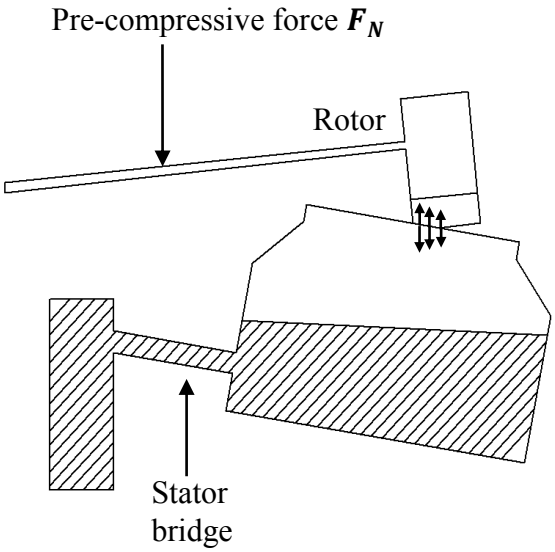

Figure 2.9: Cross-sectional view of stator-rotor contact mechanism when operating in steady-state

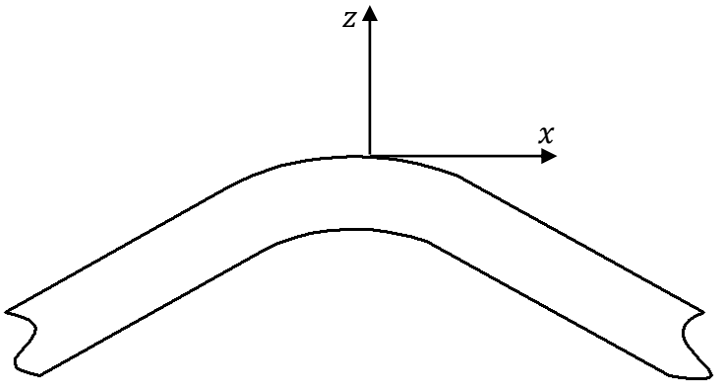

Figure 2.10: Stator traveling wave with a moving coordinate system on top of it

Chapter 3: Static modeling of the PTRUSM stator

The starting point of this work is the static PTRUSM displacement stator model. A wavelength of the SHINSEI USR60 stator can be approximated with a straight beam. The approximation is valid because the internal diameter of the stator is larger than the width of the ring (one third), and the stator wavelength is much smaller than the stator circumference (one ninth). It is demonstrated in [3] by simulations using commercial FEM software that the contribution of the stator teeth to the stiffness of the stator is small. The simulations compare the displacements of a stator wavelength with teeth on top of it versus the displacements of a stator wavelength without teeth. The results show a variation of just around 5%.

In this work a PTRUSM stator wavelength is modeled as a 2D straight beam. Teeth won't be added on top of the stator because of their small influence on the stator stiffness. Nevertheless, the mass density of the metal forming the stator is increased to include the mass of the teeth in the model. The static stator model is independent of the mass density, but the mass density is an important parameter for the dynamic stator model. The input of the static stator model is a DC voltage, and the outputs are the stator displacements.

In order to obtain an accurate PTRUSM model, it is required first to develop an accurate PTRUSM stator model. Therefore, the stator is numerically modeled. Numerical models offer lots of advantages. The advantages include: high accuracy, capability to model systems with complex shapes, and capability to control the accuracy level by changing the number of state space equations.

3.1 Static PTRUSM stator model

The stator is modeled using a FVM discretization. The equilibrium equations used to model the stator are based on the ones presented on the general static model for piezoelectric-metal cantilever beams shown in [9,10]. These references present the equilibrium equations used to obtain the

displacements of a 3D piezoelectric-metal cantilever beam. The 3D beam was numerically modeled; the discretization was performed using the FVM. In order to develop a 2D PTRUSM stator model, one needs to transform the 3D system of equilibrium equations into a 2D system of equilibrium equations.

One can find two techniques in the literature [41,42] to model 2D bodies: plane stress approximation, and plane strain approximation. For instance, plane stress is used to model beams, and plane strain is used to model shafts. The PTRUSM stator is modeled as a beam. Therefore, plane stress approximation is used to model the 2D stator.

The computational effort of a 3D model can be considerable reduced if modeled as a 2D body. In order to model a 3D body as a 2D body, one needs to remove one axis. The stator is modeled as a beam located in the xz plane. Therefore, the y axis is removed. One can mention two conditions to obtain accurate results when using plane stress to model a body. The first one is to have a small thickness compared with the dimensions in the x and z axes. The second condition is that all the external forces must be applied on the x and z axes. When using plane stress approximation, all the unknowns are considered to be independent of the y axis.

The length and height of the PTRUSM stator wavelength are much larger in magnitude with respect to the contact zone width between stator and rotor. Besides that, all the forces are applied in the x and z axes. Therefore, one can model the PTRUSM stator as a 2D body using plane stress approximation. Fig. 3.1 shows a deformed stator in static equilibrium with concentrated forces applied to it.

The procedure to obtain the 2D system of static equations is shown in Appendix A. The obtained static equations used to describe the equilibrium of a piezoelectric-metal beam are:

$$P_1 u_P - E_1 u_E - W_1 u_W - F_1 u_F - R_1 u_R - B_1(w_F - w_R) - B_2(w_{FE} - w_{RE}) + B_3(w_{FW} - w_{RW}) - B_4(w_E - w_W) - B_5(w_{FE} - w_{FW}) + B_6(w_{RE} - w_{RW}) = F_{xP} \quad (3.1)$$

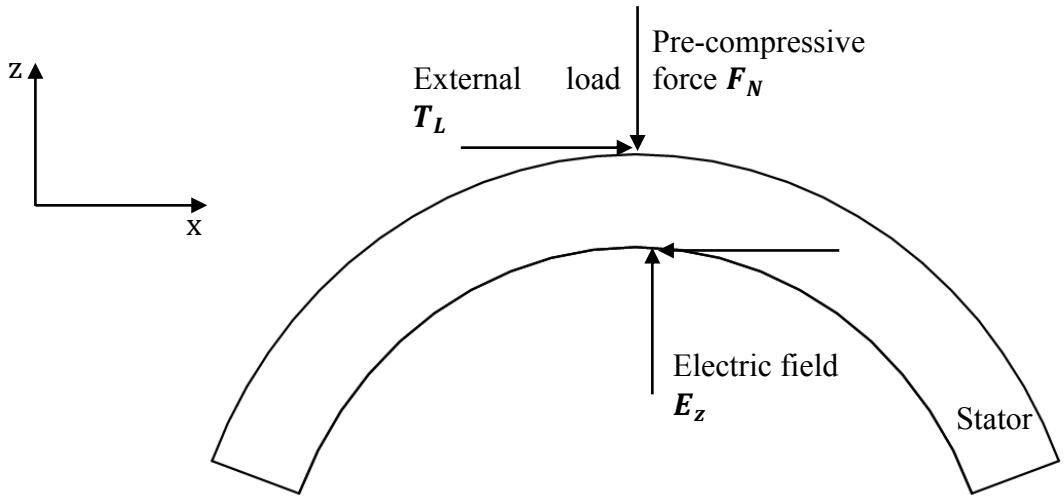

Figure 3.1: Deformed PTRUSM stator in static equilibrium with concentrated forces applied to it

$$P_2 w_P - E_2 w_E - W_2 w_W - F_2 w_F - R_1 w_R - B_7(u_F - u_R) - B_8(u_{FE} - u_{RE}) + B_9(u_{FW} - u_{RW}) - B_{10}(u_E - u_W) - B_{11}(u_{FE} - u_{FW}) + B_{12}(u_{RE} - u_{RW}) = F_{zP} \quad (3.2)$$

Equation (3.1) provides the u displacement at the center of a current control volume along the x axis. Equation (3.2) provides the w displacement at the center of a current control volume along the z axis. Equations (3.1) and (3.2) do not contain electric field terms because these equations are derived for internal control volumes. Because equations (3.1) and (3.2) do not contain electric field terms, these equations are valid to describe both, piezoelectric and metal materials. These simple algebraic equations are used to define the static equilibrium of the stator. Special equations will be derived in the next section to add the electric field at the piezoelectric material boundaries.

3.1.1 Boundary conditions

Equations (3.1) and (3.2) are the equilibrium equations defined at the center of the control volume. The center of the current control volume is labeled with the letter P. In order to solve the

system of equations, one needs to define the boundary conditions for the piezoelectric and metal materials.

As explained in [43], the boundary conditions for a piezoelectric material are divided into mechanical and electrical boundary conditions. Thus, one needs to define mechanical and electrical boundary conditions for the piezoelectric plate. For the metal plate, one just needs to define mechanical boundary conditions.

The mechanical boundary conditions are classified as displacement boundary conditions, and force boundary conditions. There are two types of displacement boundary conditions: fixed boundary conditions and free boundary conditions. If a boundary is fixed, the boundary is not allowed to move. If a boundary is free, the boundary is allowed to move in a specific direction or in any direction. The force boundary conditions refer to all mechanical forces applied to the boundaries.

The electrical boundary conditions are classified as the potentials applied at the boundary of the piezoelectric material, and the free charge contained in the piezoelectric material. The potential boundary conditions define the magnitude and polarity of the voltage applied in the piezoelectric material. The voltage defines the electric field, and through the electromechanical coupling matrix, it is transformed into a mechanical force applied at the surface of the material.

The stator model is composed of a piezoelectric beam attached to a metal beam. Therefore, it is required to define mechanical and electrical boundary conditions. Fig. 3.2 shows all the boundary conditions for the PTRUSM stator. The boundary conditions are:

- Force boundary condition at the *Front* boundary of the metal beam. Electrical and force boundary condition at the *Rear* boundary of the piezoelectric beam.
- Electrical boundary conditions at the interface between the piezoelectric and metal beams.
- Periodic boundary conditions (PBC) at the *East* and *West* boundaries of the metal and piezoelectric beams.

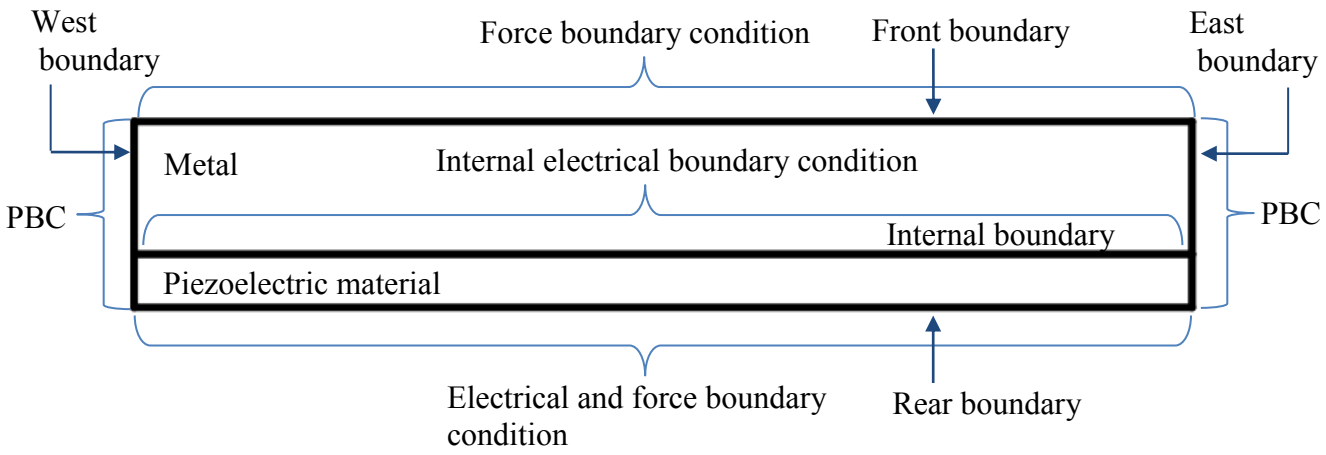

Figure 3.2: Boundary conditions for the PTRUSM stator

Mechanical boundary conditions applied at the *Front* boundary of the metal

In order to define the equations to add the force boundary conditions at the *Front* boundary of the metal, one needs to relate the external forces applied at the *Front* boundary of the metal with the internal stress produced in the metal

The normal and shear stresses are defined as equal in magnitude but opposite in direction to the normal and shear body forces applied at the surface of the continuum. Fig. 3.3 shows an external force applied at the *Front* boundary of the metal; the applied force produces a normal stress σ_z proportional to the magnitude of it.

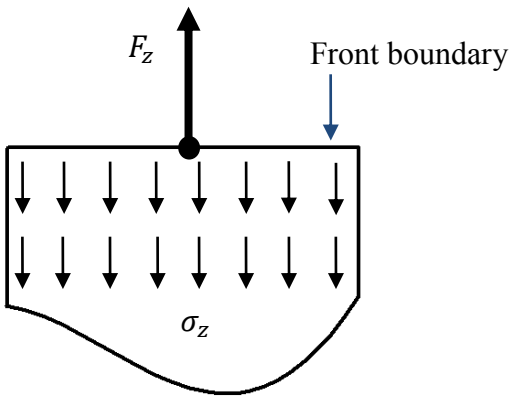

Figure 3.3: External force applied at the *Front* boundary of the metal.

The equations that describe the boundary conditions are expressed as follows:

$$\sigma_z = \frac{F_z}{\Delta A} \tag{3.3}$$

$$\tau_{zx} = \frac{F_{zx}}{\Delta A} \tag{3.4}$$

where ΔA is the cross-sectional area of the finite volume where the external force is applied.

Thus, ΔA is equivalent to:

$$\Delta A = \Delta x \, y_v \tag{3.5}$$

Equation (3.5) is substituted into equation (3.3) and (3.4). After substitution one obtains:

$$\sigma_z = \frac{F_z}{\Delta x y_v} \tag{3.6}$$

$$\tau_{zx} = \frac{F_{zx}}{\Delta x y_v} \tag{3.7}$$

Equation (3.6) is processed first. The normal stress σ_z along the z axis is expressed as a function of the strain. The normal stress is substituted with the metal constitutive matrix equation (A.12). Thus, equation (3.6) becomes:

$$c_{12}\varepsilon_{xf} + c_{11}\varepsilon_{zf} = \frac{F_z}{\Delta x y_v} \tag{3.8}$$

After substitution of the strain terms using equation (A.7), one obtains:

$$c_{12}\left(\frac{\partial u}{\partial x}\Big|_f\right) + c_{11}\left(\frac{\partial w}{\partial z}\Big|_f\right) = \frac{F_z}{\Delta x y_v} \tag{3.9}$$

The displacement partial differentials are substituted with the linear interpolations (A.43) and (A.39) to obtain:

$$c_{12}\left(\frac{u_E - u_W}{\delta_{XE} + \delta_{XW}} \cdot \frac{\delta_{ZF} - \delta_{Zf}}{\delta_{ZF}} + \frac{u_{FE} - u_{FW}}{\delta_{XFEF} + \delta_{XFWF}} \cdot \frac{\delta_{Zf}}{\delta_{ZF}}\right) + c_{11}\left(\frac{w_F - w_P}{\delta_{ZF}}\right) = \frac{F_z}{\Delta x y_v} \tag{3.10}$$

After terms manipulation one obtains:

$$\frac{c_{12}\delta_{Zf}}{c_{11}(\delta_{XFEF}+\delta_{XFWF})}.(u_{FE}-u_{FW})+w_F-w_P=\frac{\delta_{ZF}}{c_{11}}\frac{F_z}{\Delta xy_v} \tag{3.11}$$

The following notation is used in (3.11).

$$A_{F1}=\frac{c_{12}\delta_{Zf}}{c_{11}(\delta_{XFEF}+\delta_{XFWF})} \tag{3.12}$$

After substitution of notation (3.12) into equation (3.11) one obtains:

$$w_F=w_P-A_{F1}(u_{FE}-u_{FW})+\frac{\delta_{ZF}}{c_{11}}\frac{F_z}{\Delta xy_v} \tag{3.13}$$

Equation (3.7) is processed in a similar way and equation (3.14) is obtained:

$$u_F=u_P-A_{F2}(w_{FE}-w_{FW})+\frac{\delta_{ZF}}{c_{55}}\frac{F_{zx}}{\Delta xy_v} \tag{3.14}$$

where A_{F2} is equal to:

$$A_{F2}=\frac{\delta_{Zf}}{\delta_{XFEF}+\delta_{XFEF}} \tag{3.15}$$

Electrical and mechanical boundary conditions applied at the *Rear* boundary of the piezoelectric plate

The piezoelectric material is located at the *Rear* boundary of the metal. Thus, it is required to define the electrical and mechanical boundary conditions at the *Rear* piezoelectric boundary.

The starting points to derivate the equations to add the *Rear* boundary conditions for the PTRUSM stator model are again equations (3.6) and (3.7). Equation (3.6) is processed first. The normal stress σ_z along the z axis is expressed as a function of the strain using the piezoelectric constitutive matrix equation (A.6). The obtained equation is:

$$c_{31}\varepsilon_{xr}+c_{33}\varepsilon_{zr}-e_{33}E_z=\frac{F_z}{\Delta xy_v} \tag{3.16}$$

Equation (3.16) contains the boundary electric field E_z and the external boundary force F_z. It is important to mention that the external force F_z at the rear boundary is zero. One can substitute the strain terms in equation (3.16) with equation (A.7). After substitution, one obtains:

$$c_{31}\left(\frac{\partial u}{\partial x}\right)\Big|_r + c_{33}\left(\frac{\partial w}{\partial z}\right)\Big|_r - e_{33}E_z = \frac{F_z}{\Delta xy_v} \tag{3.17}$$

The displacement partial differentials are substituted with the linear interpolation (A.44) and (A.40), and equation (3.18) is obtained.

$$c_{31}\left(\frac{u_E - u_w}{\delta_{XE} + \delta_{XW}}.\frac{\delta_{ZR} - \delta_{Zr}}{\delta_{ZR}} + \frac{u_{RE} - u_{RW}}{\delta_{XRER} + \delta_{XRWR}}.\frac{\delta_{Zr}}{\delta_{ZR}}\right) + c_{33}\left(\frac{w_P - w_R}{\delta_{ZR}}\right) - e_{33}E_z = \frac{F_z}{\Delta xy_v} \tag{3.18}$$

After terms manipulation equation (3.18) becomes:

$$\frac{c_{31}\delta_{Zr}}{c_{33}(\delta_{XRER} + \delta_{XRWR})}.(u_{RE} - u_{RW}) + w_P - w_R - \frac{e_{33}\delta_{ZR}E_Z}{c_{33}} = \frac{\delta_{ZR}}{c_{33}}\frac{F_z}{\Delta xy_v} \tag{3.19}$$

The following notations are used to express the coefficients of the displacements:

$$A_{R1} = \frac{c_{31}\delta_{Zr}}{c_{33}(\delta_{XRER} + \delta_{XRWR})} \tag{3.20}$$

$$A_{R2} = \frac{\delta_{ZR}}{c_{33}}e_{33} \tag{3.21}$$

$$A_{R3} = \frac{\delta_{ZR}}{c_{33}\Delta xy_v} \tag{3.22}$$

After substitution of notations (3.20), (3.21), and (3.22) into equation (3.19) one obtains:

$$w_R = w_P + A_{R1}(u_{RE} - u_{RW}) - A_{R2}E_z - A_{R3}F_z \tag{3.23}$$

Equation (3.7) is processed in a similar way and equation (3.24) is obtained:

$$u_R = u_P + A_{R4}(w_{RE} - w_{RW}) - \frac{\delta_{ZR}}{c_{55}}\frac{F_{zx}}{\Delta xy_v} \tag{3.24}$$

In (3.24) A_{R4} is:

$$A_{R4} = \frac{\delta_{Zr}}{\delta_{XRER} + \delta_{XRWR}} \tag{3.25}$$

Internal boundary conditions

The next step is to define the internal electrical boundary conditions at the *Front* boundary of the piezoelectric material. It is called an internal boundary condition because one needs to define the electric field at the internal boundary between the metal and piezoelectric material.

In order to obtain the equation to define the internal electrical boundary condition, one needs to define the stress relationship at the boundary between the piezoelectric material and metal. The normal and shear stresses at the internal boundary between metal and piezoelectric material are defined as equal in magnitude and opposite in direction. Fig. 3.4 shows the stresses produced at the interface between metal and piezoelectric material.

This is expressed with equations (3.26) and (3.27):

$$\sigma_{zm}|_I = \sigma_{zp}\big|_I \tag{3.26}$$

$$\tau_{zxm}|_I = \tau_{zxp}\big|_I \tag{3.27}$$

where the subscript I stands for the internal point where the stress is defined. The stresses σ_{zm}, σ_{zp}, τ_{zxm}, τ_{zxp} refer to normal stress applied in the z direction at the metal point I, normal stresses applied along the z direction at the piezoelectric point I, shear stresses applied at the metal point I, and shear stresses applied at the piezoelectric point I, respectively.

The normal stress σ_z on equation (3.26) is substituted as a function of the strain and the electric field. The piezoelectric material constitutive matrix equation (A.6) and metal constitutive matrix equation (A.12) are substituted into equation (3.26) and equation (3.28) is obtained:

$$c_{12m}\varepsilon_{xm}|_I + c_{11m}\varepsilon_{zm}|_I = c_{31p}\varepsilon_{xp}\big|_I + c_{33p}\varepsilon_{zp}\big|_I - e_{33}E_z \tag{3.28}$$

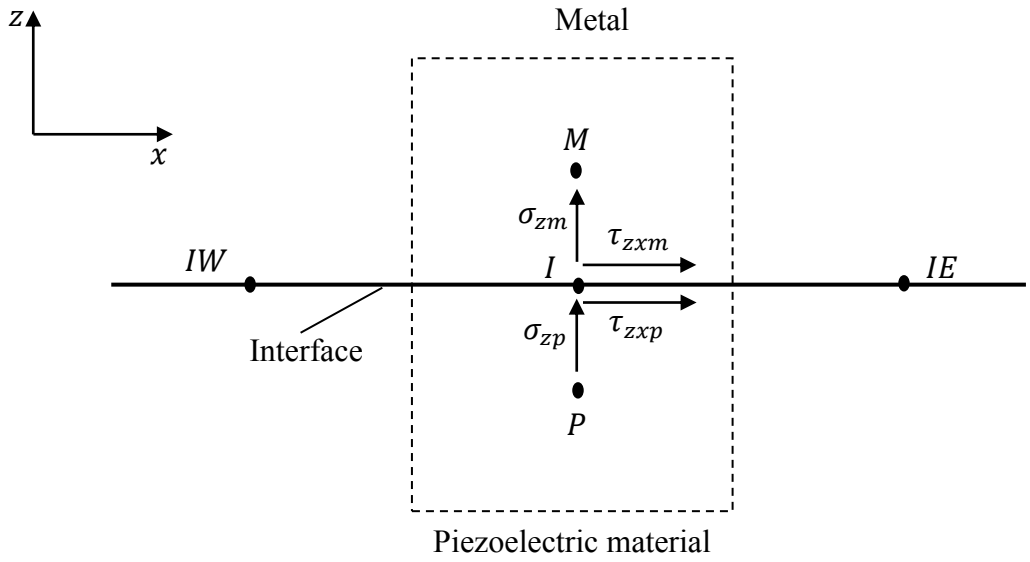

Figure 3.4: Stresses produced at the internal boundary of the PTRUSM stator

The strains in equation (3.28) are substituted with the strain definition of equation (A.7). After substitution, equation (3.28) becomes:

$$c_{12m}\left.\frac{\partial u_m}{\partial x}\right|_I + c_{11m}\left.\frac{\partial w_m}{\partial z}\right|_I = c_{31p}\left.\frac{\partial u_p}{\partial x}\right|_I + c_{33p}\left.\frac{\partial w_p}{\partial z}\right|_I - e_{33}E_z|_I \tag{3.29}$$

The displacement partial differentials are substituted with linear interpolations. After substitution one obtains:

$$c_{12m}\frac{u_{IE}-u_{IW}}{\delta_{XIEI}+\delta_{XIWI}} + c_{11m}\frac{w_M-w_I}{\delta_{ZMI}} = c_{31p}\frac{u_{IE}-u_{IW}}{\delta_{XIEI}+\delta_{XIWI}} + c_{33p}\frac{w_I-w_P}{\delta_{ZPI}} - e_{33}E_z|_I \tag{3.30}$$

Fig. 3.5 shows the distances used in the equations at the interface between metal and piezoelectric material control volumes.

After terms manipulations one obtains the displacement w at point I:

$$w_I = \frac{w_P\frac{c_{33p}}{\delta_{ZPI}} + w_M\frac{c_{11m}}{\delta_{ZMI}} - (u_{IE}-u_{IW})\frac{c_{31p}-c_{12m}}{\delta_{XIEI}+\delta_{XIWI}} + e_{33}E_z|_I}{\left(\frac{c_{33p}}{\delta_{ZPI}}+\frac{c_{11m}}{\delta_{ZMI}}\right)} \tag{3.31}$$

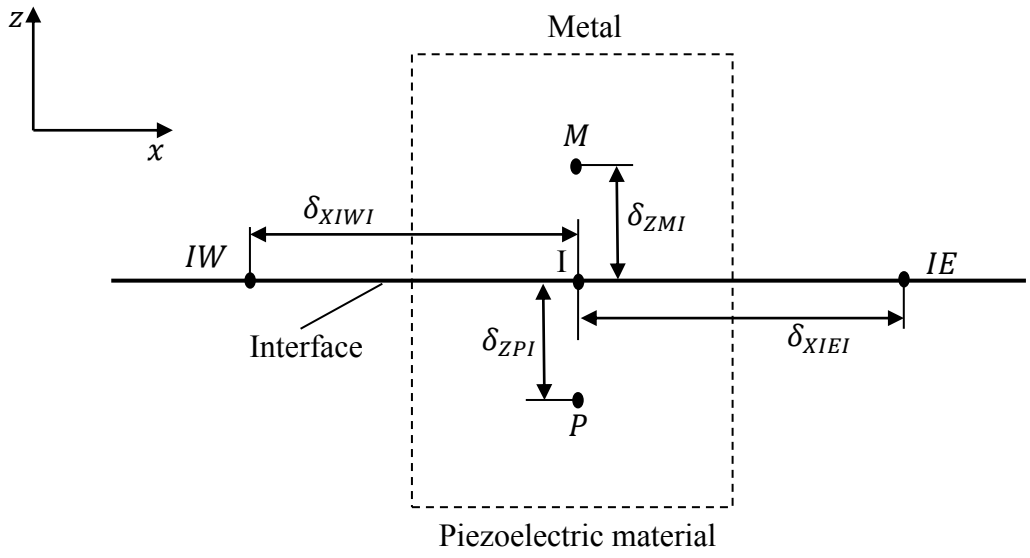

Figure 3.5: Distances at the internal boundary of the PTRUSM stator

The following notations are used to express the coefficients of equation (3.31):

$$A_{I1} = \frac{\frac{c_{33p}}{\delta_{ZPI}}}{\frac{c_{33p}}{\delta_{ZPI}} + \frac{c_{11m}}{\delta_{ZMI}}} \tag{3.32}$$

$$A_{I2} = \frac{\frac{c_{11m}}{\delta_{ZMI}}}{\frac{c_{33p}}{\delta_{ZPI}} + \frac{c_{11m}}{\delta_{ZMI}}} \tag{3.33}$$

$$A_{I3} = \frac{\frac{c_{31p-}c_{12m}}{\delta_{XIEI} + \delta_{XIWI}}}{\frac{c_{33p}}{\delta_{ZPI}} + \frac{c_{11m}}{\delta_{ZMI}}} \tag{3.34}$$

$$A_{I4} = \frac{e_{33}}{\frac{c_{33p}}{\delta_{ZPI}} + \frac{c_{11m}}{\delta_{ZMI}}} \tag{3.35}$$

After substitution of equations (3.32), (3.33), (3.34), and (3.35) into equation (3.31) one obtains equation (3.36) for w_I.

$$w_I = A_{I1}w_P + A_{I2}w_M - A_{I3}(u_{IE} - u_{IW}) + A_{I4}E_z|_I \tag{3.36}$$

Equation (3.27) is processed in a similar way. The resulting equation is:

$$u_I = A_{I5}u_P + A_{I6}u_M - A_{I7}(w_{IE} - w_{IW}) \tag{3.37}$$

where the coefficients A_{I5}, A_{I6} and A_{I7} are equal to:

$$A_{I5} = \frac{\frac{c_{55p}}{\delta_{ZPI}}}{\frac{c_{55p}}{\delta_{ZPI}} + \frac{c_{33m}}{\delta_{ZMI}}} \tag{3.38}$$

$$A_{I6} = \frac{\frac{c_{33m}}{\delta_{ZMI}}}{\frac{c_{55p}}{\delta_{ZPI}} + \frac{c_{33m}}{\delta_{ZMI}}} \tag{3.39}$$

$$A_{I7} = \frac{\frac{c_{55p} - c_{55m}}{\delta_{XIEI} + \delta_{XIWI}}}{\frac{c_{55p}}{\delta_{ZPI}} + \frac{c_{33m}}{\delta_{ZMI}}} \tag{3.40}$$

Periodic boundary conditions

As explained before, the PTRUSM stator is a ring, but the proposed model is a straight beam. Because of that, the *East* and *West* boundaries of both, the metal and the piezoelectric material are modeled with PBC. That means the *East* face of each control volume located at the *East* boundary is connected to a corresponding *West* face of a control volume located at the *West* boundary. In other words, each control volume located at the *West* boundary is virtually connected to a corresponding control volume located at the *East* boundary. The last assumption will model the continuity at the stator edges. Fig. 3.6 shows a meshed PTRUSM stator with PBC at the *East* and *West* boundaries.

Displacement boundary conditions

In addition to the force, electrical, and periodic boundary conditions one needs to provide displacement boundary conditions. All the stator boundaries are defined with free displacement boundary conditions. That means all the stator boundaries are free to move in any directions.

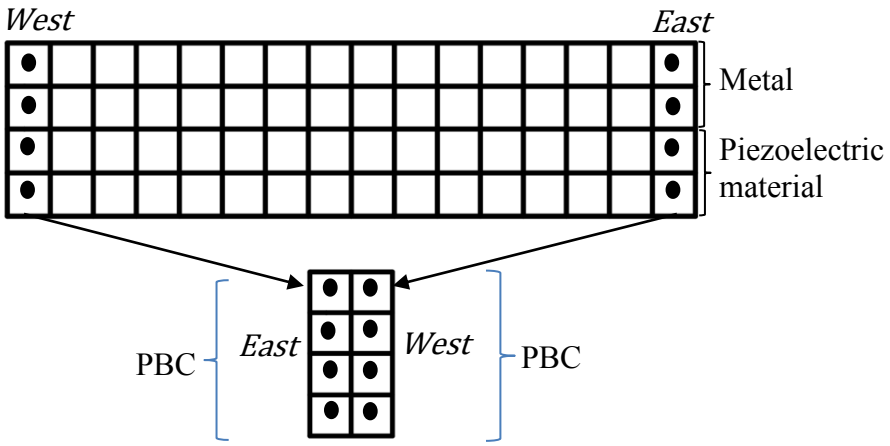

Figure 3.6: Meshed PTRUSM stator with PBC at the *East* and *West* boundaries

The PTRUSM stator is attached to a bridge, as shown in Fig. 3.7. The PTRUSM stator bridge provides the reaction forces against the forces produced in the stator-rotor contact interface. Because of that, it is required to add the bridge influence into the stator model to get accurate results. In addition, every numerical structural mechanic model needs a reference or connection to physical "ground". Therefore, the bridge will be modeled with springs. That means the PTRUSM stator model is supported by a spring foundation. The springs are defined at the center of the metal beam, as shown in Fig. 3.8.

It is required to define two springs at the center of each control volume attached to the bridge. One spring provides support in the x direction, and the second spring provides support in the z direction. The spring foundation is added to the equilibrium equations (3.1) and (3.2).

The spring foundation model developed in this work differs from the one used in FEM [42]. The reason is because the FVM control volume only has one node at its center. The springs are modeled as linear springs. The equation used to model the horizontal springs is processed first. The equation used to define the linear springs along the x axis is:

$$F_k = k_x u_{Pk} \tag{3.41}$$

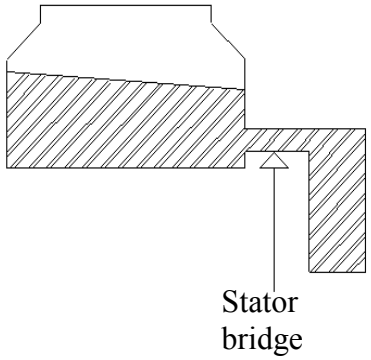

Figure 3.7: Cross sectional view of USR60 stator bridge

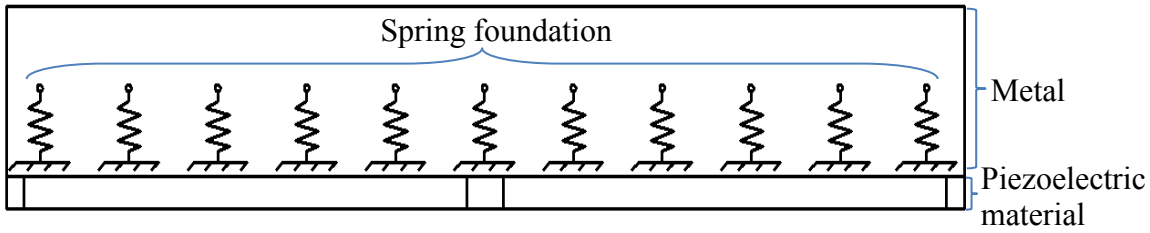

Figure 3.8: Spring foundation of the PTRUSM stator

In equation (3.41), F_k is the reaction force produced in the spring, k_x is the spring constant along the x axis, and u_{Pk} is the spring right end displacement along the x axis. The reaction force is directly proportional to the spring elongation. As shown in Fig. 3.9, the left end of the horizontal spring is fixed and the right end, denoted by u_{Pk}, is free to move in the x direction.

The linear spring element is incorporated into the static equilibrium equation (3.1). The force term F_{xP} in equation (3.1) is substituted by the spring force F_k. After substituting equation (3.41) into (3.1) one obtains:

$$P_1u_P - E_1u_E - W_1u_W - F_1u_F - R_1u_R - B_1(w_F - w_R) - B_2(w_{FE} - w_{RE}) + B_3(w_{FW} - w_{RW}) - B_4(w_E - w_W) - B_5(w_{FE} - w_{FW}) + B_6(w_{RE} - w_{RW}) = k_xu_{Pk} \quad (3.42)$$

The horizontal displacement of the current control volume is equal to the displacement of the spring node. Thus, one can write:

$$u_P = u_{Pk} \tag{3.43}$$

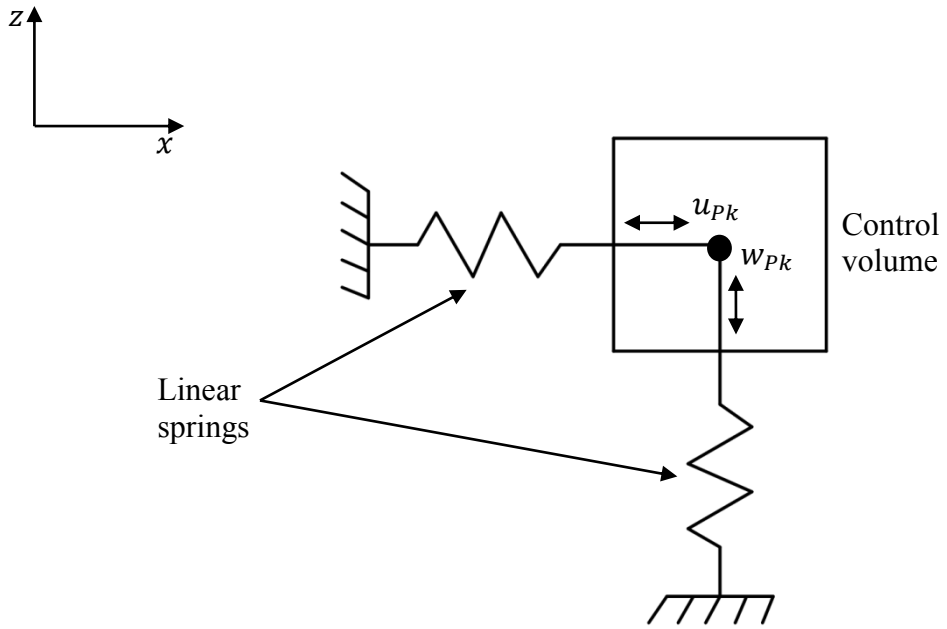

Figure 3.9: Current control volume supported by two linear springs

The u_{Pk} term of equation (3.42) is replaced with u_P**.** Therefore, the equation becomes:

$$P_1u_P - E_1u_E - W_1u_W - F_1u_F - R_1u_R - B_1(w_F - w_R) - B_2(w_{FE} - w_{RE}) + B_3(w_{FW} - w_{RW}) - B_4(w_E - w_W) - B_5(w_{FE} - w_{FW}) + B_6(w_{RE} - w_{RW}) = k_xu_P \tag{3.44}$$

After term manipulation one obtains:

$$(P_1 - k_x)u_P - E_1u_E - W_1u_W - F_1u_F - R_1u_R - B_1(w_F - w_R) - B_2(w_{FE} - w_{RE}) + B_3(w_{FW} - w_{RW}) - B_4(w_E - w_W) - B_5(w_{FE} - w_{FW}) + B_6(w_{RE} - w_{RW}) = 0 \tag{3.45}$$

Equation (3.2) is processed in a similar way and equation (3.46) is obtained:

$$(P_2 - k_z)w_P - E_2w_E - W_2w_W - F_2w_F - R_1w_R - B_7(u_F - u_R) - B_8(u_{FE} - u_{RE}) + B_9(u_{FW} - u_{RW}) - B_{10}(u_E - u_W) - B_{11}(u_{FE} - u_{FW}) + B_{12}(u_{RE} - u_{RW}) = 0 \tag{3.46}$$

3.1.2 Solution of the system of equations

The system of equations describing the static equilibrium of a 2D stator is composed by the equilibrium equations (3.1) and (3.2). These equations are defined at the center node P of every control volume forming the mesh. The u and w displacements in the x and z directions are the unknowns of the equilibrium equations. Besides that, the boundary equations (3.13), (3.14), (3.23), (3.24), (3.36), and (3.37) must be added at the *Front*, *Rear,* and internal boundary between metal and piezoelectric material. The periodic boundary conditions are used to connect the equilibrium equations (3.1) and (3.2) at the *East* and *West* boundaries. Equations (3.1) and (3.2) are simple algebraic equations.

The static equations have the matrix form:

$$AX + BU = F_P \tag{3.47}$$

where matrix A contains the coefficients of the current control volume and the internal adjacent control volumes. Matrix B contains the coefficients of the boundary control volumes adjacent to the current control volume. F_P and X are vectors that contain all the concentrated forces and the average unknown displacements u and w at the centers of the control volumes, respectively. For instance, the vector X contains two unknowns for a control volume as follows:

$$X = \begin{bmatrix} u_P \\ w_P \end{bmatrix} \tag{3.48}$$

In equation (3.47) U is a vector that contains the average unknown u and w displacements at the boundary faces of the boundary control volumes. For instance, the vector contains two unknowns (u, w displacements) for the *Front*, *Rear*, and internal boundaries control volumes as follows:

$$U = \begin{bmatrix} u_B \\ w_B \end{bmatrix} \tag{3.49}$$

The boundary equation (3.23) contains both, the electrical and mechanical boundary conditions. Therefore, one can take this equation as a reference to define the general boundary control volume equation of the PTRUSM stator. The general boundary equation is defined as follows:

$$U = CX + DU + F_E + F_M \tag{3.50}$$

In equation (3.50) matrices C and D contain the coefficients of the internal displacements and the coefficients of the boundary displacements of the boundary control volumes, respectively. F_E and F_M are vectors that contain the forces produced by the electric field and the mechanical forces applied at the current control volume boundary, respectively.

It is required to express equation (3.50) as a function of the boundary displacement *U*. After matrices manipulation one obtains:

$$U = CX(I - D)^{-1} + F_E(I - D)^{-1} + F_M(I - D)^{-1} \tag{3.51}$$

By substituting equation (3.51) into (3.47) equation (3.52) is obtained:

$$AX + B[CX(I - D)^{-1} + F_E(I - D)^{-1} + F_M(I - D)^{-1}] = F_P \tag{3.52}$$

After matrices manipulation in equation (3.52) one obtains:

$$[A + BC(I - D)^{-1}]X = -BF_E(I - D)^{-1} - F_M(I - D)^{-1} + F_P \tag{3.53}$$

The following notations are used in equation (3.53):

$$A_1 = [A + BC(I - D)^{-1}] \tag{3.54}$$

$$F_T = -BF_E(I - D)^{-1} - F_M(I - D)^{-1} + F_P \tag{3.55}$$

By substituting notations (3.54) and (3.55) into equation (3.53) one obtains equation (3.56):

$$A_1X = F_T \tag{3.56}$$

The last equation is the equilibrium equation of the PTRUSM stator. In (3.56) A_1 is the global stiffness matrix, X is a vector that contains the unknown displacements, and F_T is a vector that contains all the forces applied to the PTRUSM stator. The forcing vector contains the mechanical boundary

forces, the forces produced by the action of the electric field, and the forces applied at the center of the control volumes.

From equation (3.56) one can calculate the displacements in the vector X as:

$$X = A_1^{-1} F_T \tag{3.57}$$

3.2 Numerical results. Static PTRUSM stator simulation

In this section the discrete system of equations is used to model one stator wavelength. The goal is to determine the PTRUSM displacements under the action of a DC voltage. A stator wavelength is discretized and a constant electric field is applied at the piezoelectric material boundaries. The electric field produces a distributed force along the piezoelectric material, and the bridge produces the reaction forces. All the system forces are balanced; that means the stator is a system in equilibrium.

The USR60 is taken as an example to model the stator. The diameter of the USR60 is 0.06 m and the stator width is 0.0075 m. In order to obtain a planar model of the stator wavelength, one needs to calculate the stator circumference at the middle of the stator ring. The stator circumference is calculated at the middle to obtain its average value. Then, because the USR60 stator contains nine wavelengths, one can divide the obtained circumference to nine. Thus, the calculated USR60 stator wavelength is 0.01832 m.

As shown in Fig. 3.10, the piezoelectric material forming the stator wavelength is divided in active and passive regions. Thus, the stator is composed of two active regions and three passive regions. The active regions are polarized, one with positive and the other with negative polarization. The passive regions have no polarization.

The dimensions used to model the stator wavelength are:

$$L_{p1} = 0.00035 \text{ m}$$

$$L_a = 0.00846 \text{ m}$$

$$L_{p2} = 0.0007 \text{ m}$$

$$h_p = 0.0005 \text{ m}$$

$$h_m = 0.00255 \text{ m}$$

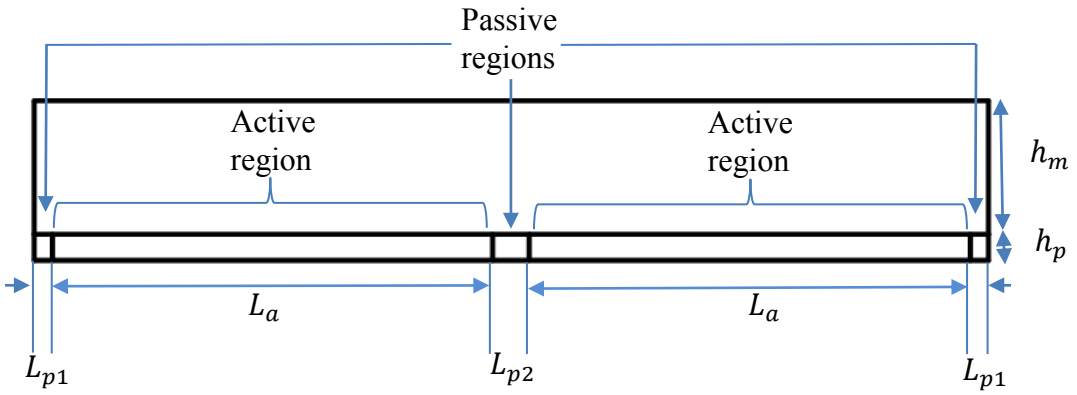

Figure 3.10: USR60 wavelength dimensions

Fig. 3.11 shows the final static stator model for one stator wavelength λ. Copper and lead zirconate titanate are chosen to model the metal and piezoelectric material, respectively. The elasticity matrices of copper and lead zirconate titanate are presented in Appendix B. A DC voltage of 100 V is applied to the piezoelectric material. The total spring stiffness k_{totx} and k_{totz} used to model the bridge stiffness along the x and z axes are 7.56 E^6 N/m and 1 E^8 N/m, respectively. In order to obtain these spring foundation values, the static model of Fig. 3.11 was implemented in COMSOL Multiphysics, the total spring constants along the x and z axes were obtained with trial and error method. These are the minimum spring values that allow convergence in the commercial software.

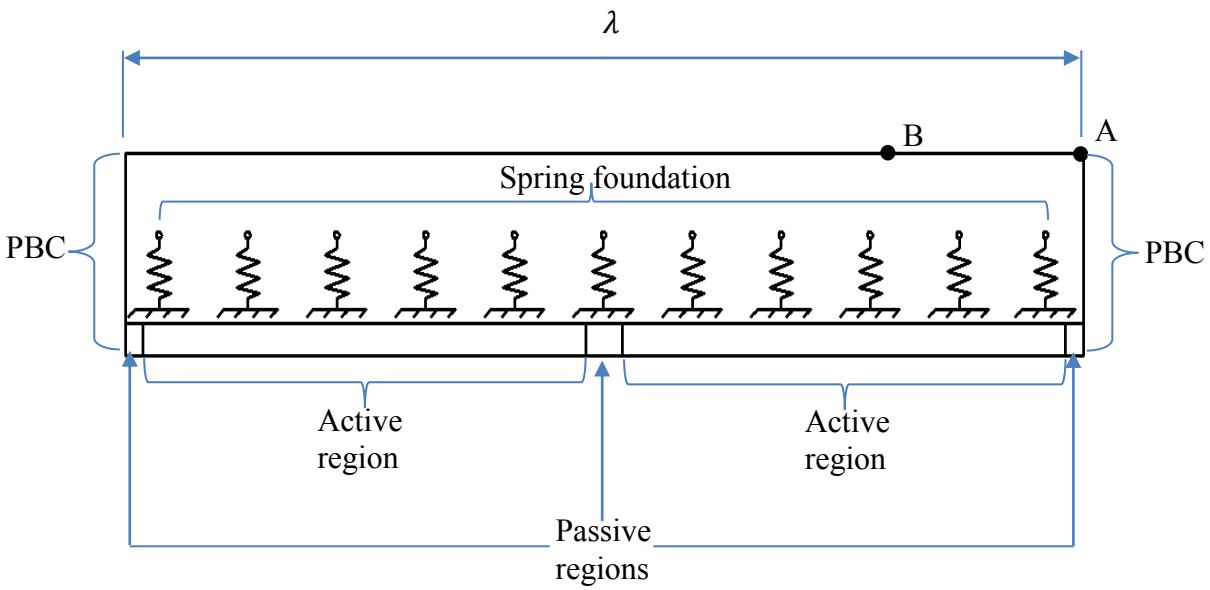

Figure 3.11: Static 2D stator modeled using the FVM

A convergence study of the final static stator model was conducted. The results were compared versus the commercial software COMSOL Multiphysics. The results are shown in Table 3.1 and Table 3.2.

The convergence study starts with a mesh of 300 control volumes. The stator is divided into 50 control volumes along the x axis and 6 control volumes along the z axis (3 for the metal and 3 for the piezoelectric material). This is the minimum possible number of control volumes because with this configuration one control volume is used to mesh the corner passive regions, and at least three control volumes are required to vertically mesh the metal because the spring foundation needs to be in the center of the metal beam. With this mesh, the passive regions L_{p1} are horizontally and vertically divided with just one control volume.

Table 3.1: Convergence study of the *u* displacement

2D system of equations using the FVM				
Number of control volumes n_z*n_x in the FVM model	Degrees of freedom	Average control volume area [mm^2]	Displacement *u* at A [μm]	Displacement deviation [%]
6*50=300	600	1.8625 E^{-4}	0.02253215	-13.76
8*50=400	800	1.3969 E^{-4}	0.02280097	-12.73
8*100=800	1600	0.6984 E^{-4}	0.02393860	-8.38
8*200=1600	3200	0.3492 E^{-4}	0.02433295	-6.87
17*200=3400	6800	0.1643 E^{-4}	0.02482787	-4.98
17*300=19800	39600	0.0282 E^{-4}	0.02493181	-4.58
COMSOL Multiphysics				
Number of elements in COMSOL Multiphysics	Degrees of freedom	Average element area [mm^2]	Displacement u at A [μm]	Displacement deviation [%]
443039	5396990	0.000126 E^{-4}	0.0261293	0.0

Table 3.1 shows the results of the convergence study showing the *u* displacement in the *x* direction at point A of Fig. 3.11 with the implemented stator model using the FVM. The reference value is taken to be the best approximated value using COMSOL Multiphysics simulations. The reference *u* displacement of point A has a value equal to 0.0261293 μm calculated with 5396990 degrees of freedom in COMSOL.

Table 3.2 shows the results of the convergence study showing the *w* displacement in the *z* direction at point B of Fig. 3.11 with the implemented stator model using the FVM. The reference value is taken to be the best approximated value using COMSOL Multiphysics simulations. The reference *w* displacement of point B has a value equal to 0.0849026 μm calculated with 5396990 degrees of freedom in COMSOL.

Table 3.2: Convergence study of the *w* displacement

2D system of equations based on the FVM				
Number of control volumes $n_x * n_z$ in the FVM model	Degrees of freedom	Average control volume area $[mm^2]$	Displacement *w* at A $[\mu m]$	Displacement deviation [%]
6*50=300	600	1.8625 E^{-4}	0.0775977	-9.41
8*50=400	800	1.3969 E^{-4}	0.0792745	-6.62
8*100=800	1600	0.6984 E^{-4}	0.0805546	-5.12
8*200=1600	3200	0.3492 E^{-4}	0.0810050	-4.59
17*200=3400	6800	0.1643 E^{-4}	0.0825693	-2.74
17*300=19800	39600	0.0282 E^{-4}	0.0826846	-2.61
COMSOL Multiphysics				
Number of elements in COMSOL Multiphysics	Degrees of freedom	Average element area $[mm^2]$	Displacement *u* at A $[\mu m]$	Displacement deviation [%]
443039	5396990	0.000126 E^{-4}	0.0849026	0.0

The FVM stator model was compared versus a very similar stator model using commercial FEM software. The main difference between both models is that the FEM model calculates the electric field over the piezoelectric material, and the FVM model for simplicity considers the electric field inside the piezoelectric material constant along the *z* direction. The convergence study shows a displacement deviation in the *x* and *z* direction of just -4.58 % and -2.61%, respectively, with 19800 control volumes using the simplified FVM stator model. It can be observed from the convergence study that the implemented model with the FVM discretization has a faster convergence rate.

Chapter 4: Dynamic modeling of the PTRUSM stator

In order to develop a complete model for the PTRUSM, one needs to accurately model the stator traveling wave. Therefore, in this chapter is developed a dynamic numerical model for the PTRUSM stator traveling wave. The dynamic model presented here provides the stator surface velocities required to obtain the rotor velocity.

As mentioned before, the horizontal movement of the stator surface points is the one responsible for moving the PTRUSM rotor. Therefore, an accurate model of the stator motion is mandatory.

4.1 Dynamic PTRUSM stator model

As mentioned in Appendix A, the governing equation describing the motion of an elastic body is Cauchy's first law of motion. Thus, the 2D motion equations (A.58, A.71) derived in Appendix A are used here to model the stator movement. The semidiscrete equations of motion are:

$$m_P \frac{d^2 u_P}{dt^2} + P_1 u_P - E_1 u_E - W_1 u_W - F_1 u_F - R_1 u_R - B_1(w_F - w_R) - B_2(w_{FE} - w_{RE}) + B_3(w_{FW} - w_{RW}) - B_4(w_E - w_W) - B_5(w_{FE} - w_{FW}) + B_6(w_{RE} - w_{RW}) = F_{xP} \tag{4.1}$$

$$m_P \frac{d^2 w_P}{dt^2} + P_2 w_P - E_2 w_E - W_2 w_W - F_2 w_F - R_1 w_R - B_7(u_F - u_R) - B_8(u_{FE} - u_{RE}) + B_9(u_{FW} - u_{RW}) - B_{10}(u_E - u_W) - B_{11}(u_{FE} - u_{FW}) + B_{12}(u_{RE} - u_{RW}) = F_{zP} \tag{4.2}$$

Equation (4.1) describes the u motion at the center of the current control volume along the x axis. Equation (4.2) describes the w motion at the center of the current control volume along the z axis. The boundary equations (3.13), (3.14), (3.23), (3.24), (3.36), and (3.37), showed in Chapter 3, are

valid to perform the dynamic analysis of the PTRUSM stator. The difference is that the electric field is now time dependent.

As shown in [44], the semidiscrete governing equation used to model the motion of a continuum has the form:

$$M\ddot{X} + C\dot{X} + KX = F \tag{4.3}$$

In (4.3) M is a matrix that contains the masses of the control volumes forming the stator. C and K are matrices that represent the viscous damping and stiffness of the stator, respectively. $\ddot{X}$, $\dot{X}$, and X are vectors that contain the accelerations, velocities, and displacements of every control volume in the discretized stator. It is important to mention that accelerations, velocities, and displacements are evaluated at the centers of the control volumes.

The model for the stiffness matrix K is the same one used to solve the static problem. In order to model the stator motion, one needs to provide a model for the stator mass M and stator damping C. The mass model is treated first.

One needs to include the contribution of the mass into the dynamic model, because it refers to the inertial forces produced in the stator. In the literature there are available two kinds of mass matrix models for discrete systems: consistent and lumped-mass matrix, (refer to [45]).

Because the stator is discretized with control volumes composed of just one node located at the center of it, lumped-mass matrix is the only option to model the stator masses. With a lumped-mass model one assumes that the mass of the control volume is concentrated at its center. Therefore, the motion of each control volume is modeled as a rigid body because the mass is concentrated at its center. The rest of the control volume is considered massless. The mass matrix M is a diagonal matrix containing the concentrated masses of the control volumes.

The mass of a body is defined as the mass density of the body times its volume.

$$m = \rho V \tag{4.4}$$

In (4.4) m, ρ, V, are the mass, mass density, and volume, respectively. In order to obtain the mass matrix M, one needs to calculate the mass of every control volume in the stator mesh. The mass of a current control volume is:

$$m = \rho \Delta x \Delta z y_w \tag{4.5}$$

All the parameters contained in equation (4.5) are defined in Appendix A.

Now, one needs to define the model for the PTRUSM stator damping. The viscous damping matrix C is obtained with the Rayleigh damping model. With this method, the damping is defined as proportional to the stiffness K and mass M matrices. According to [46], the damping equation is:

$$C = c_K K + c_M M \tag{4.6}$$

In (4.6), c_K and c_M are constants. These constants are defined by the analyst; experiments can be performed to help one to define these parameters. As explained in [46], these constants are real numbers. The units for c_K and c_M are seconds s and units per seconds $1/s$, respectively.

4.2 Solution of the system of equations

In order to solve (4.3), one needs to define initial conditions. The initial displacements and velocities of every control volume forming the stator mesh must be defined. These equations are:

$$X(0) = X_0 \tag{4.7}$$

$$\dot{X}(0) = \dot{X}_0 \tag{4.8}$$

In (4.7) and (4.8) $X(0)$ and $\dot{X}(0)$ are the displacements and velocities vectors evaluated at time zero. X_0 and $\dot{X}_0$ are the values assigned to these vectors at time zero. Commonly, the initial displacements and velocities are defined as zero. With the assumption of initial displacements and velocities equal to zero, the initial accelerations can be obtained as follows:

$$\ddot{X}(0) = M^{-1} F(0) \tag{4.9}$$

In order to solve the motion equation (4.3), one can use a direct integration method. The direct integration method is classified as explicit and implicit.

Newmark [47] proposed an implicit algorithm that has been widely used in the FEM models to solve the semidiscrete motion equation (4.3). The displacement X, velocity $\dot{X}$, and acceleration $\ddot{X}$ are assumed to be known at the time step t_n, but these parameters are unknown at the time step t_{n+1}. The solution of the motion equation (4.3) is approximated using the following algebraic equations:

$$\dot{X}_{n+1} = \dot{X}_n + \Delta t(1-\gamma)\ddot{X}_n + \Delta t\gamma\ddot{X}_{n+1} \tag{4.10}$$

$$X_{n+1} = X_n + \Delta t\dot{X}_n + \frac{\Delta t^2}{2}(1-2\beta)\ddot{X}_n + \Delta t^2\beta\ddot{X}_{n+1} \tag{4.11}$$

Equations (4.10) and (4.11) are the approximation of the velocities and displacements at the time step t_{n+1}. Using these equations, the acceleration $\ddot{X}_{n+1}$ at time step t_{n+1} is obtained first. After that, one can obtain the velocities $\dot{X}_{n+1}$ and dispalcements X_{n+1} at time step t_{n+1}.

γ and β in equations (4.10) and (4.11) are real values smaller than one. These parameters specify what percentage of the acceleration is considered to compute the velocities and displacements at the end of the current time step.

According to [44], a value of β of one quarter means a constant acceleration during the time step. The acceleration is the average value of the initial and final accelerations in the current time step. γ must be equal to one half (refer to [47]). If γ is different than one half, a damping will be introduced. Thus, the values of β and γ are:

$$\beta = \frac{1}{4} \tag{4.12}$$

$$\gamma = \frac{1}{2} \tag{4.13}$$

The Newmark method, when used with these values of β and γ, is called the average acceleration or trapezoidal rule method. The method is unconditionally stable when used with these β and γ values, (refer to [44]).

Alternatively to equations (4.10) and (4.11), one can solve the system of algebraic equations with the displacements X_{n+1} as primary unknown, (refer to [48]). The solution of the semidiscrete motion equation (4.3) is approximated alternatively using the following algebraic equations:

$$\ddot{X}_{n+1} = \frac{1}{\beta\Delta t^2}(X_{n+1} - X_n) - \frac{1}{\beta\Delta t}\dot{X}_n - \left(1 - \frac{1}{2\beta}\right)\ddot{X}_n \tag{4.14}$$

$$\dot{X}_{n+1} = \frac{\gamma}{\beta\Delta t}(X_{n+1} - X_n) - \left(\frac{\gamma}{\beta} - 1\right)\dot{X}_n - \left(\frac{\gamma}{2\beta} - 1\right)\Delta t\ddot{X}_n \tag{4.15}$$

Therefore, equation (4.3) can be expressed in terms of the approximate algebraic equations as follows:

$$M\ddot{X}_{n+1} + C\dot{X}_{n+1} + KX_{n+1} = F_{n+1} \tag{4.16}$$

After substitution of equations (4.14) and (4.15) into (4.16) one obtains:

$$M\left[\frac{1}{\beta\Delta t^2}(X_{n+1} - X_n) - \frac{1}{\beta\Delta t}\dot{X}_n - \left(1 - \frac{1}{2\beta}\right)\ddot{X}_n\right]$$

$$+ C\left[\frac{\gamma}{\beta\Delta t}(X_{n+1} - X_n) - \left(\frac{\gamma}{\beta} - 1\right)\dot{X}_n - \left(\frac{\gamma}{2\beta} - 1\right)\Delta t\ddot{X}_n\right] + KX_{n+1} = F_{n+1} \tag{4.17}$$

After terms manipulation, equation (4.17) becomes:

$$\left[\frac{1}{\beta\Delta t^2}M + \frac{\gamma}{\beta\Delta t}C + K\right]X_{n+1}$$

$$= F_{n+1} + M\left[\frac{X_n}{\beta\Delta t^2} + \frac{\dot{X}_n}{\beta\Delta t} + \left(1 - \frac{1}{2\beta}\right)\ddot{X}_n\right]$$

$$+C\left[\frac{\gamma X_n}{\beta\Delta t} + \left(\frac{\gamma}{\beta} - 1\right)\dot{X}_n + \left(\frac{\gamma}{2\beta} - 1\right)\Delta t\ddot{X}_n\right] \tag{4.18}$$

The following notations are used in equation (4.18):

$$K_T = \left[\frac{1}{\beta \Delta t^2} M + \frac{\gamma}{\beta \Delta t} C + K\right] \tag{4.19}$$

$$F_T = F_{n+1} + M\left[\frac{X_n}{\beta \Delta t^2} + \frac{\dot{X}_n}{\beta \Delta t} + \left(1 - \frac{1}{2\beta}\right)\ddot{X}_n\right]$$

$$+C\left[\frac{\gamma X_n}{\beta \Delta t} + \left(\frac{\gamma}{\beta} - 1\right)\dot{X}_n + \left(\frac{\gamma}{2\beta} - 1\right)\Delta t \ddot{X}_n\right] \tag{4.20}$$

After substitution of equations (4.19) and (4.20) into (4.18) one obtains:

$$X_{n+1} = K_T^{-1} F_T \tag{4.21}$$

The solution of equation (4.21) is the numerical solution of the semidiscrete motion equation (4.3).

The steps used to perform the dynamic analysis of the PTRUSM stator are:

1. Define the stiffness *K*, mass *M,* and viscous damping *C* matrices of the semidiscrete motion equation (4.3).
2. Set the initial displacements $X(0)$ and velocities $\dot{X}(0)$ of each control volume in the stator mesh to zero.
3. Compute the initial accelerations $\ddot{X}(0)$ using equation (4.9).
4. Compute the matrix K_T. All the elements in this matrix are constant.
5. Compute the force vector F_{n+1}. This vector contains time dependent elements.
6. Compute the matrix F_T.
7. Solve for the displacements X_{n+1} at the end of the current time step using equation (4.21).
8. Solve for the accelerations $\ddot{X}_{n+1}$ and velocities $\dot{X}_{n+1}$ at the end of the current time step using equations (4.14) and (4.15) respectively.
9. Increase the time step to t_{n+1}. Where $t_{n+1} = t_n + \Delta t$.
10. Return to step 5.

4.3 Numerical results. Time domain PTRUSM stator simulation

In order to generate a PTRUSM stator traveling wave, one needs to have at least three wavelengths. Two wavelengths are used to generate two standing waves. These two standing waves represent the two phases of the PTRUSM. The phases are excited applying alternate voltages with a phase shift of 90 degrees. The third wavelength is required to separate the two standing waves. The third wavelength must be distributed into three parts. One quarter of wavelength is used to separate the two standing waves, and the rest of it is added at the *West* and *East* sides of the beam. Fig. 4.1 shows the three wavelengths.

One needs to choose the appropriate number of control volumes to discretize the PTRUSM stator. Newmark [47] reports that the number of lumped masses is inversely proportional to the permissible time interval of the time domain analysis. Because of that, the number of control volumes should be as small as possible. Besides that, the computational effort should be kept as small as possible. The static analysis of the PTRUSM stator shows an error of less than nine percent when divided into 800 control volumes. Therefore, the mesh defined to perform the dynamic analysis is composed of 2400 control volumes. The PTRUSM stator is horizontally divided into 300 control volumes, and vertically divided into 8 control volumes. The metal is vertically divided into 5 control volumes, and the piezoelectric material is vertically divided into 3 control volumes.

Before proceeding we need to obtain the operating excitation frequency of the 2D PTRUSM stator model. This is the eigenfrequency of the stator. COMSOL Multiphysics is used to perform an eigenfrequency analysis of the 2D stator model. The energy dissipation of the USM60 stator is not provided by the manufacturer, due to that, loses are not considered in the eigenfrequency study. The obtained eigenfrequency is 40538 Hz. Fig. 4.2 shows a picture of the stator deformation when excited with the obtained eigenfrequency.

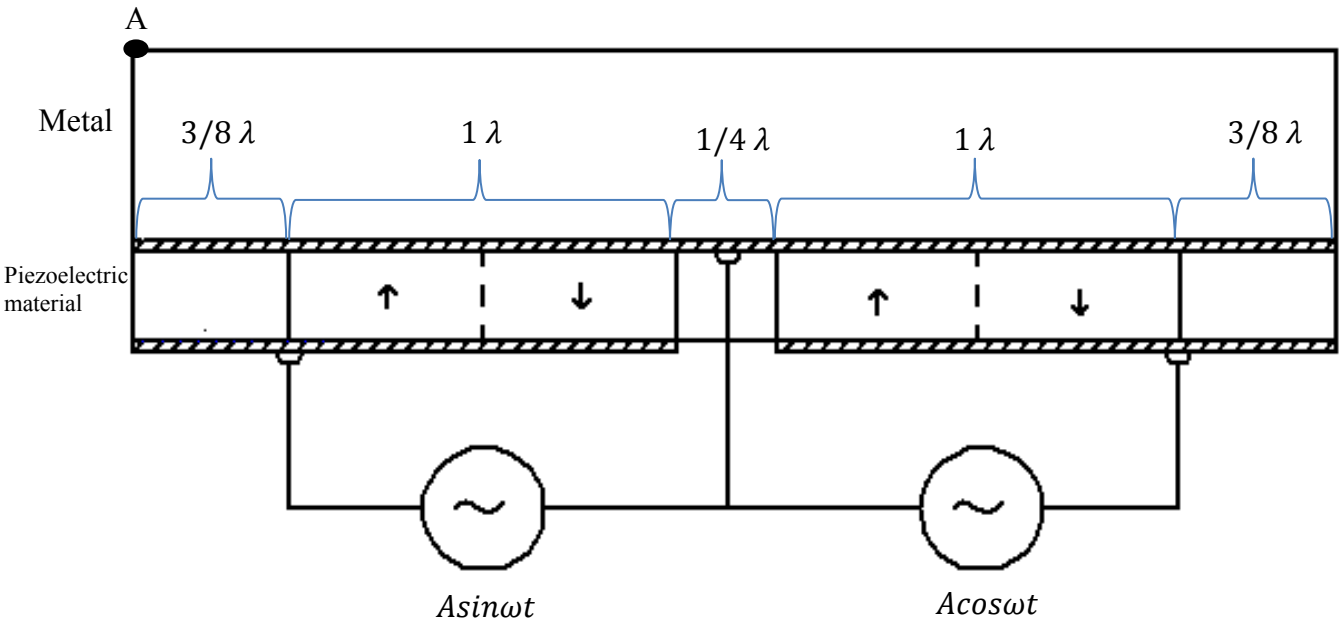

Figure 4.1: Dynamic PTRUSM stator model

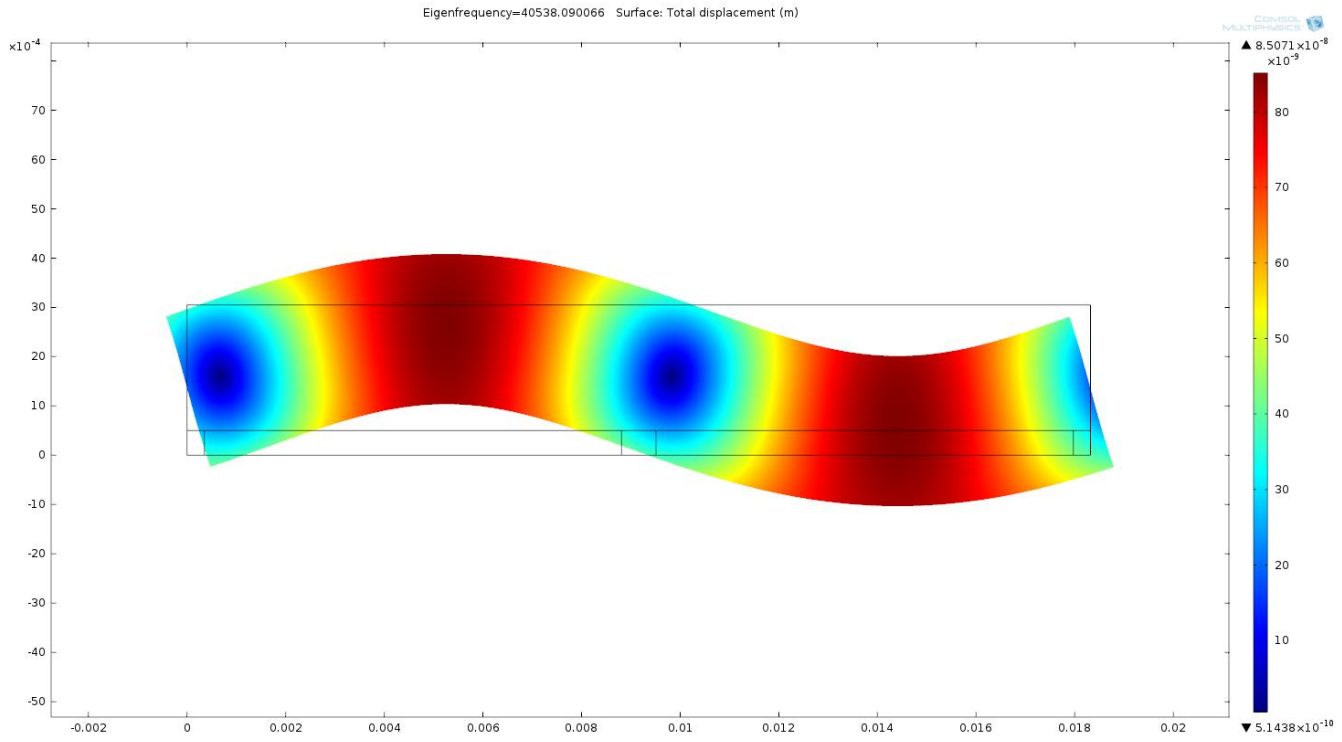

Figure 4.2: Eigenfrequency analysis with COMSOL Multiphysics

The driving voltage used to excite phases A and B is 130 Vrms. Phase A is excited with $\sqrt{(2)}130sin(40538\text{t})\ V$ and phase B is excited with $\sqrt{(2)}130cos40538\text{t}$ V. The values of the viscous damping constants c_K and c_M used during the time domain simulation are 39.58 E-6 and 100 E-12, respectively. These values were obtained with the trial and error method. It was observed that 39.58 E-6 is the minimum permissible value of c_K to avoid oscillations. It was observed too that the contribution of c_M is virtually zero; because of that, a small value was used to do the time domain analysis. The dynamic PTRUSM stator model is used to simulate the stator traveling wave. The time domain simulation is limited to an interval of 30 E-6 s. It is approximately the time interval found for a point located at the stator surface to complete a cycle of the elliptical motion.

Giles [49] provides a rule to choose the time step length for a trapezoidal integration. This rule is $\Delta t\omega_0 < 0.3$, it corresponds to 20 time steps per period. The increment of time used during the dynamic analysis has a value of 0.5 E-6 s, and it corresponds to around 50 time steps per period. The increment of time is kept constant during the entire analysis. The analysis starts at time 0 and finishes at time 30 E-6 s. At time 0 the stator is considered to be at the rest position. Figs. 4.3 to 4.8 show the stator surface displacements along the z axis at times 5 E-6 s, 10 E-6 s, 15 E-6 s, 20 E-6 s, 25 E-6 s and 30 E-6 s. These figures show the stator traveling wave. A dot on top of the first wave crest was added to show the direction of the traveling wave. One can observe that the traveling wave moves from left to right.

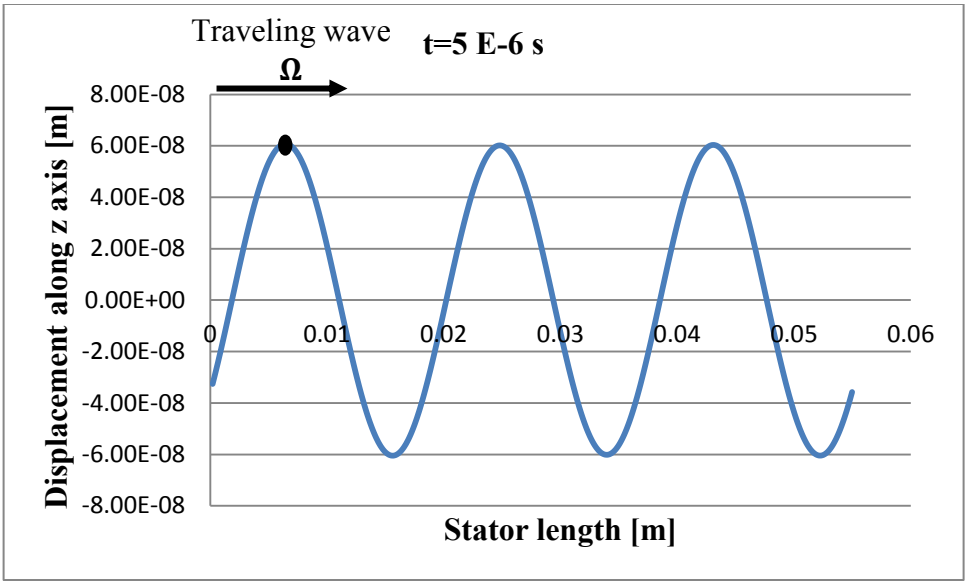

Figure 4.3: Stator surface vertical displacement at time 5 E-6 s

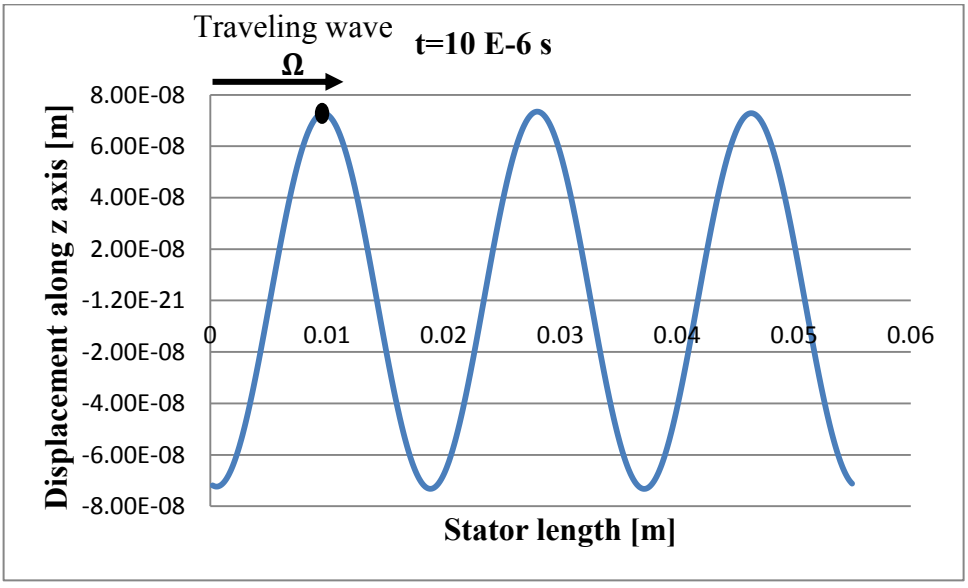

Figure 4.4: Stator surface vertical displacement at time 10 E-6 s

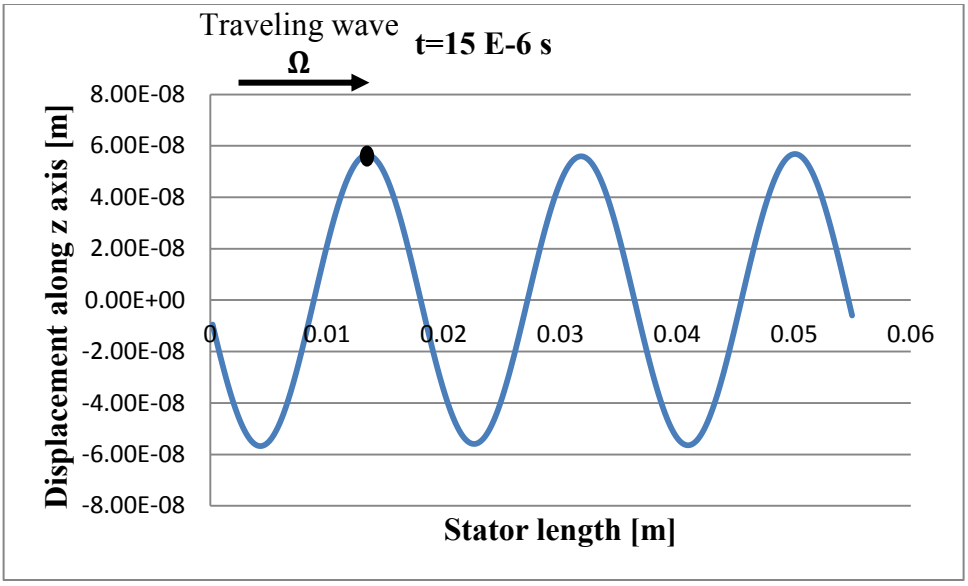

Figure 4.5: Stator surface vertical displacement at time 15 E-6 s

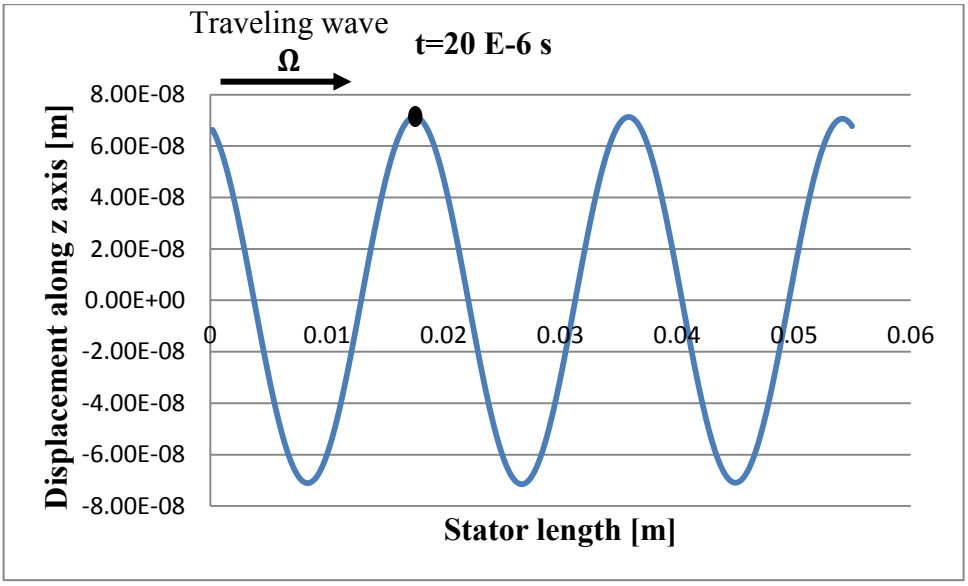

Figure 4.6: Stator surface vertical displacement at time 20 E-6 s

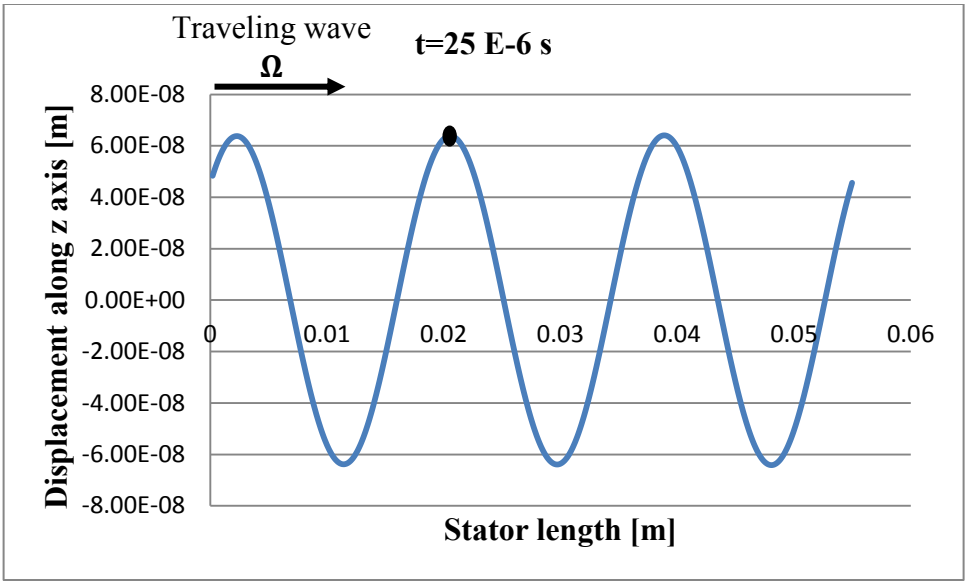

Figure 4.7: Stator surface vertical displacement at time 25 E-6 s

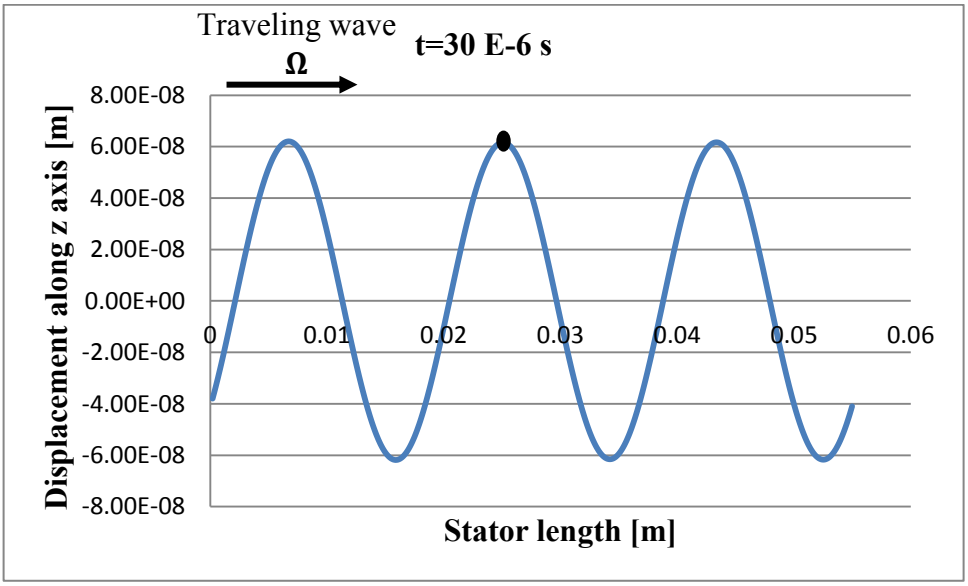

Figure 4.8: Stator surface vertical displacement at time 30 E-6 s

The obtained average value of the maximum displacement of the stator traveling wave along the z axis during the time interval is 6.5271 E-8 m.

As mentioned before, the elliptical motion of the PTRUSM stator is the one responsible for moving the rotor. Because of that, one needs to have both: the stator surface vertical and horizontal displacements. Fig. 4.9 shows the elliptical motion at point A of Fig. 4.1 during the time interval.

The horizontal velocity of the traveling wave at the end of the interval is shown in Fig. 4.10.

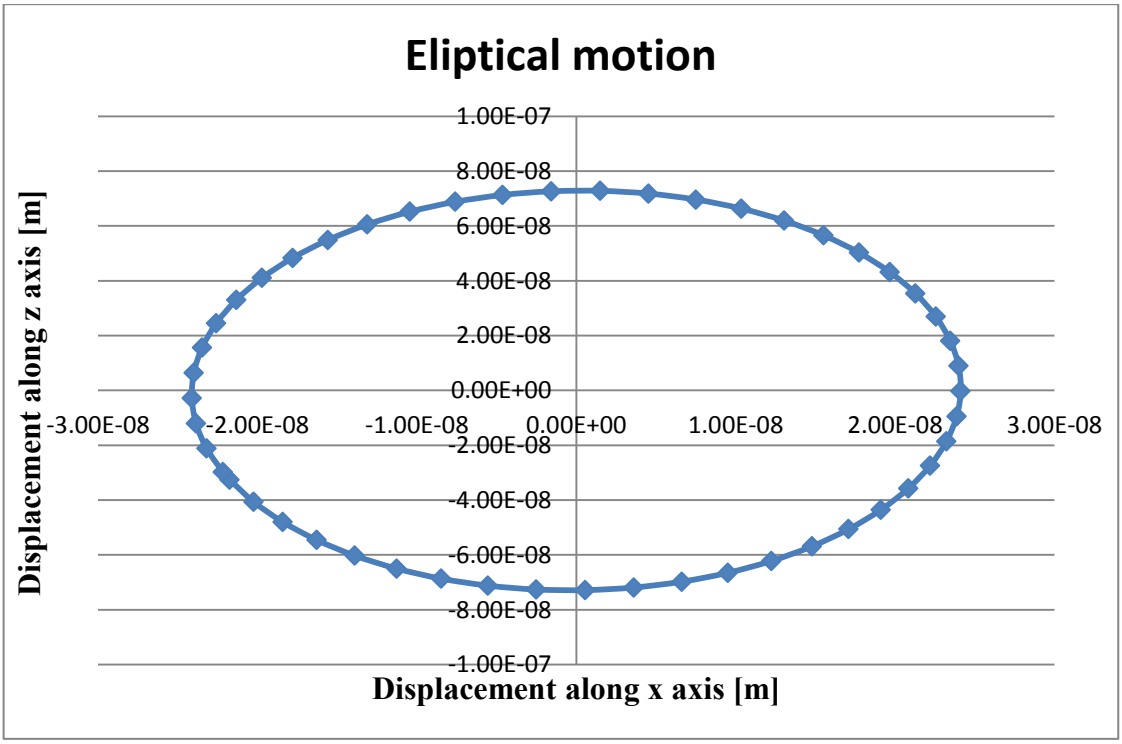

Figure 4.9: Elliptical motion produced at the stator surface

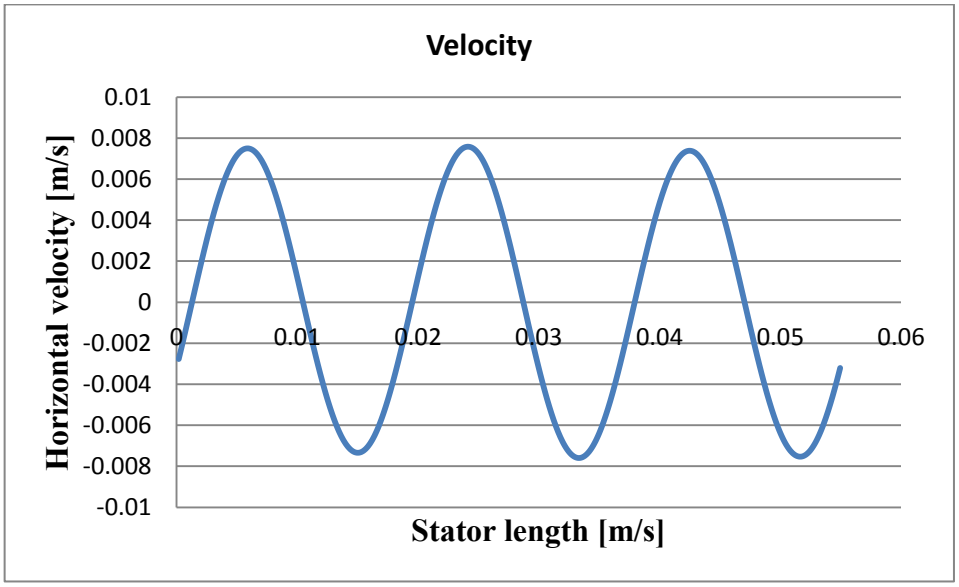

Figure 4.10: Horizontal velocity of the stator traveling wave

Chapter 5: Contact model of the PTRUSM

As mentioned in Chapter 2, a moving reference coordinate system on top of the stator traveling wave was introduced. With the moving coordinate system, the contact between stator and rotor becomes a time independent problem, (refer to [4]).

In order to compute the normal and tangential force distribution over the contact zone, it is assumed to have independency of normal force distribution with respect to tangential force distribution. The assumption was previously used in [15, 17]. This allows one to solve first for normal force distribution problem, then, tangential forces can be computed as a function of the normal ones. Nevertheless, it was observed that the higher the driving load of the USR60 is, the lower the amplitude of the traveling wave. Because of that, a method to model this phenomenon of the PTRUSM was proposed in this chapter. The normal contact problem is analyzed in the next section.

5.1 Normal contact problem

Due to the absence of adhesion between the stator and contact layer, unilateral normal contact is used to describe the PTRUSM stator-rotor contact. As shown in Fig. 5.1, three contact zones can be used to model the PTRUSM stator-rotor contact:

$$g = 0 \qquad F_N = 0 \tag{5.1}$$

$$g > 0 \qquad F_N = 0 \tag{5.2}$$

$$g < 0 \qquad F_N < 0 \tag{5.3}$$

where g refers to the gap between the stator and contact layer, and F_N refers to the normal force produced over the contact zone. A gap equal to zero is the theoretical point where both body surfaces touch each other but no penetration is present in the materials. The normal force is zero when having a gap equal to zero. A gap bigger than zero refers to the non-contact zone. The third zone models the rotor penetration. In this zone the normal contact force will be smaller than zero.

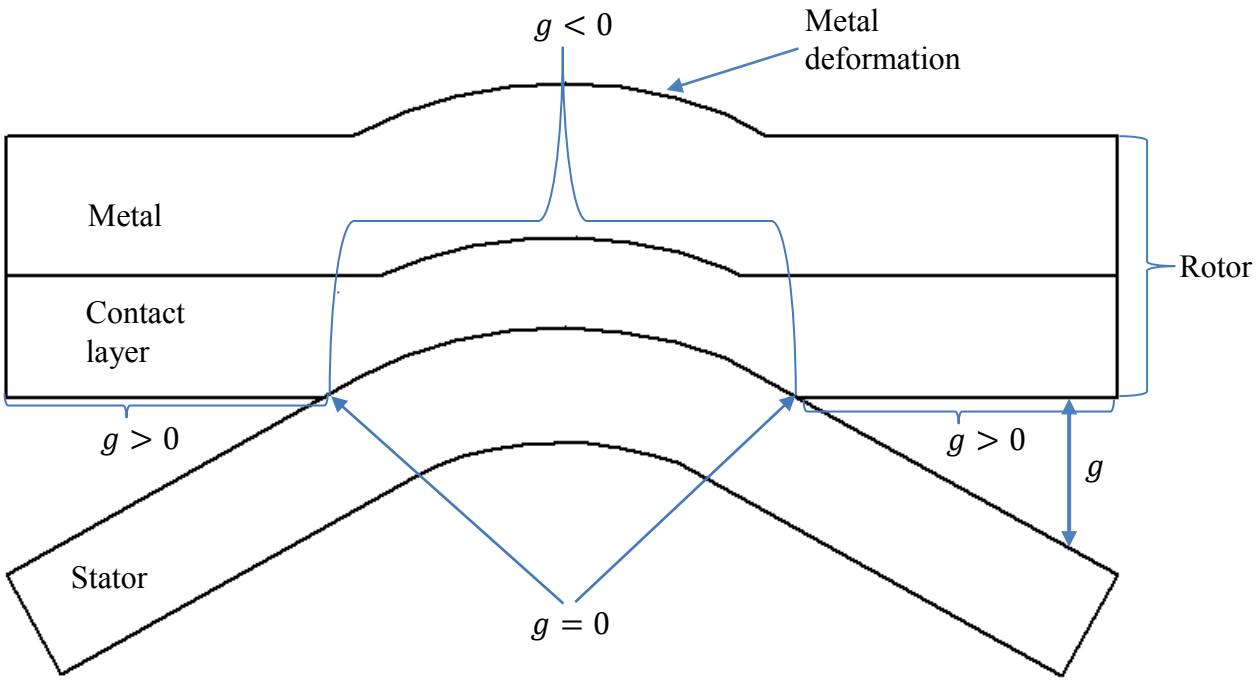

Figure 5.1: Contact zones between stator and rotor

As shown in Fig. 5.1, the PTRUSM rotor (metal) and contact layer suffer a vertical deformation when in contact with the stator traveling wave. Therefore, the rotor (metal) and contact layer are both modeled as a layer of parallel spring elements attached to a rigid body. That means the elasticity of both, metal and contact layer is considered into the model. Fig. 5.2 shows the PTRUSM rotor model. The PTRUSM rotor (metal) was previously modeled with linear springs in [7].

The finite normal force generated in the contact surface is modeled with the formula used in the penalty-based contact formulation, (refer to [50, 51]). This formula is:

$$F_N(g_n) = g_n\, k_n \tag{5.4}$$

In equation (5.4) k_n is the imaginary spring stiffness. This term expresses the relationship between the normal force and the penetration of the rotor along the vertical direction. g_n is the

penetration of the imaginary spring (rotor). The spring normal force is assumed to be linearly dependent of the rotor and contact layer penetration.

Even if the stator is modeled as a linear elastic material, and the rotor is modeled as a linear spring, the model of the PTRUSM contact is a non-linear problem because it is described with inequalities. The reason is because the contact zone of the stator and rotor surfaces is not a priori known; reference [52] explains this characteristic of contact problems. Therefore, we developed an algorithm to solve the normal contact problem. In [53, 54] contact algorithms used in FEM are presented.

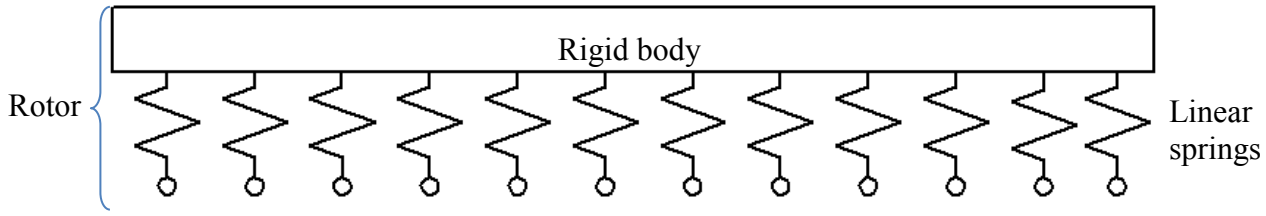

Figure 5.2: PTRUSM rotor model

5.1.1 Normal contact algorithm

In this section we present the method developed to model the contact between stator and rotor. The analysis is static. Therefore, this section is limited to the analysis of the normal forces produced in the PTRUSM contact interface.

The analysis of the normal forces produced at the stator-rotor contact interface is handled as an equilibrium problem. An equilibrium problem is composed of two stages: the first stage is the instant when forces are applied to the body before deformation, and the second stage is the instant when the deformation of the body subject to forces stops. In order to find the PTRUSM static contact equilibrium, one needs to develop an algorithm.

The algorithm developed here starts with the assumption of no deformation of the stator and rotor when the motor is not powered. Fig. 5.3 shows the stator-rotor contact interface when the motor is not powered. Suppose that one applies an excitation voltage to the PTRUSM stator. At this instant, the stator-rotor deformation begins. The normal contact algorithm is started to find the static equilibrium of the stator-rotor contact interface. The algorithm ends when the static equilibrium of the stator-rotor contact interface is found.

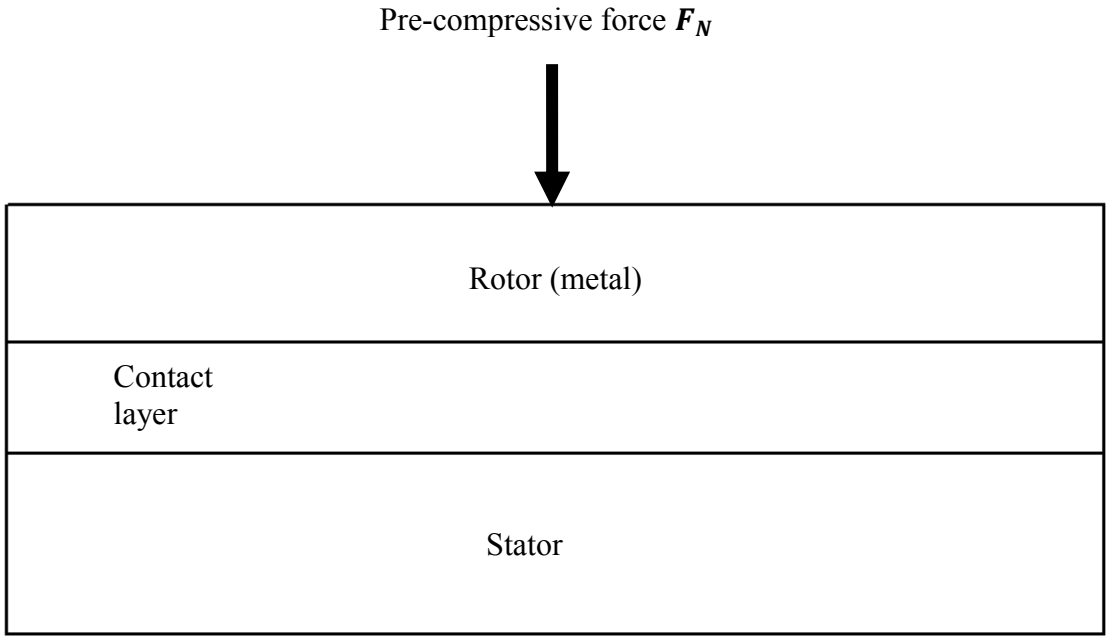

Figure 5.3: PTRUSM stator-rotor contact interface when the motor is not powered

The steps of the algorithm used to statically analyze the PTRUSM stator-rotor contact interface are:

1. **Discretize the PTRUSM stator**. The procedure to discretize the stator is presented in Chapter 3. Fig. 5.4 shows a discretized stator.

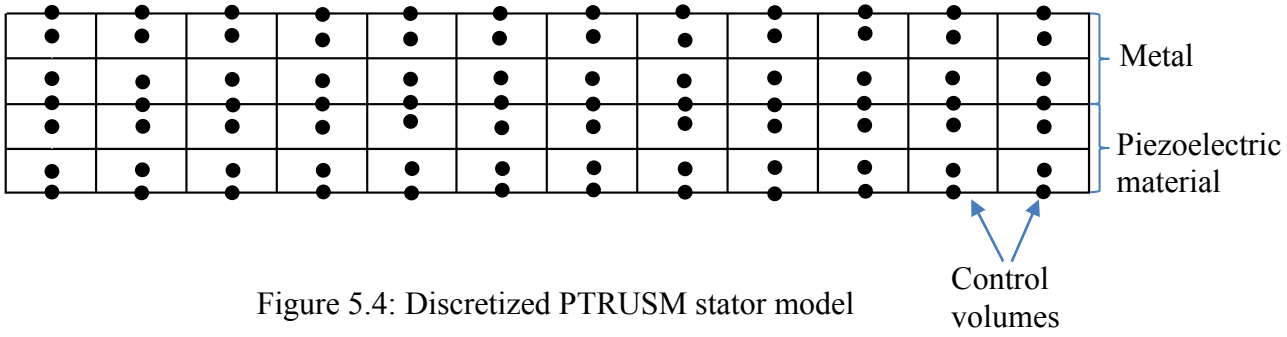

Figure 5.4: Discretized PTRUSM stator model

2. **Calculate the pre-compressive force F_N distribution for an undeformed stator**, (refer to Fig. 5.3). In this step one needs to calculate the distribution of the pre-compressive force when the PTRUSM is not powered. The equation used here to calculate the pre-compressive force distribution is:

$$F_{Ni} = \frac{F_N}{n} \tag{5.5}$$

In (5.5) F_{Ni} is the normal force applied on top of the current stator control volume. F_N and n are the normal force applied during the motor assembly process and the assumed number of stator control volumes in contact with the rotor. In this step, the normal force distribution is assumed to be constant. Fig. 5.5 shows a discretized stator with the constant normal force distribution on top of it. This is the normal force distribution applied on top of the stator when the PTRUSM is not powered.

3. **Apply the normal force distribution F_{Ni} on top of the stator and the DC voltage on the stator's piezoelectric material.** Fig. 5.6 shows a discretized stator before deformation with the distributed normal force and the DC voltage applied on it.

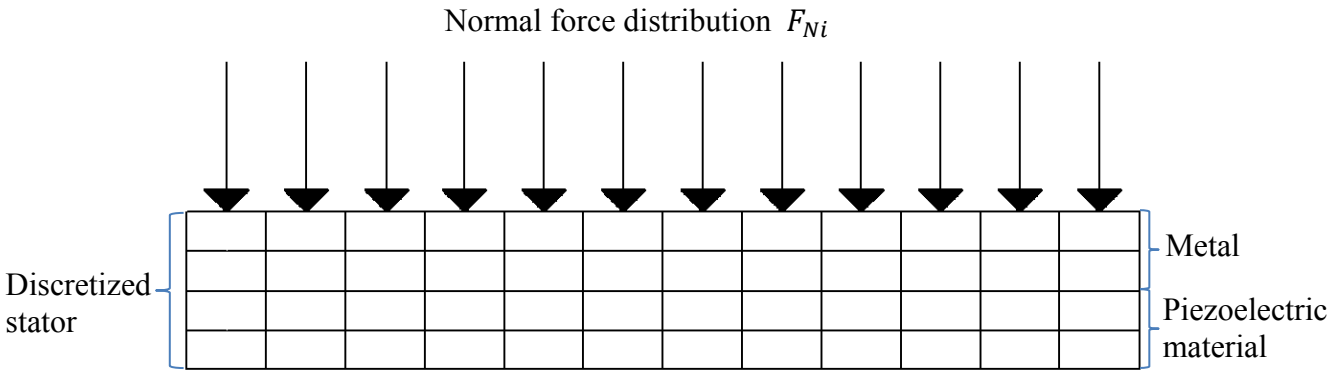

Figure 5.5: Constant normal force distribution applied over the discretized stator surface

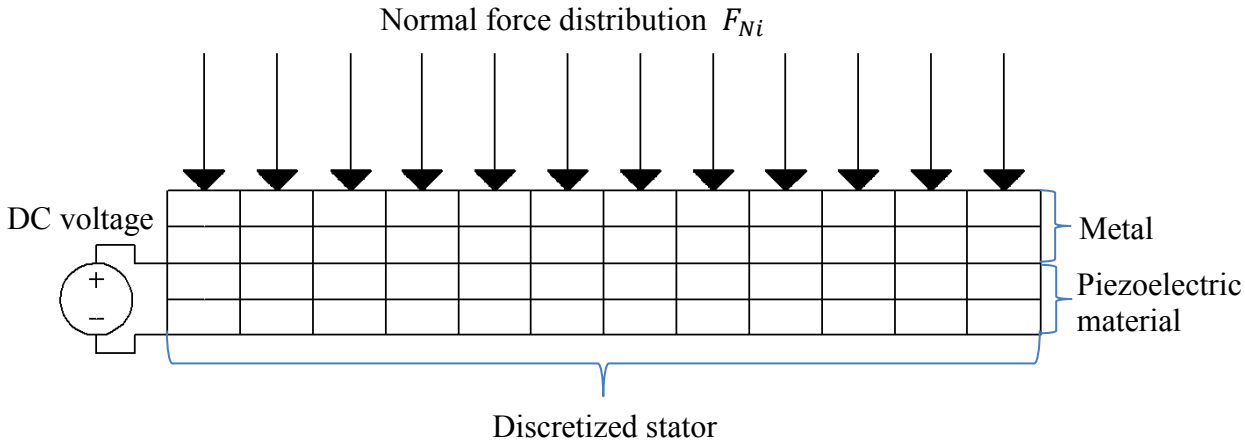

Figure 5.6: Discretized stator with normal force and DC voltage applied on it

4. **Obtain the stator stiffness matrix A_1 and the total force vector F_T**. The procedure to obtain the stator stiffness and total force vector is explained in Chapter 3.
5. **Solve the static system of equations.** Using equation (3.57) one can obtain the vector X containing the stator displacements of each degree of freedom.

6. **Calculate the rotor rigid body vertical displacement.** When the discretized stator and rotor (linear springs) deform, the rotor rigid body suffers a vertical displacement, refer to Fig. 5.7. First, let us define the equilibrium equation that defines the normal force distribution. This equation is:

$$F_N = K_n \sum_{i=1}^{n} (Z_i - Z_{RVD}) \tag{5.6}$$

where K_n, Z_i, Z_{RVD} are the equivalent rotor spring stiffness (metal and contact layer), vertical displacement of each stator control volume involved in the contact and the vertical displacement of the rigid body respectively.

After terms manipulation, one can define the vertical displacement of the rigid body.

$$Z_{RVD} = \frac{F_N - K_n \sum_{i=1}^{n} Z_i}{-nK_n} \tag{5.7}$$

In (5.7) n is the current number of stator control volumes involved in contact. The rigid body vertical displacement is a function of the normal force, rotor stiffness, surface stator vertical displacement, and the number of stator control volumes in contact with the rotor.

The number of stator control volumes involved in contact is unknown. Therefore, during this step the surface stator control volumes with positive vertical displacement are assumed to be in contact. With this assumption, one can use equation (5.7) to calculate the rotor rigid body vertical displacement.

7. **Calculate the penetration g_n of the rotor (linear springs).** One needs to calculate the penetration after deformation produced for each surface stator control volume in contact with the rotor. The overlap between stator and rotor is defined as the penetration of the rotor. This equation is:

$$g_{ni} = Z_i - Z_{RVD} \tag{5.8}$$

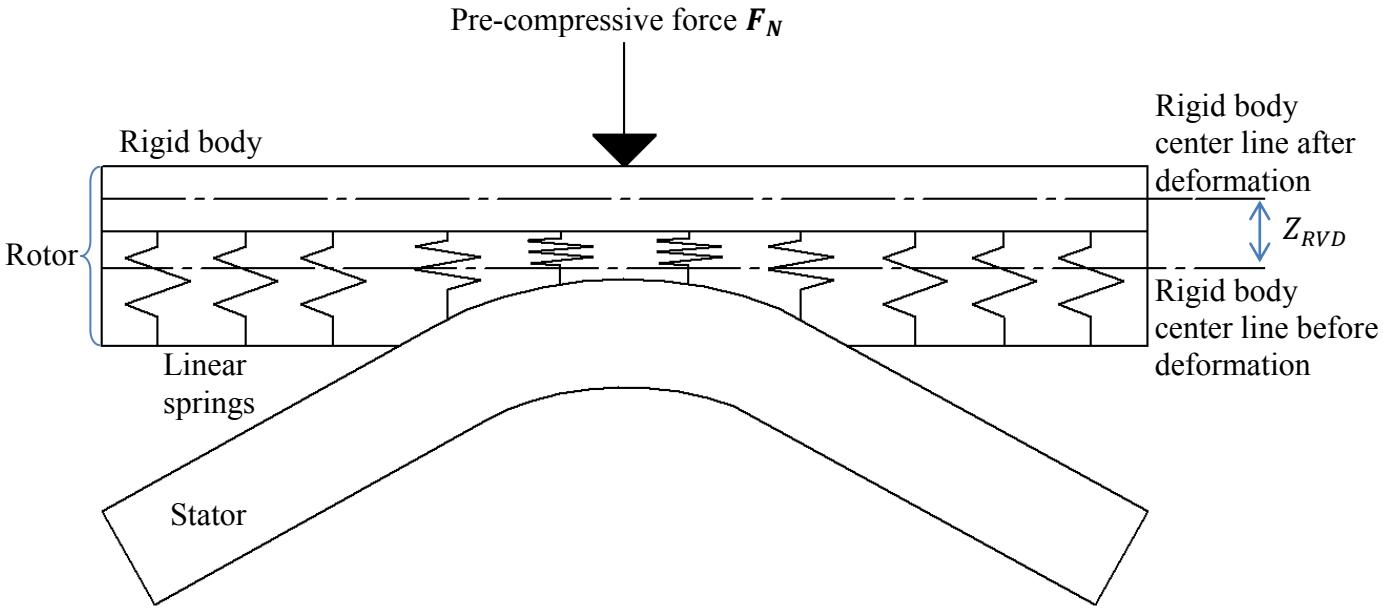

Figure 5.7: Rotor rigid body vertical displacement

g_{ni} is a vector that associates a penetration value to each stator control volume involved in contact.

8. **Check the sign of each value of the g_{ni} vector.** If the penetration of a current control volume is positive, it means that the previous assumption of considering the current control volume as a control volume in contact with the rotor is true. Therefore, the current control volume will be still considered in contact during the next iteration. If the penetration of a current control volume is negative, it means that the previous assumption of considering the current control volume as a control volume in contact is false. Therefore, the current control volume will not be considered in contact during the next iteration.

   If the g_{ni} vector contains negative values, one can go to step 9. If the g_{ni} vector does not contain negative values, must go to step 10.

9. **Calculate the rotor rigid body vertical displacement.** Similar to step 6, the rotor vertical displacement is calculated with equation (5.7). The difference is that the stator control volumes assumed to be in contact are the ones obtained in step 8. One must now return to step 7.
10. **Calculate the normal force distribution over the contact zone**. In this step one needs to calculate the normal force distribution produced in the stator-rotor contact zone after deformation. The normal force distribution is calculated with the following equation:

$$F_{Ni} = K_n(Z_i - Z_{RVD}) \tag{5.9}$$

F_{Ni} is the contact normal force produced in the current stator control volume. Fig. 5.8 shows a deformed stator with the contact normal force distribution on top of it.

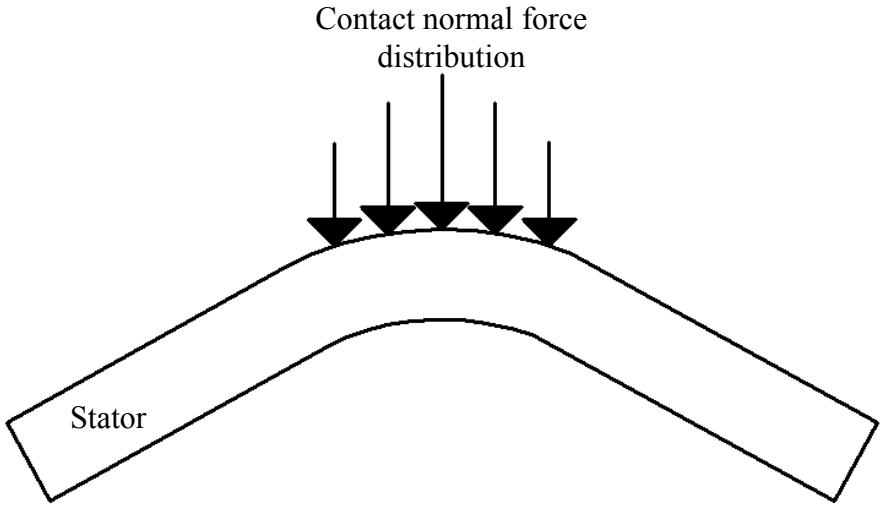

Figure 5.8: Stator with contact normal force distribution on top of it

11. **Check the convergence of the maximum value of the normal force vector distribution.** The equation used is:

$$F_i \approx F_{i+1} \tag{5.10}$$

The current normal force is compared to the normal force of the previous iteration. If the normal force distribution converges, the algorithm ends. If the normal force distribution does not converge, one must return to step 3.

Fig. 5.9 shows a block diagram with the normal contact algorithm.

5.2 Tangential contact problem

After computing the normal force distribution over the contact zone, the tangential force distribution is calculated. Due to the relative motion between stator and rotor, two situations happen between the stator and rotor particles along the mechanical contact: stick and slip. Stick refers to the theoretical contact points where the stator and rotor particles are moving with the same velocity. Slip refers to the stator and rotor particles moving with different velocities.

According to [24], the horizontal displacement of the contact layer can be neglected because the overall contact behavior is almost the same. Besides that, the dynamic and static coefficient of friction between stator and contact layer are almost the same. Therefore, the contact layer is considered to be deformed just in the vertical direction. That means the whole contact interface is considered to be in the state of slip.

Coulomb's friction law is assumed between the stator and contact layer surface, (refer to [5]). Only slip effects are modeled, assuming a constant dynamic coefficient of friction μ_k. A sign function is added to compute the friction force direction. The friction force is calculated with (5.11).

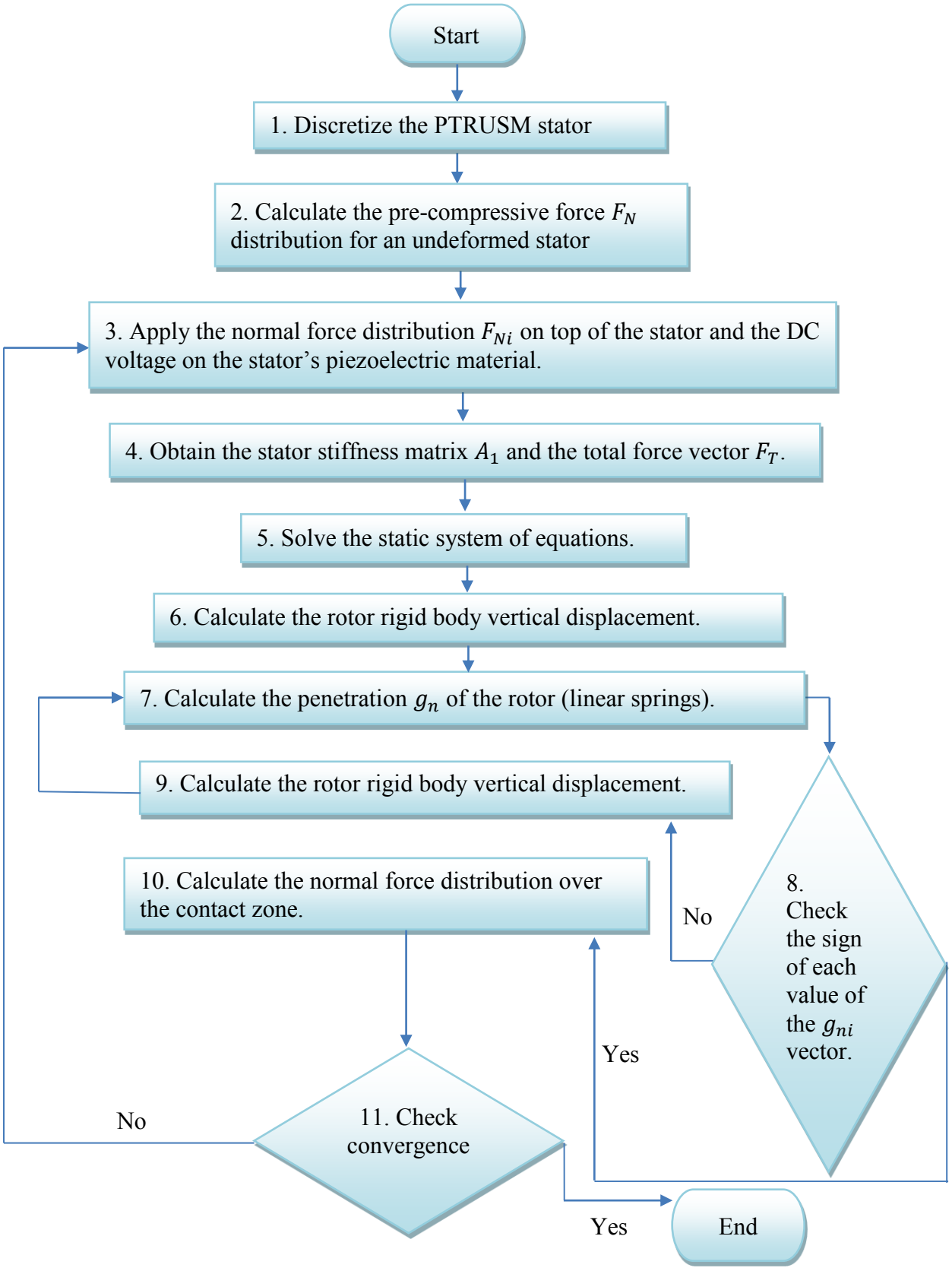

Figure 5.9: Normal contact algorithm

$$F_{Fi} = sign(V_{si} - V_R) \cdot \mu_k F_{Ni} \tag{5.11}$$

where V_{si} and V_R refer to the horizontal stator and rotor velocities, respectively. The subscript i is added to refer the tangential force, stator velocity and normal force at the current stator control volume. The horizontal velocity of the rotor is considered to be the same at every point. The tangential forces presented in the contact interface can be divided into two groups: driving and braking forces, (refer to Fig. 5.10). Driving forces are the ones presented in contact particles where the velocity of the stator is higher than the velocity of the rotor. These forces are the ones responsible of providing torque in the desired direction of movement of the rotor. Braking forces are forces presented in the contact particles where the stator velocity is lower than the rotor velocity. Breaking forces generate torque in the opposite desired direction of movement of the rotor. Due to that fact, it is required to avoid PTRUSM operation with high breaking zones. A schematic of the contact model is shown in Fig. 5.10.

One can use the dynamic model of the stator presented in Chapter 4 to model the stator surface velocities when in contact with the rotor. The horizontal velocities of the stator traveling wave are a function of its amplitude. The higher the amplitude of the traveling wave, the higher the horizontal velocity.

The external load applied to the PTRUSM influences the stator-rotor contact zone. If the driving load increases, the amplitude of the contact zone decreases, and at the same time, the width of the contact zone increases. Therefore, it is mandatory to include the load effect into the stator-rotor contact model. We use Coulomb's friction law to include the load influence into the normal contact algorithm. Using equation (5.12) one can transform the load into a normal force:

$$F_{NL} = \frac{L}{\mu_k} \tag{5.12}$$

F_{NL} is added to the pre-compressive force F_N . The normal contact force distribution is calculated using the total normal force F_{NT} .

The total normal force is:

$$F_{NT} = F_N + F_{NL} \tag{5.13}$$

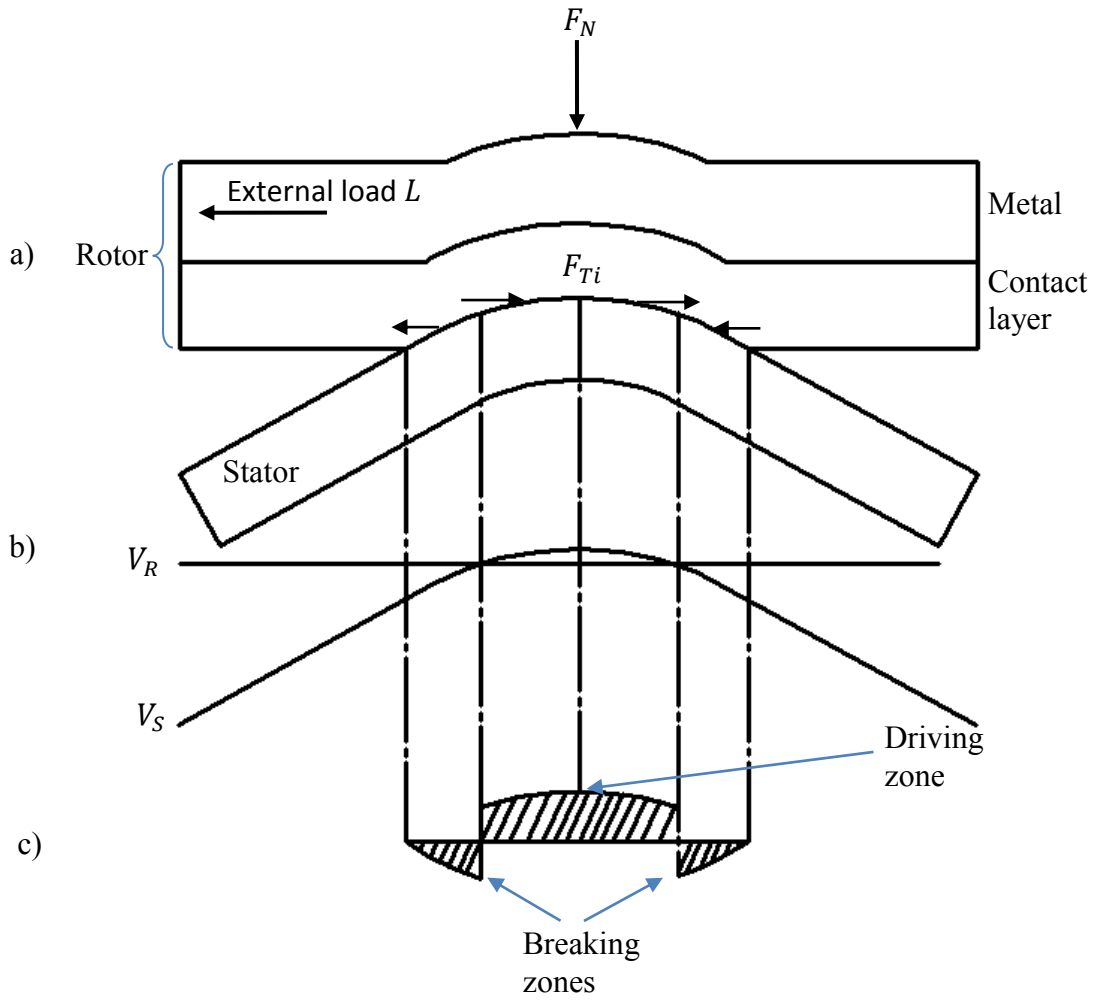

Figure 5.10: a) Stator-rotor contact interface. b). Stator surface velocity and rotor velocity. c) Tangential force distribution

5.2.1 Tangential contact algorithm

This section presents the method developed to model the tangential contact between stator and rotor. This algorithm includes the normal contact model and the dynamic stator model. The new input is the external load, and the output is the rotor velocity.

The steps of the algorithm used to analyze the PTRUSM stator-rotor tangential contact interface are:

1. **Compute the normal force produced by the external load.** One needs to use equation (5.12) for computation.
2. C**ompute the normal force distribution produced at the stator-rotor contact interface**. One needs to use the normal contact algorithm to obtain it. The primary outputs of the normal contact algorithm are the contact normal force distribution and the amplitude of the traveling wave.
3. **Compute the surface horizontal velocities of the stator traveling wave V_s.** One needs to use the dynamic stator model developed in Chapter 4 to obtain the horizontal stator velocities. The traveling wave needs to have the amplitude obtained in step 2. One needs to adjust the input voltage of the stator to obtain a traveling wave with the desired amplitude.
4. **Assign a horizontal velocity value of the vector V_s to the surface of the stator control volumes of the contact model.** In this step, a velocity value is assigned to the control volumes of the static stator model in contact with the rotor.
5. **Compute the tangential force distribution.** First, use Coulomb's law to compute the absolute value of the tangential force vector. This equation is:

$$|F_{Fi}| = \mu_k F_{Ni} \tag{5.14}$$

The total friction force produced at the stator-rotor contact interface has to be equal to the external load. This equation is:

$$F_{FT} = L \tag{5.15}$$

The sum of friction forces obtained with equation (5.14) has to be equal to the total friction force. This equation is:

$$\sum_{i=1}^{n} F_{Fi} = F_{FT} \tag{5.16}$$

6. **Compute the rotor velocity V_R.** One can express the total friction force as follows:

$$\sum_{i=1}^{n} F_{Fi} = \sum_{i=1}^{n} sign(V_{si} - V_R) \cdot \mu_k F_{Ni} = L \tag{5.17}$$

The only unknown in equation (5.17) is the rotor velocity. Therefore, one can obtain the rotor velocity with equation (5.17). One needs to remember that the stator model is discrete. Thus, equation (5.17) can be expressed as follows:

$$\sum_{i=1}^{n} F_{Fi} = \sum_{i=1}^{n} sign(V_{si} - V_R) \cdot \mu_k F_{Ni} \approx L \tag{5.18}$$

Fig. 5.11 shows a block diagram of the tangential contact algorithm. At this point the proposed steady-state model of the PTRUSM is finished. Fig. 5.12 shows a schematic of the complete model.

5.3 Numerical results. PTRUSM stator-rotor contact simulation

The USR60 has 9 wavelengths, but the behavior of all the wavelengths is the same at a specific moment in time. Therefore, one just needs to model the contact zone of one wavelength. The vibration amplitude of the USR60 stator is around 1μm, refer to [1]. In order to obtain similar amplitudes with the static stator model, one needs to characterize as accurate as possible the model parameters such as the exciting voltage and the spring foundation (bridge) constants.

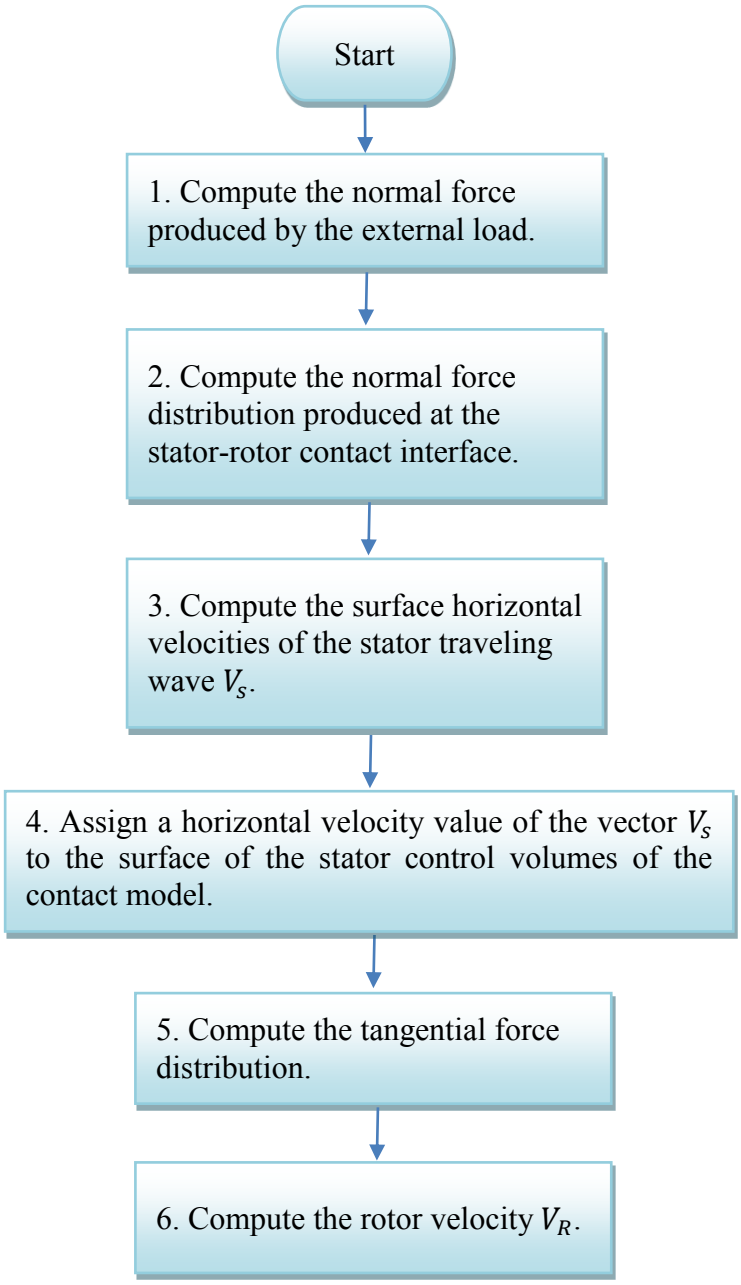

Figure 5.11: Tangential contact algorithm

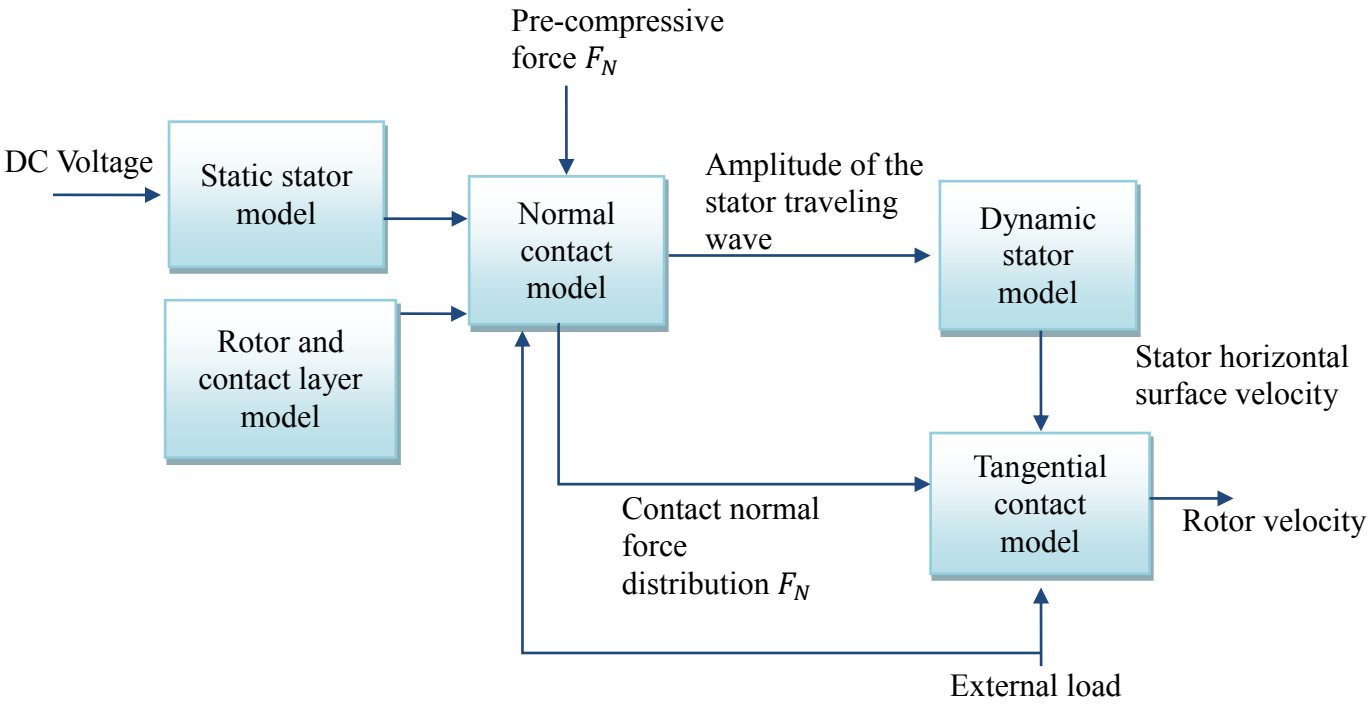

Figure 5.12: Complete steady state model of the PTRUSM

The stator model of the stator-rotor contact model is excited with a DC voltage, and it does not have teeth on top of it. Therefore, one needs to obtain the required DC voltage to generate displacements of the stator similar to the ones produced by the USR60 traveling wave at resonance.

In order to estimate the stator model excitation voltage, a static model of the PTRUSM was created using COMSOL Multiphysics. This model is composed of a discretized stator in contact with a discretized rotor with contact layer. The materials used to form the rotor model are aluminum and epoxy resin. Fig. 5.13 shows the static contact model made in COMSOL Multiphysics.

The required DC voltage and spring foundation constants were obtained with the trial and error method. The reference vertical displacement of the stator is 1μm. The combination of DC voltage and the spring foundation vertical and horizontal constants that produces a displacement of 1μm are 1500 V,

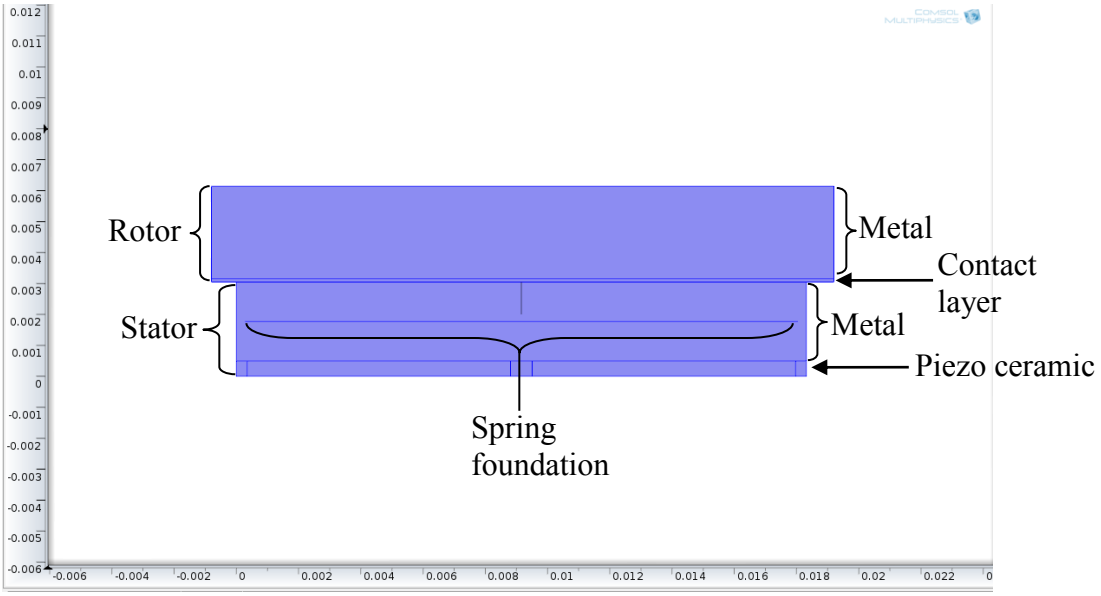

Figure 5.13: Static contact model made in COMSOL Multiphysics

3 E^{8} N/m and 7.56 E^{6} N/m, respectively. In order to obtain these voltage and spring foundation values, the static contact model of Fig. 5.13 was implemented in COMSOL Multiphysics, the voltages and total spring constants were obtained with the trial and error method. One needs to consider that the spring foundation vertical constant must be high enough to support the stator when subject to the normal forces produced by the stator-rotor contact interface.

Reference [2] presents a range of pre-compressive forces from 100 to 250 N used to test the friction coefficient of the PTRUSM contact zone. Reference [1] used a pre-compressive force of 132 N to obtain the output characteristic of the PTRUSM, but the maximum output torque obtained with this pre-compressive force was of just 0.5 Nm. Therefore, we assumed a pre-compressive force of 250 N.

The plot of the USR60 torque-speed characteristic (Fig. 2.8) shows the unloaded motor case, and the 0.2, 0.4, 0.6, 0.8 and 1.0 Nm load cases. The total normal forces (refer to equation (5.13)) of the USR60 model was applied to the contact model made in COMSOL Multiphysics. Then, by applying equation (5.6), the stator surface vertical displacements and the rotor vertical displacement obtained

with the contact model made in COMSOL Multiphysics were used to find the rotor imaginary spring stiffness. The obtained average value of the imaginary rotor spring stiffness is 7E^6 N/m. In reference [18] the dynamic coefficient of friction of the PTRUSM was measured with a friction tester. The obtained dynamic coefficient of friction was 0.7. This value is used in this dissertation to model the friction forces.

Now that we defined the parameters of the USR60 steady state contact model, the torque-speed characteristic of the USR60 can be obtained. One needs to obtain the normal force distribution of the stator-rotor contact interface, amplitude of the traveling wave, surface velocity of the stator traveling wave, tangential force distribution (driving and breaking zones), and finally the rotor velocity. These parameters are obtained for the driving loads: 0, 0.2, 0.4, 0.6, 0.8 and 1.0 Nm.

Figs. 5.14-5.19 show the normal force distribution at the stator-rotor contact interface when the motor is unloaded and loaded with 0.2, 0.4, 0.6, 0.8 and 1.0 Nm, respectively.

- **Case 1 (unloaded):**

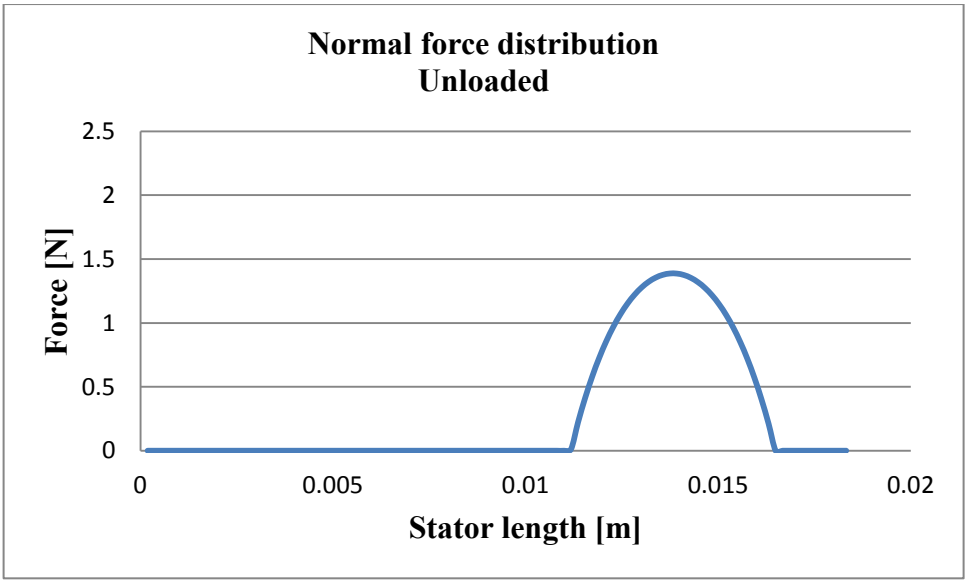

Figure 5.14: Normal force distribution at the stator-rotor contact interface when the motor is unloaded

The contact length and the maximum stator vertical displacement when the motor is unloaded are:

Contact length= 0.00531 m

Maximum stator vertical displacement = 6.35569E^{-07} m

- **Case 2 (load 0.2 Nm):**

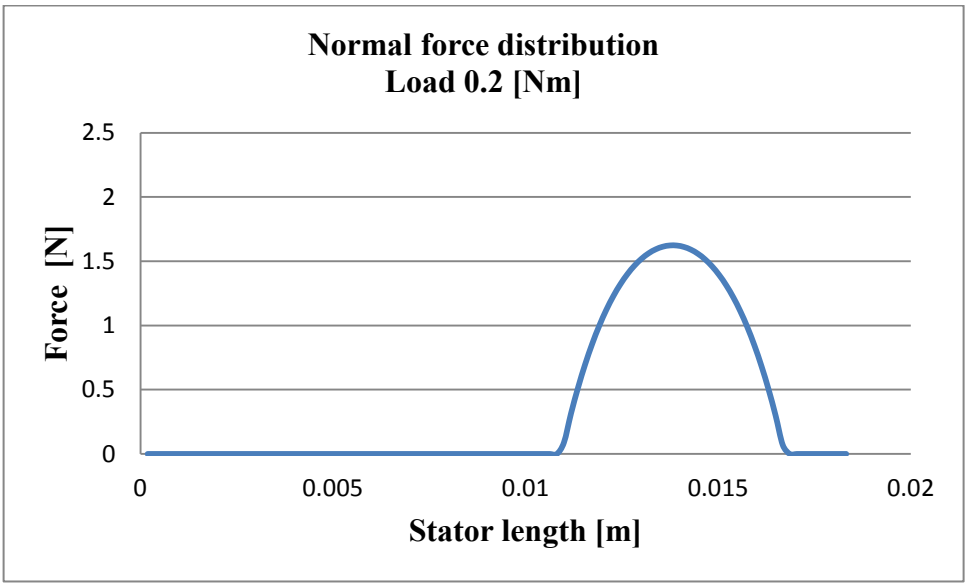

Figure 5.15: Normal force distribution at the stator-rotor contact interface when the motor has a load of 0.2 [Nm]

The contact length and the maximum stator vertical displacement when the motor is loaded with 0.2 Nm are:

Contact length= 0.00586 m

Maximum stator vertical displacement = 5.86792E^{-07} m

- **Case 3 (load 0.4 Nm):**

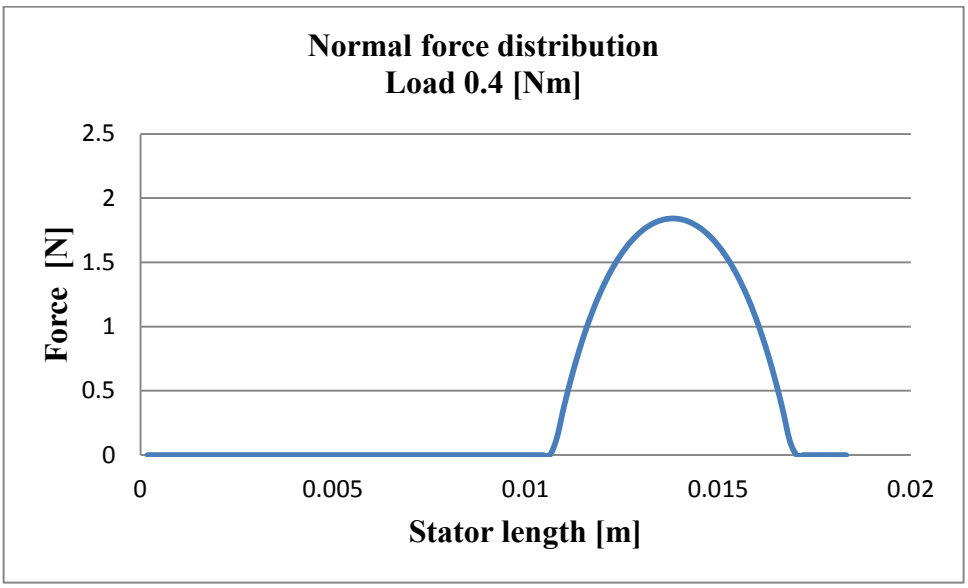

Figure 5.16: Normal force distribution at the stator-rotor contact interface when the motor has a load of 0.4 [Nm]

The contact length and the maximum stator vertical displacement when the motor is loaded with 0.4 Nm are:

Contact length= 0.00622 m

Maximum stator vertical displacement = 5.38991E^{-07} m

- **Case 4 (load 0.6 Nm):**

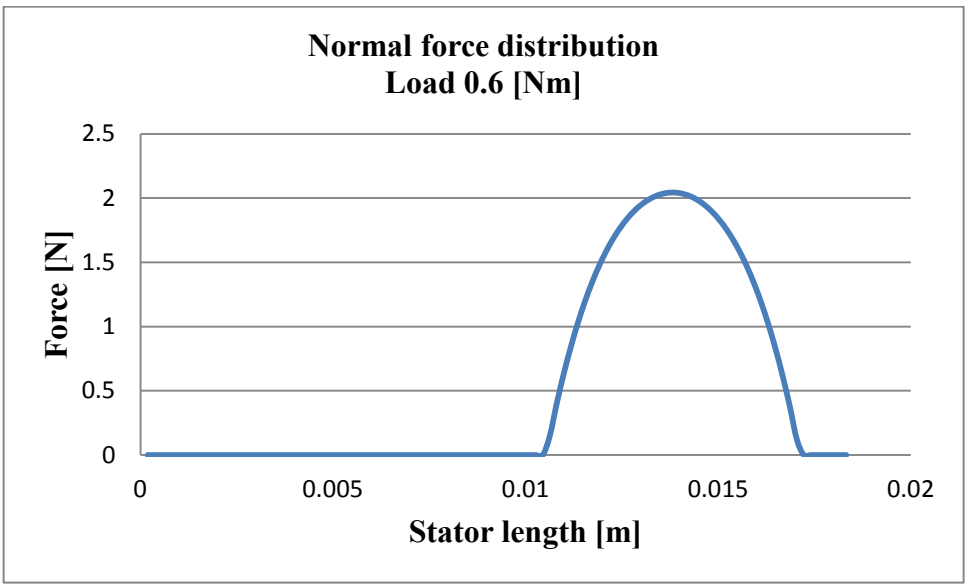

Figure 5.17: Normal force distribution at the stator-rotor contact interface when the motor has a load of 0.6 [Nm]

The contact length and the maximum stator vertical displacement when the motor is loaded with 0.6 Nm are:

Contact length= 0.00659 m

Maximum stator vertical displacement = 4.92330E^{-07} m

- **Case 5 (load 0.8 Nm):**

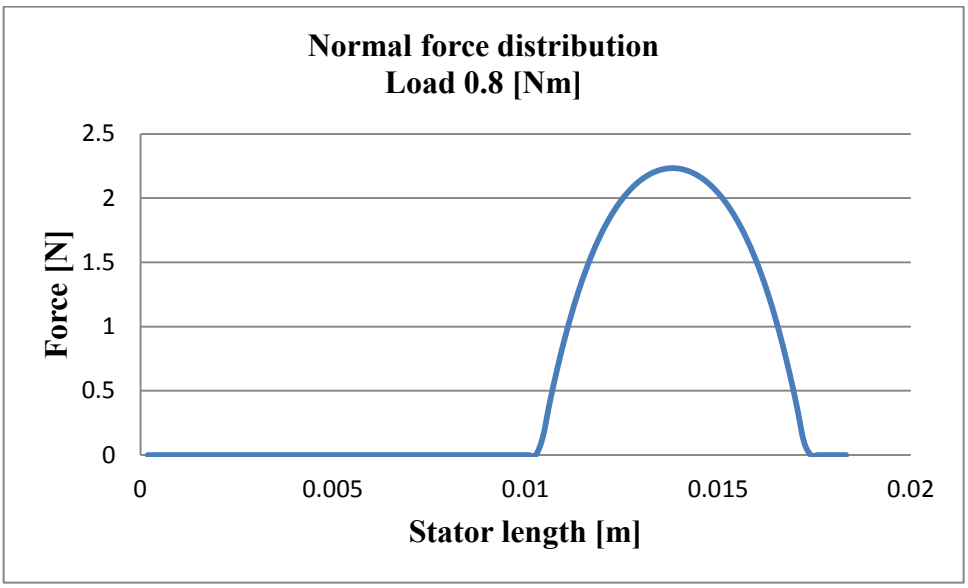

Figure 5.18: Normal force distribution at the stator-rotor contact interface when the motor has a load of 0.8 [Nm]

The contact length and the maximum stator vertical displacement when the motor is loaded with 0.8 Nm are:

Contact length= 0.00696 m

Maximum stator vertical displacement= 4.46718E^{-07} m

- **Case 6 (load 1.0 Nm):**

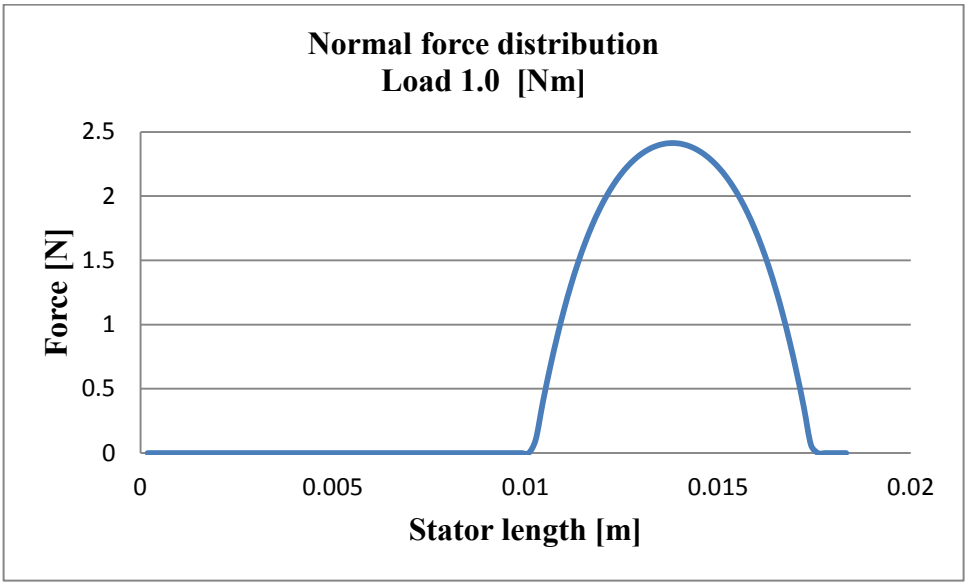

Figure 5.19: Normal force distribution at the stator-rotor contact interface when the motor has a load of 1.0 [Nm]

The contact length and the maximum stator vertical displacement when the motor is loaded with 1.0 Nm are:

Contact length= 0.00732 m

Maximum stator vertical displacement= 4.02041E^{-07} m

The results obtained with the normal contact model were compared versus the results of the model made in COMSOL Multiphysics. Fig. 5.20 shows the deformation of the static stator-rotor contact model using COMSOL Multiphysics. In this comparison a normal force of 27.77 N was applied on top of the rotor. Fig. 5.21 shows the normal contact pressure distribution between stator and rotor obtained with COMSOL Multiphysics. The normal pressure distribution obtained with the proposed model is shown in Fig. 5.22.

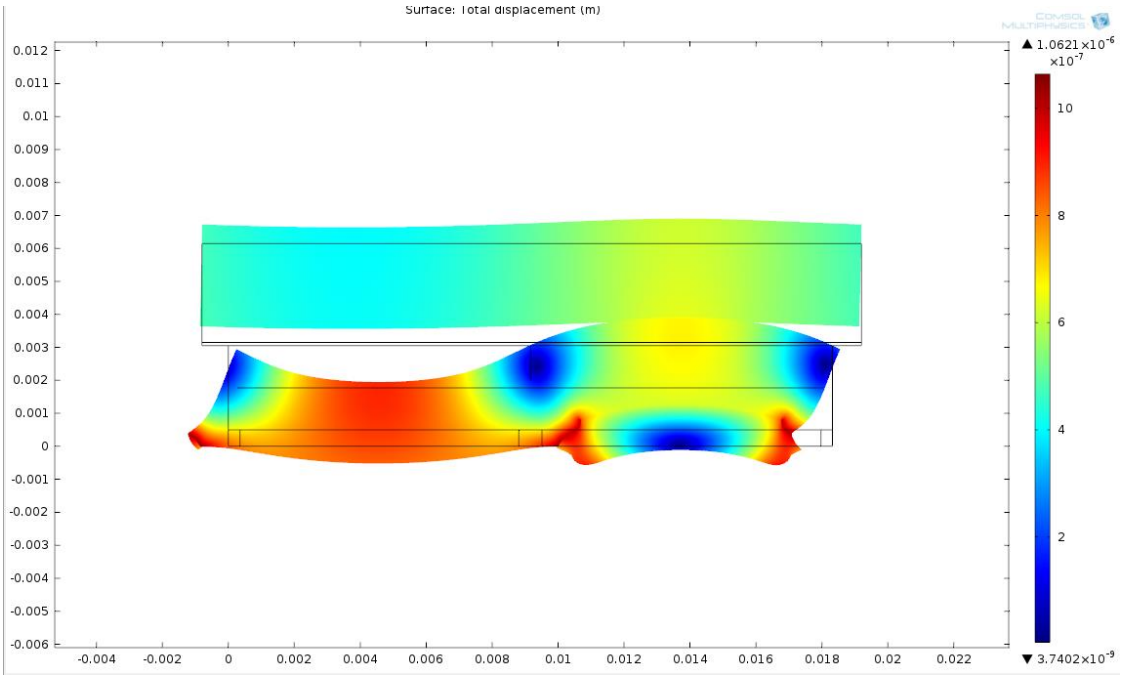

Figure 5.20: Deformation of stator-rotor (contact model using COMSOL Multiphysics)

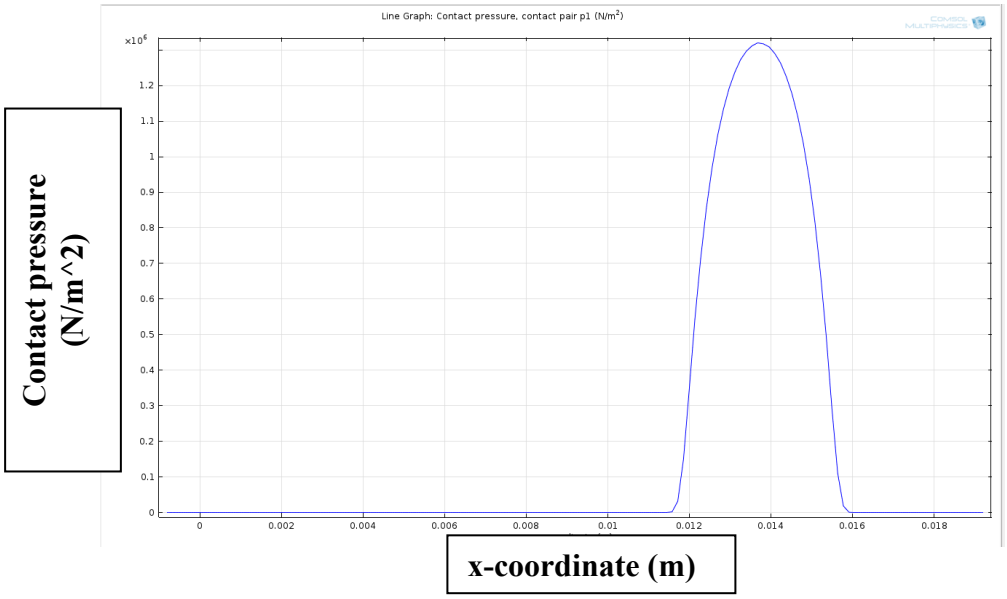

Figure 5.21: Contact pressure distribution between stator and rotor obtained with COMSOL Multiphysics

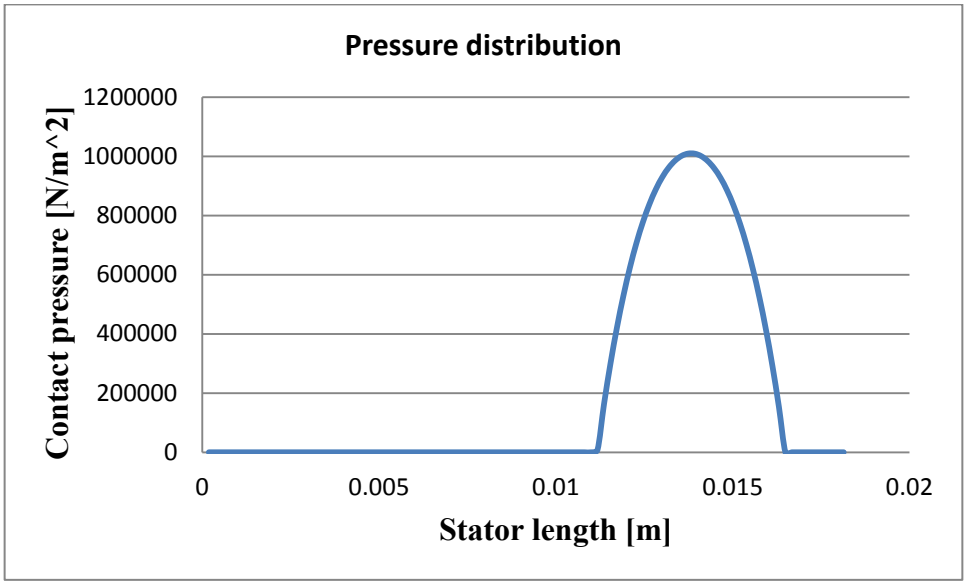

Figure 5.22: Contact pressure distribution between stator and rotor obtained with the proposed model

The results obtained with COMSOL Multiphysics are used as a reference. One can see that the proposed model presents a good agreement. One needs to consider that the proposed model is much simpler than the one made in COMSOL. Thus, the computational effort was significantly reduced. The proposed model allows one to model in detail the forces produced in the stator-rotor contact interface with a relative low computational effort.

By using the obtained maximum stator vertical displacement one can model the stator horizontal surface velocity when subjected to the mentioned loads. Figs. 5.23- 5.28 show the stator horizontal surface velocity for the studied cases.

- **Case 1 (unloaded):**

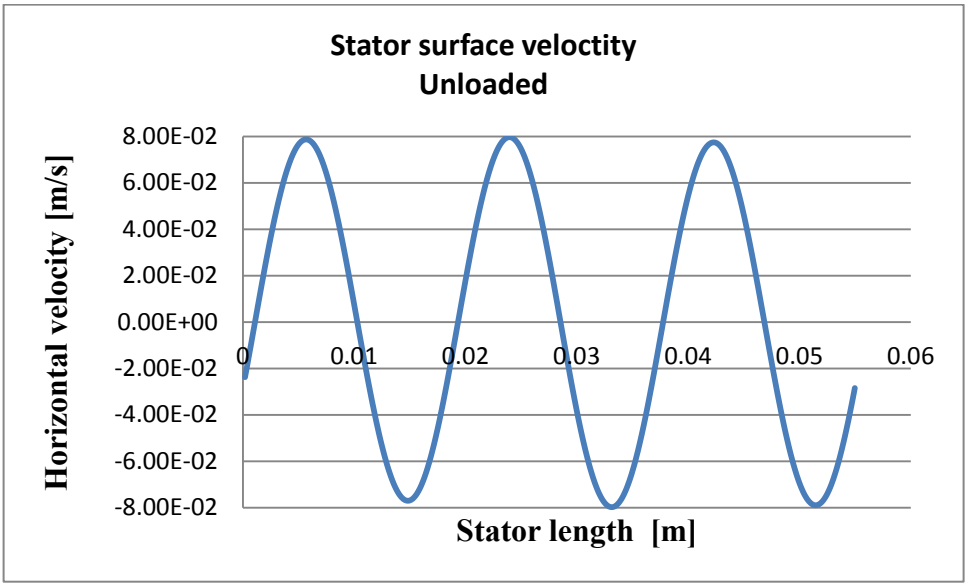

Figure 5.23: Stator horizontal surface velocity when the motor is unloaded

- **Case 2 (load 0.2 Nm):**

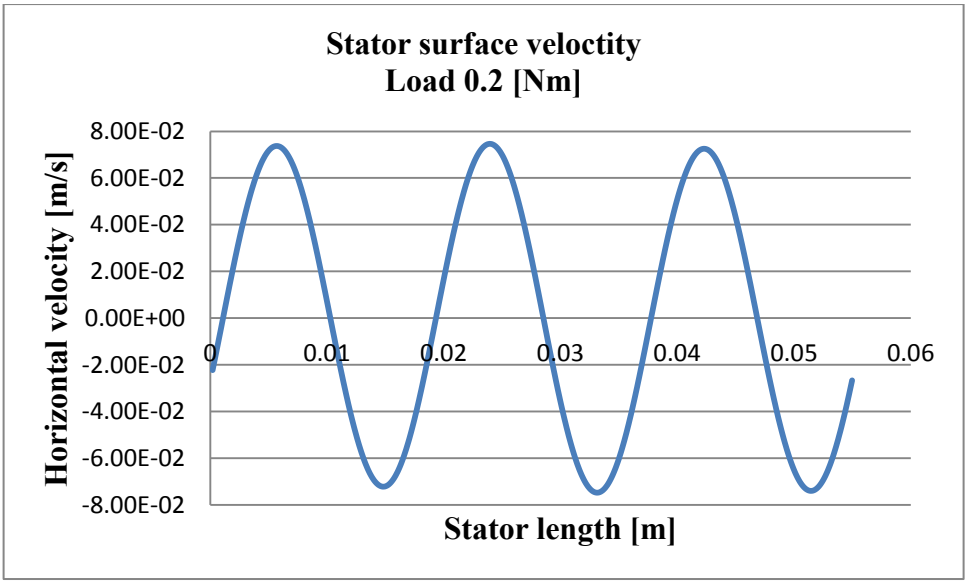

Figure 5.24: Stator horizontal surface velocity when the motor has a load of 0.2 [Nm]

- **Case 3 (load 0.4 Nm):**

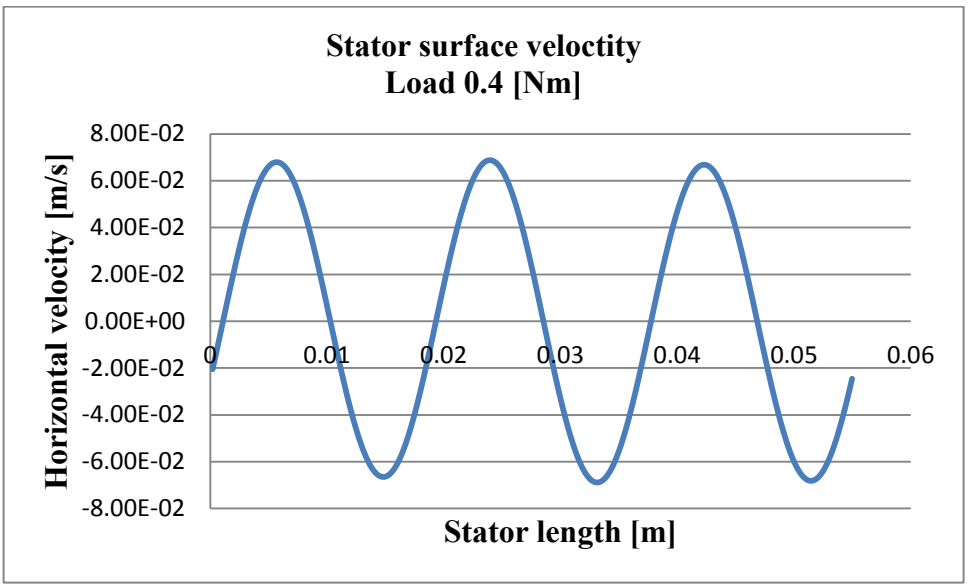

Figure 5.25: Stator horizontal surface velocity when the motor has a load of 0.4 [Nm]

- **Case 4 (load 0.6 Nm):**

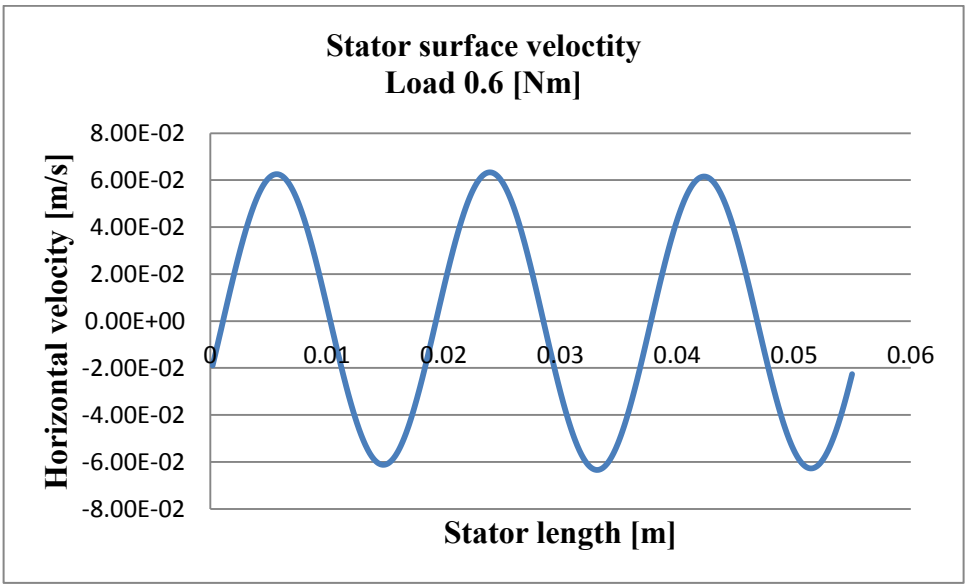

Figure 5.26: Stator horizontal surface velocity when the motor has a load of 0.6 [Nm]

- **Case 5 (load 0.8 Nm):**

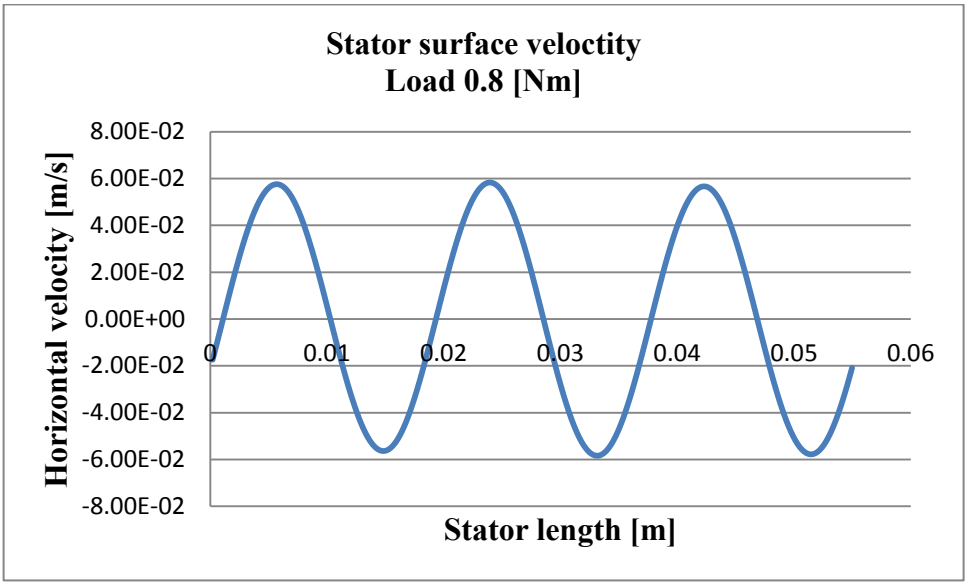

Figure 5.27: Stator horizontal surface velocity when the motor has a load of 0.8 [Nm]

- **Case 6 (load 1.0 Nm):**

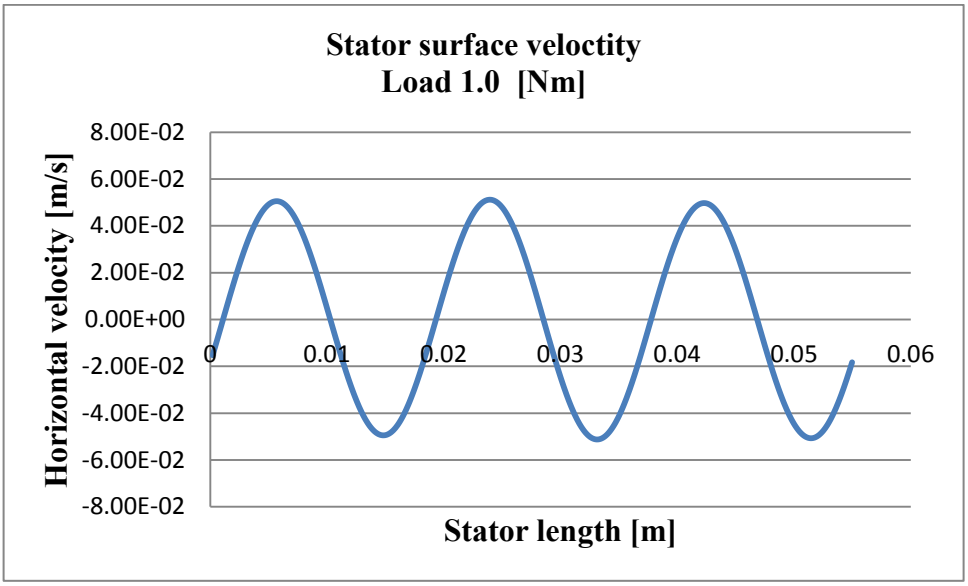

Figure 5.28: Stator horizontal surface velocity when the motor has a load of 1.0 [Nm]

By using the normal force distribution one can calculate the absolute value of the tangential force distribution. Then, the driving and breaking zones are calculated. Figs. 5.29-5.34 show the tangential force distribution at the stator-rotor contact interface when the motor is unloaded and loaded with 0.2, 0.4, 0.6, 0.8 and 1.0 Nm, respectively.

- **Case 1 (unloaded):**

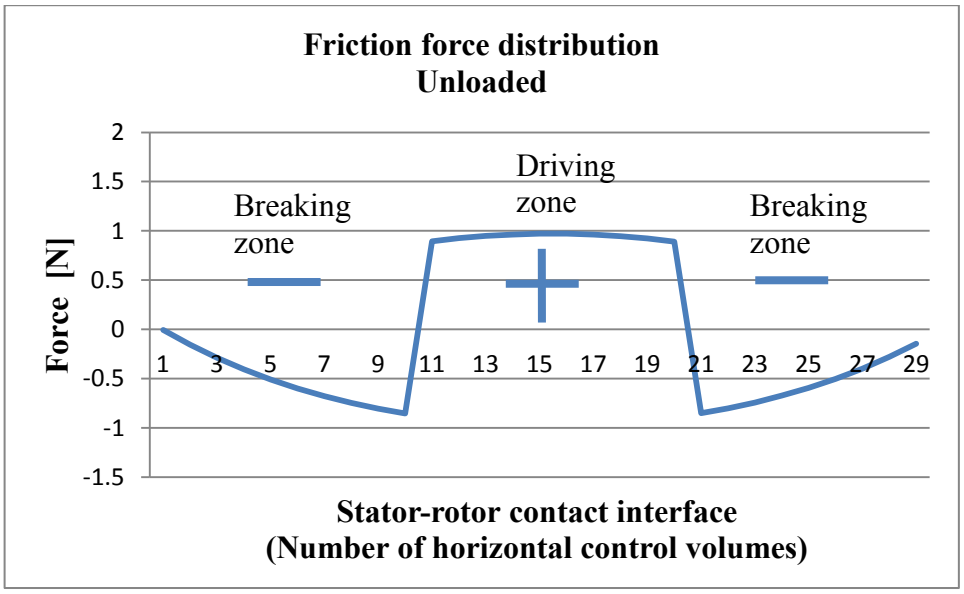

Figure 5.29: Friction force distribution at the stator-rotor contact interface when the motor is unloaded

- **Case 2 (load 0.2 Nm):**

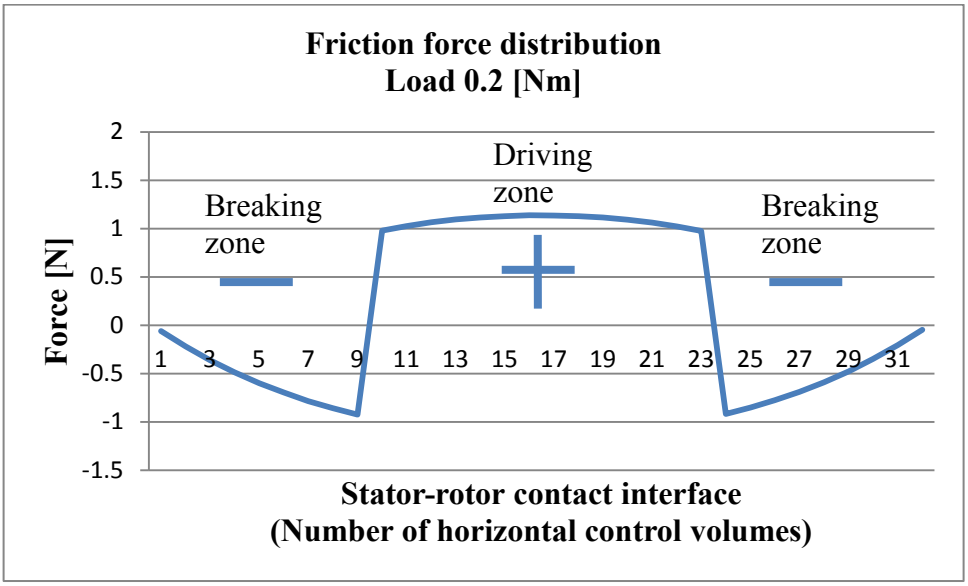

Figure 5.30: Friction force distribution at the stator-rotor contact interface when the motor has a load of 0.2 [Nm]

- **Case 3 (load 0.4 Nm):**

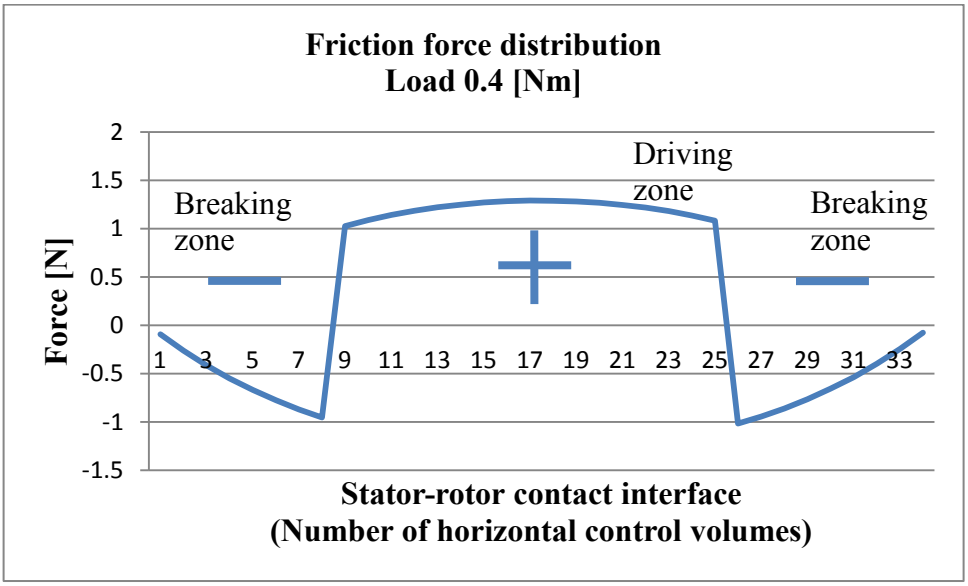

Figure 5.31: Friction force distribution at the stator-rotor contact interface when the motor has a load of 0.4 [Nm]

- **Case 4 (load 0.6 Nm):**

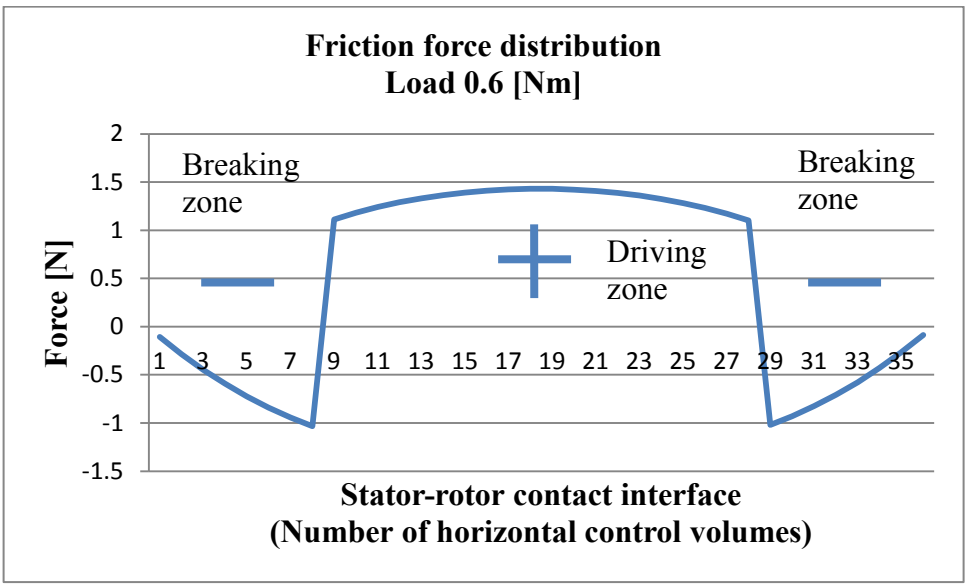

Figure 5.32: Friction force distribution at the stator-rotor contact interface when the motor has a load of 0.6 [Nm]

- **Case 5 (load 0.8 Nm):**

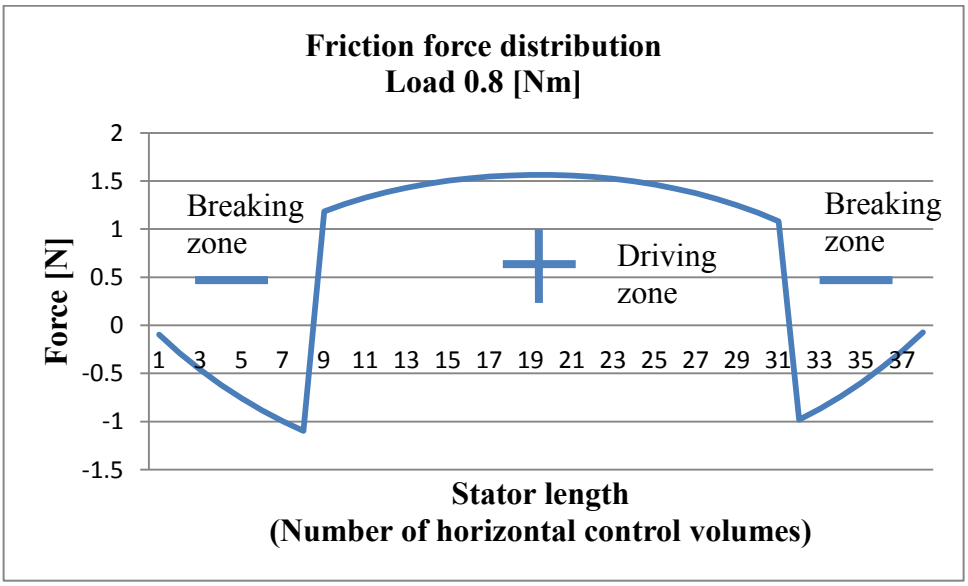

Figure 5.33: Friction force distribution at the stator-rotor contact interface when the motor has a load of 0.8 [Nm]

- **Case 6 (load 1.0 Nm):**

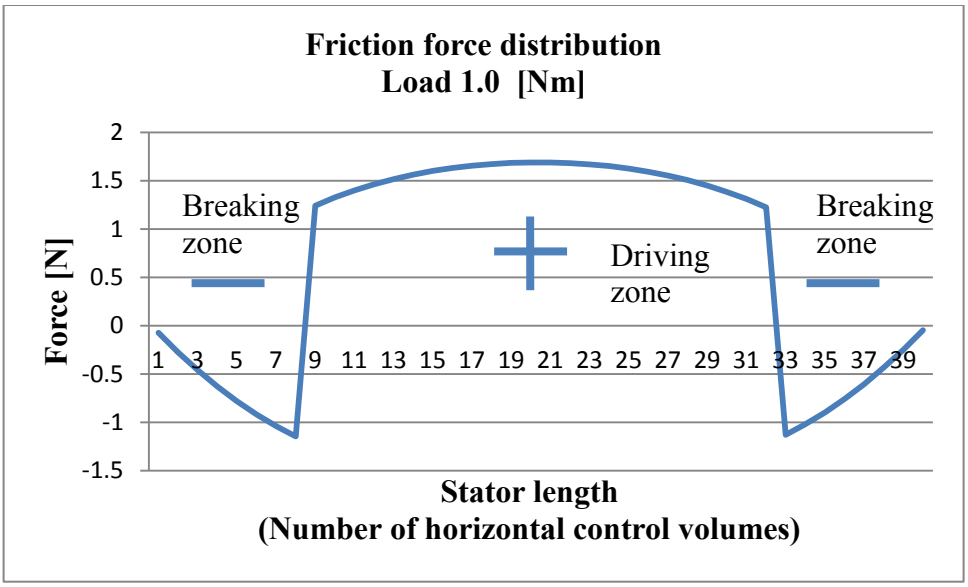

Figure 5.34: Friction force distribution at the stator-rotor contact interface when the motor has a load of 1.0 [Nm]

After the driving and breaking zones were obtained, one needs to assign a velocity value at each stator control volume with a tangential force different of zero. At this point the only unknown is the rotor velocity. This can be obtained with equation (5.18). Fig. 5.35 and 5.36 show a comparison between the experimental and the modeled USR60 torque-speed characteristic.

One can see a very good agreement between the proposed model and the torque-speed characteristic of the USR60. One needs to consider that several simplifications were used to develop the model. The most important simplifications are:

- The stator is modeled as a 2D beam.
- The contact zone is modeled as a line of contact (instead of an area of contact).
- The rotor is modeled as a linear spring.

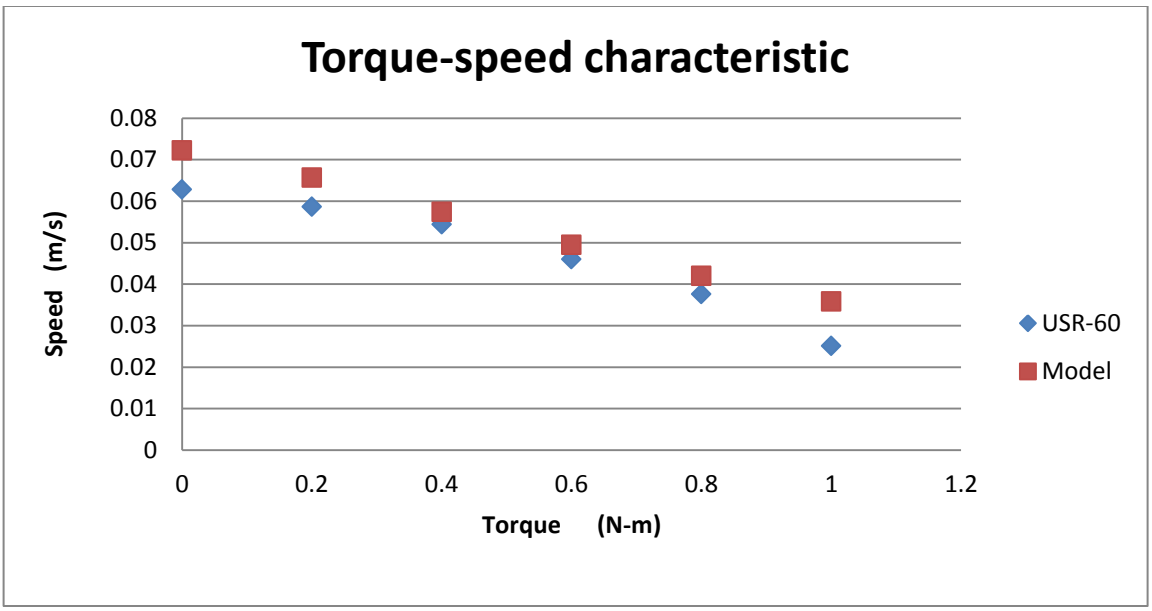

Figure 5.35: USR60 torque-speed characteristic expressed in m/s

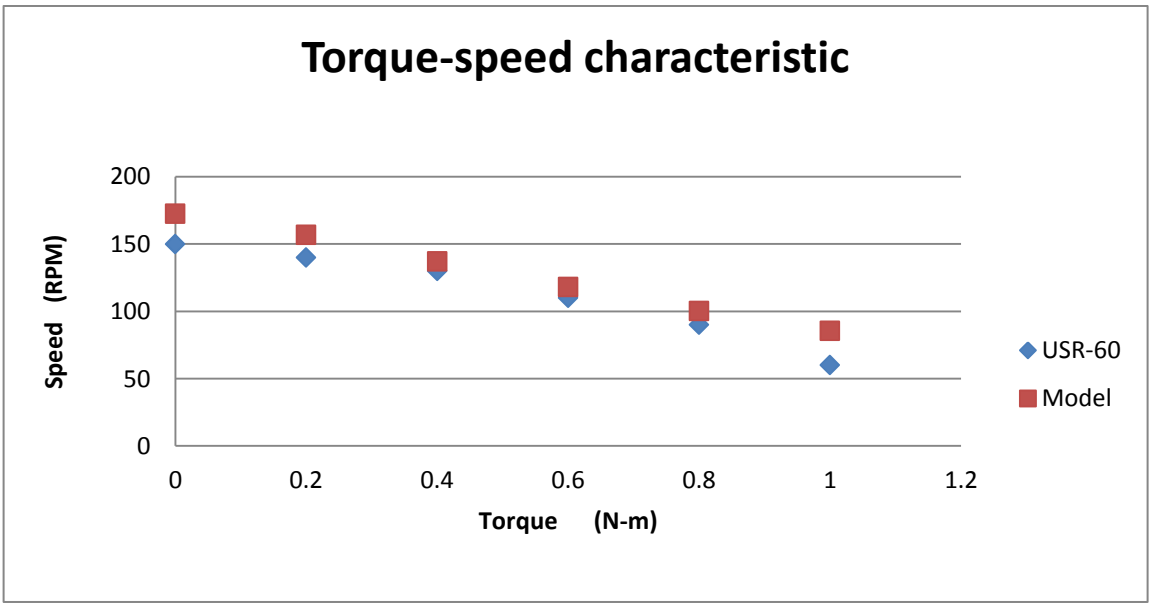

Figure 5.36: USR60 torque-speed characteristic expressed in RPM

- The normal contact problem was assumed to be independent of the tangential contact problem.
- Coulomb's friction law was assumed at the contact zone between stator and rotor.
- The contact slip between stator and rotor that happens along the y axis was neglected.
- The coefficient of friction was assumed to be constant.

The output velocities of the USR60 obtained with the proposed model have a linear behavior. The reason is because the rotor was modeled as a linear spring, and the friction forces generated at the stator rotor-contact zone were modeled with Coulomb's law. This law considers that the tangential forces are linearly dependent of the normal forces and the coefficient of friction.

The 2D model neglects the contact slip between stator and rotor along the y axis. The contact along the y axis increases the area of the breaking zones [2]. Thus, the 2D model has higher driving zones than the real ones. The higher driving zones produce higher output velocities. This phenomenon can explain why the velocities obtained with the proposed model are higher than the real velocities of the motor.

The highest output velocities deviations of the proposed model with respect to the experimental output velocity of the motor are for the unloaded and maximum load cases. Fortunately, this two cases are not usually implemented (the rated output torque is 0.5 Nm).

Based on the obtained results, one can conclude that the proposed model successfully reflects the output characteristic of the PTRUSM.

Chapter 6: Conclusions, contributions and future work

6.1 Conclusions

The purpose of this dissertation was to develop a complete and accurate mathematical model of the PTRUSM. The motivation of this work was the need of a complete model of the motor able of being used as the backbone of a model-based control strategy. A model of the PTRUSM able of been implemented in a control strategy needs to accurately reflect the behavior of the PTRUSM stator, rotor and the stator-rotor contact interface.

The inputs of the complete PTRUSM model are the voltages applied to the stator piezoelectric material, pre-compressive force, and external load. The output of the model is the rotor velocity. This set of inputs and output are required in a model able of being implemented in a control strategy.

Because of the complexity of the problem concerning the PTRUSM modeling, certain valid simplifications were introduced. The PTRUSM was modeled in 2D because the contact between stator and rotor happens in a zone with a small thickness, and a moving reference coordinate system on top of the stator traveling wave was introduced. This simplifies the steady-state modeling, as one can reduce a time dependent problem into a time independent problem. Because the steady-state modeling of the PTRUSM is a time independent problem, the contact between stator and rotor was modeled with a static model.

The problem concerning the stator modeling was treated first. Two models of the PTRUSM stator were proposed: a static one and a dynamic one. A 3D system of equations that models a piezoelectric-metal cantilever beam [9, 10] was used to develop the model of the PTRUSM stator. The stator was discretized with the FVM. The reason of using FVM is that it was observed in [10] that a piezoelectric-metal cantilever beam discretized with the FVM has a faster convergence rate than a piezoelectric-metal cantilever beam discretized with the FEM.

It is important to consider that the stator is attached to the motor case with a bridge. Therefore, a model of the PTRUSM stator bridge was added to obtain accurate results. The bridge was modeled as a spring foundation. Because the stator is modeled as a straight beam, a technique to model periodic boundary conditions at the *West* and *East* boundaries of the stator model was proposed.

One wavelength of the stator was modeled with the static stator model. A convergence study of the complete static stator model was performed. The convergence study of the u and w displacements shows that the solution converges with just 3400 control volumes (6800 degrees of freedom). One can observe in Tables 3.1 and 3.2 that the system of equations reaches convergence with 3400 control volumes because the displacement deviation is almost the same with bigger meshes (19800 control volumes). The results of the convergence study were compared versus the commercial software COMSOL Multiphysics. In this software the stator was meshed with 443039 finite elements (5396990 degrees of freedom). An error of just 4.98% and -2.74% for the u and w displacements, respectively, were obtained for a stator discretized with 3400 control volumes.

The system of equations of the static stator model was used to develop the dynamic stator model. In order to generate a traveling wave at least three wavelengths are required. Thus, the dynamic stator model was composed of three wavelengths. One requires an algorithm to solve the dynamic equation, and Newmark method was used to perform the time domain analysis. The dynamic stator model was used to calculate the surface horizontal velocities of the stator traveling wave. In addition, the model was used to obtain the elliptical motion of the stator traveling wave.

The problem concerning the rotor modeling is relatively simple. It was found by using FEM software (COMSOL Multiphysics) that the rotor (metal) deforms vertically when in contact with the stator. Therefore, the deformation of the rotor (metal) was considered into the model. The rotor and contact layer were both modeled as linear springs attached to a rigid body.

In order to obtain the rotor horizontal velocity, the static and dynamic stator models were coupled with the rotor model to develop the stator-rotor contact interface model. The stator-rotor contact interface model was described with inequalities. Therefore, two algorithms were developed to couple the stator and rotor models. First an algorithm was developed to solve the normal contact problem. With this algorithm one can compute the contact zone width and height, vertical displacement of the stator traveling wave, and the normal force distribution produced over the contact interface. After the normal contact algorithm was established, a tangential contact algorithm was developed to compute the tangential force distribution. The absolute value of the tangential force distribution was calculated from the normal force distribution using Coulomb's law. Subsequently, the motor driving and braking zones were obtained with the tangential force distribution. Finally, the rotor horizontal velocity was calculated.

In order to validate the results of the proposed PTRUSM model, the torque-speed characteristic of the USR60 was calculated and compared to the real torque-speed characteristic of the motor. One can see a very good agreement between the proposed model and the torque-speed characteristic of the USR60. Based on the obtained results, one can conclude that the proposed model successfully reflects the output characteristic of the PTRUSM.

6.2 Contributions

The following paragraphs describe the contributions of this dissertation regarding the complete mathematical model of the PTRUSM:

- **2D system of equations that numerically models a piezoelectric-metal cantilever beam.** This contribution is the implementation of plane stress approximation to reduce from 3D to 2D the system of equations presented in [9,10]. The derivation is presented in Appendix A.
- **Static model of the PTRUSM stator.** A static model of the PTRUSM stator was developed. The 2D system of equations that models the piezoelectric-metal cantilever beam was used to model the stator. In order to generate this model, an equation to model the stator bridge as a spring foundation

and a technique to model periodic boundary conditions were proposed. The static model of the PTRUSM stator is presented in Chapter 3.

- **Dynamic model of the PTRUSM stator**. The static stator model was used to develop a dynamic stator model. The time domain analysis provides the velocities of the stator traveling wave. This model is used as well to model the elliptical motion of the stator surface. The dynamic model of the PTRUSM stator is presented in Chapter 4.
- **PTRUSM rotor model.** A static model of the rotor and contact layer with the capability of being coupled with the discrete stator model was developed.
- **Stator-rotor contact model of the PTRUSM**. This is the complete model of the PTRUSM. Two algorithms were developed to model the stator-rotor contact interface: a normal contact model and a tangential contact model. These algorithms provide the contact length, amplitude of the stator traveling wave (when subject to mechanical contact with the rotor), normal force distribution, tangential force distribution, driving and breaking zones, and rotor horizontal velocity. The stator-rotor contact model is presented in Chapter 5.

6.3 Future work

The future work of this dissertation could be focused on the adaptation and implementation of the proposed mathematical model of the PTRUSM to develop control strategies for these motors. The proposed future work is:

- **Include the temperature effect into the PTRUSM model**. If the motor is operated for a short time the temperature effect can be neglected, but if the motor is operated for a long time the temperature effect needs to be considered into the model. Therefore, this phenomenon has to be investigated, and the temperature effect could be included into the model of the PTRUSM.

- **Apply model order reduction to the PTRUSM model**. The computational effort of the proposed model is relatively high. The reasons are that the stator was modeled with a numerical technique, and because the contact problem is solved with an algorithm. One can implement a model order reduction technique to simplify the PTRUSM model, (refer to [55]).
- **Develop an equivalent circuit of the model that could be implemented (coupled) to a control scheme.** Once model order reduction is applied to the proposed PTRUSM model, one can develop an equivalent circuit of the PTRUSM. The equivalent circuit could be used to couple the model with control schemes and simulate the model in circuit simulation software such as PSpice.
- **Develop control strategies.** The transfer function of the plant (motor) could be obtained with the equivalent circuit. The transfer function of the motor could be used to develop a model-based control strategy for these motors.

References

[1] T. Sashida, “An introduction to ultrasonic motors,” ed. Oxford science publications, Oxford New York.

[2] C. Zhao, “Ultrasonic motors technologies and applications,” Springer, Science Press Beijing.

[3] V. Bolborici, “Modeling of the stator of piezoelectric traveling wave rotary ultrasonic motors,” PhD. Dissertation, Dept. of Electrical and Computer Engineering, University of Toronto, Toronto, ON, Canada, 2009.

[4] T. Sattel, “Modeling of ultrasonic motors,” PhD. Dissertation, VomFachbereich mechanic der technischenUniversitatDarmstadzurErlangung des grades eines, Darmstadt 2003.

[5] J. Maas, P. Ide, N. Fröhleke, and H. Grotstollen, “Simulation model for ultrasonic motors powered by resonant converters”, *IEEE industry applications conference,* Orlando, FL, 1995, pp. 111-120.

[6] J. Wallaschek, “Piezoelectric ultrasonic motors”, *Journal of intelligent material systems and structures,* vol. 6, no. 1, pp. 71-83, Jan. 1995.

[7] N. W. Hagood, and A. McFarland, “Modeling of a piezoelectric rotary ultrasonic motor”, *IEEE Trans. on ultrasonics, ferroelectrics, and frequency control,* vol. 42, no. 2, pp. 210-224, March 1995.

[8] J. Pons, H. Rodríguez, R. Ceres, and L. Calderón, “Novel modeling technique for the stator of traveling wave ultrasonic motors” IEEE Trans. on ultrasonics, and frequency control, vol. 50, no. 11, pp. 1429-1435, Nov. 2003.

[9] V. Bolborici, F. Dawson, and M. Pugh, “Modeling of piezoelectric devices with the finite volume method”, I*EEE Trans. on ultrasonics, ferroelectrics, and frequency control,* vol. 57, no. 7, pp. 1673-1691,July 2010.

[10] V. Bolborici, Francis Dawson, and Mary Pugh, "Modeling of composite piezoelectric structures with the finite volume method", *IEEE Trans. on ultrasonics, ferroelectrics, and frequency control,* vol. 59, no. 1, pp. 156-162, Jan. 2012.

[11] V. Bolborici, F. Dawson, and M. Pugh, "A finite volume method and experimental study of a stator of a piezoelectric traveling wave rotary ultrasonic motor", *ELSEVIER Ultrasonics,* vol. 54, no. 3, pp. 809-820, March 2014.

[12] J. Jia, "Essentials of applied dynamic analysis," Springer, Springer-Verlag Berlin Heidelberg.

[13] H. Rodriguez, R. Ceres, L. Calderon, and J. Pons, "Modelling of travelling wave piezoelectric motor stator: an integrated review and new perspective", *Boletín de la sociedad española de cerámica y vidrio,* vol. 43, no. 3, pp. 698-705, 2004.

[14] J. Maas, T. Schulte, and N. Frohleke, "Model-based control for ultrasonic motors," *IEEE/ASME Trans.On mechatronic,* vol. 21, no. 3, pp. 165-180, June 2000.

[15] J. P. Schmidt, P. Hagedorn, and M. Bingqi, "A note on the contact problem in an ultrasonic travelling wave motor", *International journal of non-linear mechanics,* vol. 31, no. 6, pp. 915-924, Nov. 1996.

[16] J. Schmidt, "Ein mechanisches model des stator-rotor-kontaktes beim ultrasonic-waderwellenmotor," PhD Dissertation, Dept. of Mechatronics, Vom Fachbereich mechanic der technischen Universitat Darmstad zur Erlangung des grades eines, Darmstadt 2003.

[17] T. Sattel, P. Hagedorn, and J. Schmidt, "The contact problem in ultrasonic traveling-wave motors," *Journal of applied mechanics,* vol. 77, no. 3, May 2010.

[18] T. Maeno, T. Tsukimoto, and A. Miyake, "Finite-element analysis of the rotor/stator contact in a ring-type ultrasonic motor," *IEEE Trans. on ultrasonics, ferroelectrics, and frequency control,* vol. 39, no. 6, pp. 668-674, Nov. 1992.

[19] M. Zhu, "Contact analysis and mathematical modeling of traveling wave ultrasonic motors*," IEEE Trans. on ultrasonics, ferroelectrics, and frequency control,* vol. 51, no. 6, pp. 668-679, June 2004.

[20] F. Zohra Kebbab, Z. Boumous, and S. Belkhiat, "Traveling wave ultrasonic motor type Daimler-Benz AWM90-X: Modeling and simulation mechanical characteristics," *3th international Conf. on electrical engineering,* Algiers, 2009, pp. 24-29.

[21] J. Qu, F. Sun, and C. Zhao, "Performance evaluation of traveling wave ultrasonic motor based on a model with visco-elastic friction layer on stator," *ELSEVIER ultrasonics,* vol. 45, no. 1-4, pp. 22-31, Dec. 2006.

[22] B. Radi, and A. El Hami, "The study of the dynamic contact in ultrasonic motor," *ELSEVIER applied mathematical modelling,* vol. 34, no. 12, pp. 3767-3777, Dec. 2010.

[23] X. Ca, and J. Wallaschek, "Estimation of the tangential stresses in the stator/rotor contact of travelling wave ultrasonic motors using visco-elastic foundation models," *2th Internat. Conf. CONTACT MECHANICS,* Ferrara, 1995.

[24] J. Wallaschek, "Contact mechanics of piezoelectric ultrasonic motors", *Smart materials and structures,* vol. 7, no. 3, pp. 369-381, June 1998.

[25] H. Hirata, and S. Ueha, "Characteristics estimation of a traveling wave type ultrasonic motor", *IEEE Trans. on ultrasonics, ferroelectrics, and frequency control,* vol. 40, no. 4, pp. 402-406, July 1993.

[26] Y. Izuno, R. Takeda, and Mutsuo Nakaoka, "New fuzzy reasoning–based high-performance speed/position control schemes for ultrasonic motor driven by two-phase resonant inverter", *Industry applications society annual meeting*, USA, 1990, pp. 325-330.

[27] Y. Izuno, R. Takeda, and M. Nakaoka, "New fuzzy reasoning-based high-performance speed/position servo control schemes incorporation ultrasonic motor", *IEEE Trans. on industrial applications*, vol. 28, no. 3, pp. 613-618, June 1992.

[28] I. S. Cha, H. A. Park, H. I. Back, G. J. Yu, and Y. D. Kim, “The characteristics of compensation on temperature of ultrasonic motor with robot actuator by fuzzy controller," *IEEE Conference on Emerging Technologies and Factory Automation*, EFTA '96, vol. 2, pp. 752-758, 1996.

[29] Y. Yano, K. Iida, T. Sakabe, K. Yabugami, and Y. Nakata, “Approach to speed control using temperature characteristics of ultrasonic motor”, *The 47th IEEE international Midwest symposium on circuits and systems*, vol. 3, pp. 155-158, July 2004.

[30] T. Senjyu, S. Yokada, and K. Uezato, “Speed control of ultrasonic motors using fuzzy neural network”, *Journal of intelligent and fuzzy systems*, vol. 9, no. 2, pp. 135-146, 2000.

[31] G. Bal, E. Bekiroglu, “A highly effective load adaptive servo drive system for speed control of travelling-wave ultrasonic motor”, *IEEE trans. on power electronics*, vol. 20, pp. 1143-1149, 2005.

[32] J. Maas, T. Schulte, “High performance speed control for ultrasonic motors”, *IEEE/ASME international conf. on advance intelligence mechatronics*, Atlanta, pp. 91-196, Sep. 1999.

[33] T. Sattel, “Dynamic phenomena in traveling wave-type ultrasonic motors,” *in Proc. Int. Congr. Acoust.*, Kyoto Japan, pp. 413-416, 2004.

[34] J. Maas, T. Schulte, and N. Frohleke, “Model-based control for ultrasonic motors," *IEEE/ASME Transactions on Mechatronics*, vol. 5, no. 2, pp. 165-180, June 2000.

[35] T. Chen, C. Yu, C. Chen, and M. Tsai, “Neuro-fuzzy speed control of traveling-wave type ultrasonic motor drive using frequency and phase modulation”, *ElSEVIER*, vol. 47, no. 3, pp. 325-228, July 2008.

[36] T. Senjyu, M. Nakamura, N. Urasaki, Hideomi Sekine, and Toshihisa Funabashi, “Mathematical model of ultrasonic motors for speed control”, *Electric power components and systems*, pp. 637-648, May 2008.

[37] F. Lin, “Fuzzy adaptive model-following position control for the ultrasonic motor,” *IEEE transaction on power electronics*, vol. 12, no. 2, pp. 261-268, May 1997.

[38] L. Huafeng, Z. Chunsheng, and G. Chenglin, "Precise position control of ultrasonic motor using fuzzy control," *IEEE international ultrasonic, ferroelectrics, and frequency control Conf.*, 2004, pp. 1177-1180.

[39] J. Maas, P. Ide, and H. Grotstollen, "Characteristics of inverter-fed ultrasonic motors optimization of stator/rotor interface," *5th international Conf. on new actuators*, Bremen, 1996, pp. 241-244.

[40] P. Le Moal, P. Cusin, "Optimization of travelling wave ultrasonic motors using a three-dimensional analysis of the contact mechanics at the stator-rotor interface", *European journal of mechanics – A/Solids*, vol. 18, no. 6, pp. 1061-1084, 1999.

[41] G. R. Liu, S. S. Quek, "The finite element method: A practical course", Elsevier Ltd, 2013.

[42] M. Asghar Bhatti, "Fundamentals of finite element analysis and applications", John Wiley & Sons, 2005.

[43] R. Lerch, "Simulation of piezoelectric devices by two-and three-dimensional finite elements", IEEE Trans. on ultrasonics, and ferroelectrics and frequency control, vol. 37, no. 37, pp. 233-247, May 1990.

[44] T. J. R. Hughes, "The finite element method linear static and dynamic finite element analysis", Dover publications, Mineola New York.

[45]S. S. Rao, "Mechanical vibrations", Prentice Hall, 2011.

[46] I. Chowdhury, S. P. Dasgupta, "Computation of Rayleigh damping coefficients for large systems", *The 14th World conference on earthquake engineering,* 2008, pp. 12-17.

[47] N. Newmark, "A method of computation for structural dynamics", Journal of the engineering mechanics division, vol. 85, no. 3, pp. 67-94, July 1959.

[48] J. García de Jalón, E. Bayo, "Kinematic and dynamic simulation of multibody systems", Springer-Verlag, 1994.

[49]M. B. Giles, "Stability and accuracy of numerical boundary conditions in aeroelastic analysis", technical report 13, Oxford University Computing Laboratory, 1995.

[50] A. Stefancu, S. Melenciuc, and M. Budescu, “Penalty based algorithms for frictional contact problems,” *Buletinul institutului politehnic din iasi*, vol 7, Aug. 2011.

[51] P. Litewka, “The penalty and Lagrange multiplier methods in the frictional 3D beam-to-beam contact problem,” *Civ. environ. eng. reports*, no. 1, pp. 187-207, 2005.

[52] S. Vulovic, M. Zivkovic, and N. Grujovic, “Contact problems based on the penalty method,” *Scientific technical review*, vol 58, no. 3-4, pp. 33-36, 2008.

[53] P. Wriggers and P. Panagiotopoulos, “New developments in contact problems”, Springer, 1999.

[54] P. Wriggers. “Computational contact mechanics,” ed. Wiley. Hannover, Germany, 2002.

[55] W. Schilders, “Model order reduction: theory, research aspects and applications,” Springer, Springer-Verlag Berlin Heidelberg.

[56] IEEE standard on piezoelectricity (1987), IEEE/ANSI Std. 176-1987

[57] T. J. Chung, “General continuum mechanics”, Cambridge University Press, 1988.

[58] M. Hayes, G. Saccomandi, “Topics in finite elasticity”, Springer, 2001.

[59] H. K. Versteeg and W. Malalasekera, “An introduction to computational fluid dynamics. The finite volume method”, Longman Scienti_c & Technical, 2007.

Appendix A

Derivation of 2D equilibrium equations to model a piezoelectric-metal beam using the FVM.

References [9, 10] present the equilibrium equations to model a 3D piezoelectric-metal cantilever beam with the FVM. The procedure used in [9, 10] is followed in this appendix to obtain a 2D version of the presented static equations.

A.1.1 Constitutive equations

In order to obtain the equilibrium equations of a piezoelectric-metal beam, one needs to define the constitutive equations for both, piezoelectric and metal materials. The piezoelectric material modeling is discussed first.

The IEEE standard on piezoelectricity [56] presents the linear constitutive equations that describe the piezoelectric material behavior. The displacements produced in the PTRUSM stator are in the order of micrometers. Due to that fact, it is valid to use the linear constitutive equations.

As presented in the IEEE Standard on Piezoelectricity, the constitutive equations describing the behavior of piezoelectric materials are:

$$T = c^E S - e^t E \tag{A.1}$$

$$D = eS + \epsilon^S E \tag{A.2}$$

Equations (A.1) and (A.2) are arranged in the stress-charge form. The stress and electric displacement field are expressed as a function of the strain and electric field. Nevertheless, the piezoelectric standard theory differs when compared to the structural mechanics theory. The piezoelectric convention uses the letter T to represent stress instead of σ, and S instead of ε stands for the strain.

The PTRUSM stator is composed of a piezoelectric and a metal plate. Thus, the letters used for structural mechanics are used in this work to describe both, piezoelectric and metal plates.

Therefore, the constitutive piezoelectric equations (A.1) and (A.2) become:

$$\sigma = c^E \varepsilon - e^t E \tag{A.3}$$

$$D = e\varepsilon + \epsilon^S E \tag{A.4}$$

where the elements in equations (A.3) and (A.4) have the following meanings:

σ stands for the stress tensor vector composed of 6 elements arranged in the form:

$$\sigma = \begin{pmatrix} \sigma_x & \sigma_y & \sigma_z & \tau_{xy} & \tau_{yz} & \tau_{zx} \end{pmatrix}^T$$

The units used to measure stress are N/m^2.

c^E is a 6x6 matrix that contains the elastic stiffness constants of the piezoelectric material arranged in the form:

$$c^E = \begin{bmatrix} c_{11} & c_{12} & c_{13} & 0 & 0 & 0 \\ c_{12} & c_{22} & c_{23} & 0 & 0 & 0 \\ c_{13} & c_{32} & c_{33} & 0 & 0 & 0 \\ 0 & 0 & 0 & c_{44} & 0 & 0 \\ 0 & 0 & 0 & 0 & c_{55} & 0 \\ 0 & 0 & 0 & 0 & 0 & c_{66} \end{bmatrix}$$

These are obtained by experiments. The superscript E means that the elasticity constants are calculated at a constant electric field E. The unit used to measure the elastic stiffness coefficients is N/m^2.

ε is the strain vector composed of 6 elements arranged in the form:

$$\varepsilon = \begin{pmatrix} \varepsilon_x & \varepsilon_y & \varepsilon_z & \gamma_{xy} & \gamma_{yz} & \gamma_{zx} \end{pmatrix}^T$$

The strain is a dimensionless quantity.

e is a 3x6 matrix that contains the electro-mechanical coupling coefficients arranged in the form:

$$e = \begin{bmatrix} 0 & 0 & 0 & 0 & e_{15} & 0 \\ 0 & 0 & 0 & e_{24} & 0 & 0 \\ e_{31} & e_{32} & e_{33} & 0 & 0 & 0 \end{bmatrix}$$

The unit used to measure the electro-mechanical coefficients is C/m^2.

E is a 3x1 vector that contains the electric field components arranged in the form:

$$E = \left[E_x\ E_y\ E_z\right]^t$$

The unit used to measure the electric field components is V/m.

D is a 3x1 vector that contains the electric displacement components arranged in the form:

$$D = \left[D_x\ D_y\ D_z\right]^t$$

The unit used to measure the electric displacement components is C/m^2.

ϵ is a 3x3 matrix that contains the permittivity coefficients arranged in the form:

$$\epsilon = \begin{bmatrix} \epsilon_{11} & 0 & 0 \\ 0 & \epsilon_{22} & 0 \\ 0 & 0 & \epsilon_{33} \end{bmatrix}$$

The unit used to measure the permittivity coefficients is F/m.

The stress equation describes the behavior of the piezoelectric material when used as an actuator. This is the only constitutive equation required in this work to model the piezoelectric material behavior. Thus, equation (A.3) is the only constitutive equation of interest.

As shown in Fig. A.1, the PTRUSM is driven by a voltage applied across the electrodes connected to the piezoelectric material. Because of that, one needs to define the distribution of the electric field inside the piezoelectric material.

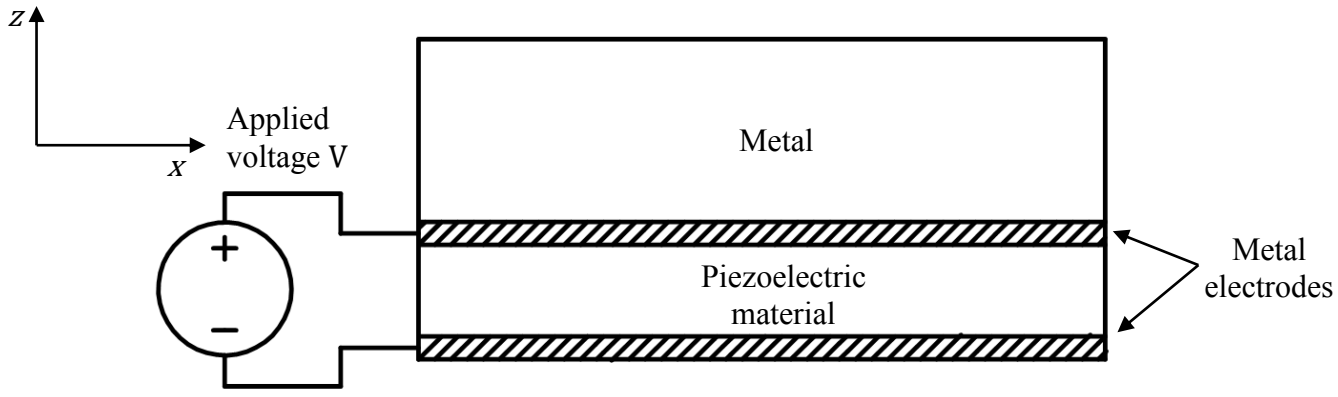

Figure A.1: Voltage applied across metal electrodes to the PTRUSM stator

The piezoelectric plate used for the PTRUSM stator has a very small thickness compared with the stator length and width. Therefore, the electric field lines are considered to be straight, and the influence of the fringing flux at the edges of the plate are neglected. Fig. A.2 shows a constant electric field applied across the piezoelectric beam. Because of the previous assumption, the electric field applied in the z direction is considered constant and equal to the voltage applied on the surface of the piezoelectric material divided by the piezoelectric beam height d. Thus, the electric field is:

$$E_z = -\frac{V}{d} \qquad (A.5)$$

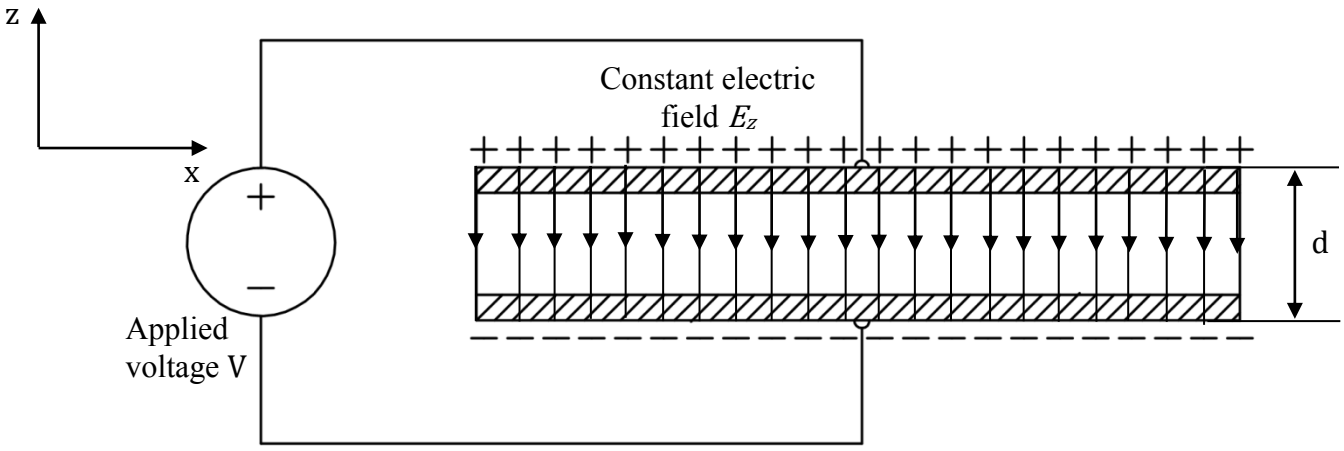

Figure A.2: Constant electric field E_z applied in the z direction

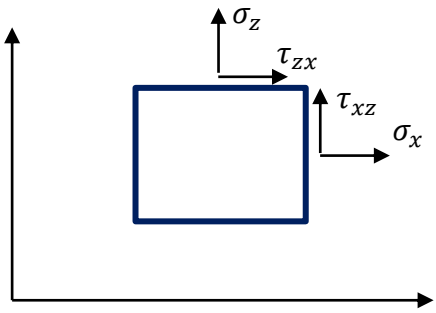

Figure A.4: 2D stress tensor components placed at a point in the solid

Fig. A.4 shows the 2D stress tensor components placed at a point in the solid. It is important to notice that the shear stresses τ_{zx} and τ_{xz} are equal. Using plane stress approximation one can express in matrix form equation (A.3) for a 2D piezoelectric body placed in the x and z planes as follows:

$$\begin{bmatrix}\sigma_x\\ \sigma_z\\ \tau_{zx}\end{bmatrix}=\begin{bmatrix}c_{11} & c_{13} & 0\\ c_{31} & c_{33} & 0\\ 0 & 0 & c_{55}\end{bmatrix}\begin{bmatrix}\varepsilon_x\\ \varepsilon_z\\ \gamma_{zx}\end{bmatrix}-\begin{bmatrix}e_{31}\\ e_{33}\\ 0\end{bmatrix}[E_z] \qquad (A.6)$$

The strain vector is defined in terms of the displacements as follows:

$$\begin{bmatrix}\varepsilon_x\\ \varepsilon_z\\ \gamma_{zx}\end{bmatrix}=\begin{bmatrix}\dfrac{\partial u}{\partial x}\\ \dfrac{\partial w}{\partial z}\\ \dfrac{\partial u}{\partial z}+\dfrac{\partial w}{\partial x}\end{bmatrix} \qquad (A.7)$$

Next, it is required to define the relationships to model the PTRUSM stator metal. The constitutive equation that describes the behavior of the stator metal is:

$$\sigma = c\varepsilon \qquad (A.8)$$

where σ, c, and ε have the same meanings as in equation (A.3). The metal is modeled as an isotropic material. That means that the material properties are the same in any direction.

In order to obtain the stiffness matrix c, one needs to provide Young's modulus $Y$and the Poisson's ratio v of the material.

For isotropic materials, the stiffness matrix c is:

$$c=\begin{bmatrix}c_{11} & c_{12} & c_{12} & 0 & 0 & 0\\ c_{12} & c_{11} & c_{12} & 0 & 0 & 0\\ c_{12} & c_{12} & c_{11} & 0 & 0 & 0\\ 0 & 0 & 0 & c_{11}-c_{12}/2 & 0 & 0\\ 0 & 0 & 0 & 0 & c_{11}-c_{12}/2 & 0\\ 0 & 0 & 0 & 0 & 0 & c_{11}-c_{12}/2\end{bmatrix}$$

where the coefficients of the matrix c are:

$$c_{11} = \frac{Y(1-v)}{(1-2v)(1+v)} \tag{A.9}$$

$$c_{12} = \frac{Yv}{(1-2v)(1+v)} \tag{A.10}$$

$$\frac{c_{11} - c_{12}}{2} = c_{33} = \frac{Y}{2(1+v)} \tag{A.11}$$

Equation (A.8) can be expressed in a matrix form for a 2D body using plane stress approximation as follows:

$$\begin{bmatrix} \sigma_x \\ \sigma_z \\ \tau_{zx} \end{bmatrix} = \begin{bmatrix} c_{11} & c_{12} & 0 \\ c_{12} & c_{11} & 0 \\ 0 & 0 & c_{33} \end{bmatrix} \begin{bmatrix} \varepsilon_x \\ \varepsilon_z \\ \gamma_{zx} \end{bmatrix} \tag{A.12}$$

A.1.2 Governing equation

After defining the constitutive equations for the piezoelectric and metal materials, the next step is to define the governing equation of the PTRUSM stator. The governing equation describing the motion of an elastic body is Cauchy's first law of motion, (refer to [57] and [58]). It is expressed as follows:

$$\rho \frac{d^2 u_T}{dt^2} - \nabla \cdot \sigma = F_b \tag{A.13}$$

Sometimes equation (A.13) is simply called equation of motion.

In this equation $\rho, u_T, \sigma,$ and F_b represent the material density, displacement vector, stress tensor, and the body force vector, respectively. The governing equation describes the motion of both piezoelectric material and metal. This motion equation is used to describe the dynamics of the PTRUSM stator.

Equation (A.13) can be represented in a matrix form for a 2D model using plane stress approximation as follows:

$$\rho \frac{d^2}{dt^2}\begin{bmatrix} u \\ z \end{bmatrix} - \nabla \cdot \begin{bmatrix} \sigma_x & \tau_{xz} \\ \tau_{zx} & \sigma_z \end{bmatrix} = \begin{bmatrix} F_{bx} \\ F_{bz} \end{bmatrix} \quad (A.14)$$

where ρ is the material density, u and z represent the unknown displacements in the x and z directions, respectively. σ_x and σ_z are the normal stresses applied in the x and z directions, respectively. τ_{zx} and τ_{xz} are the shear stresses applied in both directions. F_{bx} and F_{bz} are the body forces applied in the x and z directions, respectively.

Equation (A.14) is the governing equation expressed in a matrix form that describes the stator dynamics. The first term of equation (A.14) is the acceleration of the continuum. The second term is the divergence of the stress tensor. The last term is the total body force applied in the continuum.

A.1.3 Discretization of the continuum.

The FVM is used in this section to discretize the continuum. The FVM technique is explained in detail for computational fluid dynamics in [59]. The general steps to discretize a continuum using the FVM are: mesh generation, discretization, and solution of the generated system of equations. The mesh generation and discretization are treated in this appendix. The solution of the final system of equations is treated in Chapter 3.

Mesh generation

The PTRUSM stator is divided into small squares called control volumes ΔV. A current control volume is showed in the center of Fig. A.5 surrounded by adjacent neighboring control volumes. The center of the current control volume is identified with the letter P and the neighboring volumes with the letters E, RE, R, RW, W, FW, F and FE. The notation means *East*, *Rear-East*, *Rear*, *Rear-West*, *West*, *Front-West*, *Front*, and *Front-East*, respectively. Fig. A.5 also shows the notations used to represent the distances between centers of adjacent control volumes. For instance, δ_{XE} is the distance

along the horizontal axis between the center of the control volume P and the center of the control volume E placed at the *East* side of it.

One needs to define internal distances from the center of a current control volume to the four faces of it. Fig. A.6 shows the internal distances for a current control volume P.

The accuracy of the models depends on the number of control volumes used to discretize the continuum. The higher the number of control volumes, the more accurate the solution.

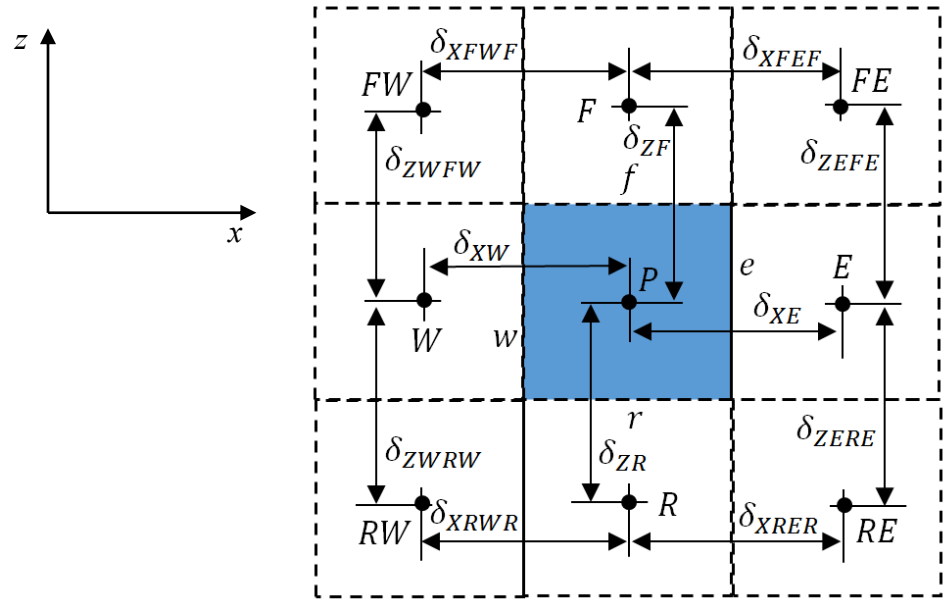

Figure A.5: Internal control volume P surrounded by neighboring control volumes placed at the xz plane

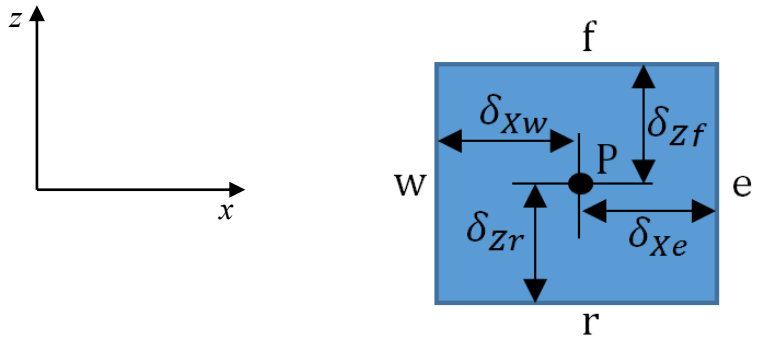

Figure A.6: Internal control volume P with notation for internal distance

Discretization

The FVM technique assumes that the parameter of interest is concentrated at the center P of the control volume. The average value of the parameter of interest into the control volume is used to compute the solution. In this case, the parameter of interest is the displacement of the continuum. The infinite displacements of the infinite points inside the current control volume are modeled as the average displacement at the center P.

The governing equation (A.14) is integrated over an internal control volume ΔV. After integration, the governing equation becomes:

$$\int_{\Delta V} \rho \frac{d^2}{dt^2} \begin{bmatrix} u \\ w \end{bmatrix} dV - \int_{\Delta V} \nabla \cdot \begin{bmatrix} \sigma_x & \tau_{xz} \\ \tau_{zx} & \sigma_z \end{bmatrix} dV = \int_{\Delta V} \begin{bmatrix} F_{bx} \\ F_{bz} \end{bmatrix} dV \qquad (A.15)$$

Where the infinitesimal volume dV is:

$$dV = dxdzdy \qquad (A.16)$$

The stator is modeled in the xz plane. Because of that, the integration of the stator width is done along the y axis, and it is independent of the x and z axis. Equation (A.15) becomes:

$$\int_{\Delta A} \left(\int_0^{y_v} dy \right) \rho \frac{d^2}{dt^2} \begin{bmatrix} u \\ w \end{bmatrix} dA - \int_{\Delta A} \left(\int_0^{y_v} dy \right) \nabla \cdot \begin{bmatrix} \sigma_x & \tau_{xz} \\ \tau_{zx} & \sigma_z \end{bmatrix} dA = \int_{\Delta A} \left(\int_0^{y_v} dy \right) \begin{bmatrix} F_{bx} \\ F_{bz} \end{bmatrix} dA \qquad (A.17)$$

where y_v represents the stator width.

After integration of the stator width, equation (A.17) becomes:

$$y_v \int_{\Delta A} \rho \frac{d^2}{dt^2} \begin{bmatrix} u \\ w \end{bmatrix} dA - y_v \int_{\Delta A} \nabla \cdot \begin{bmatrix} \sigma_x & \tau_{xz} \\ \tau_{zx} & \sigma_z \end{bmatrix} dA = y_v \int_{\Delta A} \begin{bmatrix} F_{bx} \\ F_{bz} \end{bmatrix} dA \qquad (A.18)$$

According to [3], the divergence theorem can be applied to the stress tensor matrix of equation (A.18). The area integral is transformed into a line integral on the closed perimeter of the control volume. Thus, equation (A.18) becomes:

$$y_v \int_{\Delta A} \rho \frac{d^2}{dt^2} \begin{bmatrix} u \\ w \end{bmatrix} dA - y_v \oint_{\Delta L} \begin{bmatrix} \sigma_x & \tau_{xz} \\ \tau_{zx} & \sigma_z \end{bmatrix} d\vec{l} = y_v \int_{\Delta A} \begin{bmatrix} F_{bx} \\ F_{bz} \end{bmatrix} dA \qquad (A.19)$$

The divergence theorem stands that the density within a region of space can only change if there is a flow of matter through the boundary of the closed region.

The infinitesimal area dA and length $d\vec{l}$ are expressed as follows:

$$dA = dxdz \qquad (A.20)$$

$$d\vec{l} = \vec{\imath}\, dz + \vec{k} dx \qquad (A.21)$$

After substitution of equation (A.21) into (A.19) one obtains:

$$y_v \int_{\Delta A} \rho \frac{d^2}{dt^2} \begin{bmatrix} u \\ w \end{bmatrix} dA - y_v \oint_{\Delta L} \begin{bmatrix} \sigma_x & \tau_{xz} \\ \tau_{zx} & \sigma_z \end{bmatrix} \begin{matrix} dz \\ dx \end{matrix} = y_v \int_{\Delta A} \begin{bmatrix} F_{bx} \\ F_{bz} \end{bmatrix} dA \qquad (A.22)$$

Equation (A.22) can be divided into two equations that correspond to the displacements u and w at the center P of the current control volume. The displacements are produced along the x and z axes. Thus, equation (A.22) can be written as two separate equations:

$$y_v \int_{\Delta A} \rho \frac{d^2u}{dt^2}\, dA - y_v \oint_{\Delta L} \sigma_x\, dz - y_v \oint_{\Delta L} \tau_{xz}\, dx = y_v \int_{\Delta A} F_{bx}\, dA \qquad (A.23)$$

$$y_v \int_{\Delta A} \rho \frac{d^2w}{dt^2}\, dA - y_v \oint_{\Delta L} \sigma_z\, dx - y_v \oint_{\Delta L} \tau_{zx}\, dz = y_v \int_{\Delta A} F_{bz}\, dA \qquad (A.24)$$

Equations (A.23) and (A.24) describe the motion of the continuum in the x and z axes. Equation (A.23) is processed first.

The acceleration and body force terms in equation (A.23) are integrated as the average values of the acceleration and body force terms into the current control volume. The stress tensor components are

integrated over the z and x axis as the difference of the stress across the axis. Thus, equation (A.23) becomes:

$$y_v \Delta A \rho \frac{d^2 u_P}{dt^2} - y_v \left(\int_e \sigma_x \, dz - \int_w \sigma_x \, dz \right) - y_v \left(\int_f \tau_{xz} \, dx - \int_r \tau_{xz} \, dx \right) = y_v \Delta A F_{bxP} \qquad (A.25)$$

In equation (A.25) the subscripts e, w, f, and r refer to the boundaries of the control volume *East*, *West*, *Front,* and *Rear* . Fig. A.5 shows the faces e, w, f, and r of an internal control volume placed in the xz plane. ΔA is the area of the control volume where the equation is defined.

The stress tensor components in equation (A.25) are integrated over the axis where it is applied. After integration, one obtains:

$$y_v \Delta A \rho \frac{d^2 u_P}{dt^2} - y_v (\Delta z \sigma_{xe} - \Delta z \sigma_{xw}) - y_v \left(\Delta_x \tau_{xzf} - \Delta_x \tau_{xzr} \right) = y_v \Delta A F_{bxP} \qquad (A.26)$$

In equation (A.26) Δz and Δ_x refer to the control volume height and length, respectively.

By using the constitutive piezoelectric equation expressed in the matrix form (A.6), one can express the stresses in equation (A.26) as a function of the strain and electric field. Equation (A.26) becomes:

$$y_v \Delta A \rho \frac{d^2 u_p}{dt^2} - y_v \Delta z (c_{11} \varepsilon_{xe} + c_{13} \varepsilon_{ze} - e_{31} E_z) + y_v \Delta z (c_{11} \varepsilon_{xw} + c_{13} \varepsilon_{zw} - e_{31} E_z) - y_v \Delta x \left(c_{55} \gamma_{zxf} \right)$$
$$+ y_v \Delta x (c_{55} \gamma_{zxr}) = y_v \Delta A F_{bxP} \qquad (A.27)$$

The strains in equation $(A.27)$ are substituted using the stress-displacement relationships (A.7). Thus, equation $(A.27)$ becomes:

$$y_v \Delta A \rho \frac{d^2 u_P}{dt^2} - y_v \Delta z \left(c_{11} \left. \frac{\partial u}{\partial x} \right|_e + c_{13} \left. \frac{\partial w}{\partial z} \right|_e - e_{31} E_z \right) + y_v \Delta z \left(c_{11} \left. \frac{\partial u}{\partial x} \right|_w + c_{13} \left. \frac{\partial w}{\partial z} \right|_w - e_{31} E_z \right)$$
$$- y_v \Delta x c_{55} \left(\left. \frac{\partial u}{\partial z} \right|_f + \left. \frac{\partial w}{\partial x} \right|_f \right) + y_v \Delta x c_{55} \left(\left. \frac{\partial u}{\partial z} \right|_r + \left. \frac{\partial w}{\partial x} \right|_r \right) = y_v \Delta A F_{bxP} \qquad (A.28)$$

The displacements, electric fields, and mechanical forces are evaluated at the nodal points. Nevertheless, it is required to express the displacements at the control volumes faces. Linear interpolations are defined to approximate the displacements at the control volumes faces. This method is called central differencing [59]. Reference [3] provides all the linear interpolations required for a 3D continuum. The strain-displacement relationships are expressed with linear interpolations as follows:

$$\left.\frac{\partial u}{\partial x}\right|_e = \frac{u_E - u_P}{\delta_{XE}} \tag{A.29}$$

$$\left.\frac{\partial u}{\partial x}\right|_w = \frac{u_P - u_W}{\delta_{XW}} \tag{A.30}$$

$$\left.\frac{\partial u}{\partial z}\right|_f = \frac{u_F - u_P}{\delta_{ZF}} \tag{A.31}$$

$$\left.\frac{\partial u}{\partial z}\right|_r = \frac{u_P - u_R}{\delta_{ZR}} \tag{A.32}$$

$$\left.\frac{\partial w}{\partial z}\right|_e = \frac{w_F - w_R}{\delta_{ZF} + \delta_{ZR}} . \frac{\delta_{XE} - \delta_{Xe}}{\delta_{XE}} + \frac{w_{FE} - w_{RE}}{\delta_{ZEFE} + \delta_{ZERE}} . \frac{\delta_{Xe}}{\delta_{XE}} \tag{A.33}$$

$$\left.\frac{\partial w}{\partial z}\right|_w = \frac{w_F - w_R}{\delta_{ZF} + \delta_{ZR}} . \frac{\delta_{XW} - \delta_{Xw}}{\delta_{XW}} + \frac{w_{FW} - w_{RW}}{\delta_{ZWFW} + \delta_{ZWRW}} . \frac{\delta_{Xw}}{\delta_{XW}} \tag{A.34}$$

$$\left.\frac{\partial w}{\partial x}\right|_f = \frac{w_E - w_W}{\delta_{XE} + \delta_{XW}} . \frac{\delta_{ZF} - \delta_{Zf}}{\delta_{ZF}} + \frac{w_{FE} - w_{FW}}{\delta_{XFEF} + \delta_{XFWF}} . \frac{\delta_{Zf}}{\delta_{ZF}} \tag{A.35}$$

$$\left.\frac{\partial w}{\partial x}\right|_r = \frac{w_E - w_W}{\delta_{XE} + \delta_{XW}} . \frac{\delta_{ZR} - \delta_{Zr}}{\delta_{ZR}} + \frac{w_{RE} - w_{RW}}{\delta_{XRER} + \delta_{XRWR}} . \frac{\delta_{Zr}}{\delta_{ZR}} \tag{A.36}$$

$$\left.\frac{\partial w}{\partial x}\right|_e = \frac{w_E - w_P}{\delta_{XE}} \tag{A.37}$$

$$\left.\frac{\partial w}{\partial x}\right|_w = \frac{w_P - w_W}{\delta_{XW}} \tag{A.38}$$

$$\left.\frac{\partial w}{\partial z}\right|_f = \frac{w_F - w_P}{\delta_{ZF}} \tag{A.39}$$

$$\left.\frac{\partial w}{\partial z}\right|_r = \frac{w_P - w_R}{\delta_{ZR}} \tag{A.40}$$

$$\left.\frac{\partial u}{\partial z}\right|_e = \frac{u_F - u_R}{\delta_{ZF} + \delta_{ZR}} . \frac{\delta_{XE} - \delta_{Xe}}{\delta_{XE}} + \frac{u_{FE} - u_{RE}}{\delta_{ZEFE} + \delta_{ZERE}} . \frac{\delta_{Xe}}{\delta_{XE}} \tag{A.41}$$

$$\left.\frac{\partial u}{\partial z}\right|_w = \frac{u_F - u_R}{\delta_{ZF} + \delta_{ZR}} . \frac{\delta_{XW} - \delta_{Xw}}{\delta_{XW}} + \frac{u_{FW} - u_{RW}}{\delta_{ZWFW} + \delta_{ZWRW}} . \frac{\delta_{Xw}}{\delta_{XW}} \tag{A.42}$$

$$\left.\frac{\partial u}{\partial x}\right|_f = \frac{u_E - u_W}{\delta_{XE} + \delta_{XW}} . \frac{\delta_{ZF} - \delta_{Zf}}{\delta_{ZF}} + \frac{u_{FE} - u_{FW}}{\delta_{XFEF} + \delta_{XFWF}} . \frac{\delta_{Zf}}{\delta_{ZF}} \tag{A.43}$$

$$\left.\frac{\partial u}{\partial x}\right|_r = \frac{u_E - u_W}{\delta_{XE} + \delta_{XW}} . \frac{\delta_{ZR} - \delta_{Zr}}{\delta_{ZR}} + \frac{u_{RE} - u_{RW}}{\delta_{XRER} + \delta_{XRWR}} . \frac{\delta_{Zr}}{\delta_{ZR}} \tag{A.44}$$

Expressions (A.29) to (A.36) are substituted into equation (A.28), and equation ($A.45$) is obtained.

$$\begin{aligned} & y_v \Delta A \rho \frac{d^2 u_P}{dt^2} - y_v \Delta z c_{11} \left(\frac{u_E - u_P}{\delta_{XE}}\right) - y_v \Delta z c_{13} \left(\frac{w_F - w_R}{\delta_{ZF} + \delta_{ZR}} . \frac{\delta_{XE} - \delta_{Xe}}{\delta_{XE}} + \frac{w_{FE} - w_{RE}}{\delta_{ZEFE} + \delta_{ZERE}} . \frac{\delta_{Xe}}{\delta_{XE}}\right) \\ & + y_v \Delta z e_{31} E_Z + y_v c_{11} \left(\frac{u_P - u_W}{\delta_{XW}}\right) \\ & + y_v \Delta z c_{13} \left(\frac{w_F - w_R}{\delta_{ZF} + \delta_{ZR}} . \frac{\delta_{XW} - \delta_{Xw}}{\delta_{XW}} + \frac{w_{FW} - w_{RW}}{\delta_{ZWFW} + \delta_{ZWRW}} . \frac{\delta_{Xw}}{\delta_{XW}}\right) - y_v \Delta z e_{31} E_Z \\ & - y_v \Delta x c_{55} \left(\frac{u_F - u_P}{\delta_{ZF}}\right) - y_v \Delta x c_{55} \left(\frac{w_E - w_W}{\delta_{XE} + \delta_{XW}} . \frac{\delta_{ZF} - \delta_{Xf}}{\delta_{ZF}} + \frac{w_{FE} - w_{FW}}{\delta_{XFEF} + \delta_{XFWF}} . \frac{\delta_{Zf}}{\delta_{ZF}}\right) \\ & + y_v \Delta x c_{55} \left(\frac{u_P - u_R}{\delta_{ZR}}\right) + y_v \Delta x c_{55} \left(\frac{w_E - w_W}{\delta_{XE} + \delta_{XW}} . \frac{\delta_{ZR} - \delta_{Zr}}{\delta_{ZR}} + \frac{w_{RE} - w_{RW}}{\delta_{XRER} + \delta_{XRWR}} . \frac{\delta_{Zr}}{\delta_{ZR}}\right) \\ & = y_v \Delta A F_{bxP} \end{aligned} \tag{A.45}$$

The terms in equation (A.45) are rearranged and equation (A.46) is obtained:

$$y_v \Delta A \rho \frac{d^2 u_P}{dt^2} + y_v \left[\Delta z c_{11} \left(\frac{1}{\delta_{XE}} + \frac{1}{\delta_{XW}} \right) + \Delta x c_{55} \left(\frac{1}{\delta_{ZF}} + \frac{1}{\delta_{ZR}} \right) \right] u_P - \frac{y_v \Delta z c_{11}}{\delta_{XE}} u_E - \frac{y_v \Delta z c_{11}}{\delta_{XW}} u_W$$

$$- \frac{y_v \Delta x c_{55}}{\delta_{ZF}} u_F - \frac{y_v \Delta x c_{55}}{\delta_{ZR}} u_R - y_v \left[\frac{\Delta_z c_{13}}{\delta_{ZF} + \delta_{ZR}} \left(\frac{\delta_{XE} - \delta_{Xe}}{\delta_{XE}} - \frac{\delta_{XW} - \delta_{Xw}}{\delta_{XW}} \right) \right] (w_F - w_R)$$

$$- \frac{y_v \Delta_z c_{13}}{\delta_{ZEFE} + \delta_{ZERE}} . \frac{\delta_{Xe}}{\delta_{XE}} (w_{FE} - w_{RE}) + \frac{y_v \Delta_z c_{13}}{\delta_{ZWFW} + \delta_{ZWRW}} . \frac{\delta_{Xw}}{\delta_{XW}} (w_{FW} - w_{RW})$$

$$- \frac{y_v \Delta_x c_{55}}{\delta_{XE} + \delta_{XW}} . \left(\frac{\delta_{ZF} - \delta_{Zf}}{\delta_{ZF}} - \frac{\delta_{ZR} - \delta_{Zr}}{\delta_{ZR}} \right) (w_E - w_W)$$

$$- \frac{y_v c_{55}}{\delta_{XFEF} + \delta_{XFWF}} . \left(\frac{\delta_{Zf}}{\delta_{ZF}} \right) (w_{FE} - w_{FW})$$

$$+ \frac{y_v \Delta_x c_{55}}{\delta_{XRER} + \delta_{XRWR}} . \left(\frac{\delta_{Zr}}{\delta_{ZR}} \right) (w_{RE} - w_{RW}) = y_v \Delta A F_{bxP} \qquad (A.46)$$

The following notations are used to express the coefficients of the unknown displacements u and w.

$$P_1 = y_v \left[\Delta_z c_{11} \left(\frac{1}{\delta_{XE}} + \frac{1}{\delta_{XW}} \right) + \Delta_x c_{55} \left(\frac{1}{\delta_{ZF}} + \frac{1}{\delta_{ZR}} \right) \right] \qquad (A.47)$$

$$E_1 = \frac{y_v \Delta_z c_{11}}{\delta_{XE}} \qquad (A.48)$$

$$W_1 = \frac{y_v \Delta_z c_{11}}{\delta_{XW}} \qquad (A.49)$$

$$F_1 = \frac{y_v c_{55}}{\delta_{ZF}} \qquad (A.50)$$

$$R_1 = \frac{y_v \Delta_x c_{55}}{\delta_{ZR}} \qquad (A.51)$$

$$B_1 = \frac{y_v \Delta_z c_{13}}{\delta_{ZF} + \delta_{ZR}} \left(\frac{\delta_{XE} - \delta_{Xe}}{\delta_{XE}} - \frac{\delta_{XW} - \delta_{Xw}}{\delta_{XW}} \right) \qquad (A.52)$$

$$B_2 = \frac{y_v \Delta_z c_{13}}{\delta_{ZEFE} + \delta_{ZERE}} . \frac{\delta_{Xe}}{\delta_{XE}} \qquad (A.53)$$

$$B_3 = \frac{y_v \Delta_z c_{13}}{\delta_{ZWFW} + \delta_{ZWRW}} . \frac{\delta_{Xw}}{\delta_{XW}} \tag{A.54}$$

$$B_4 = \frac{y_v \Delta_x c_{55}}{\delta_{XE} + \delta_{XW}} . \left(\frac{\delta_{ZF} - \delta_{Zf}}{\delta_{ZF}} - \frac{\delta_{ZR} - \delta_{Zr}}{\delta_{ZR}} \right) \tag{A.55}$$

$$B_5 = \frac{y_v c_{55}}{\delta_{XFEF} + \delta_{XFWF}} . \left(\frac{\delta_{Zf}}{\delta_{ZF}} \right) \tag{A.56}$$

$$B_6 = \frac{y_v c_{55}}{\delta_{XRER} + \delta_{XRWR}} . \left(\frac{\delta_{Zr}}{\delta_{ZR}} \right) \tag{A.57}$$

After substitution of expressions (A.47) to (A.57) into equation (A.46) one obtains:

$$m_P \frac{d^2 u_P}{dt^2} + P_1 u_P - E_1 u_E - W_1 u_W - F_1 u_F - R_1 u_R - B_1 (w_F - w_R) - B_2 (w_{FE} - w_{RE}) +$$
$$B_3 (w_{FW} - w_{RW}) - B_4 (w_E - w_W) - B_5 (w_{FE} - w_{FW}) + B_6 (w_{RE} - w_{RW})$$
$$= F_{xP} \tag{A.58}$$

In (A.58) m_P and F_{xP} are the total mass contained inside the finite volume and the total concentrated force applied in the x direction, respectively. Equation (A.58) is the semidiscrete motion equation of the u displacement along the x axis. The motion equation is called semidiscrete because the acceleration term was not discretized.

Equation (A.24) is processed in a similar way and equation (A.59) is obtained:

$$y_v \Delta A \rho \frac{d^2 w_P}{dt^2} + y_v \left[\Delta z c_{55} \left(\frac{1}{\delta_{XE}} + \frac{1}{\delta_{XW}} \right) + \Delta x c_{33} \left(\frac{1}{\delta_{ZF}} + \frac{1}{\delta_{ZR}} \right) \right] w_P - \frac{y_v \Delta z c_{55}}{\delta_{XE}} w_E - \frac{y_v \Delta z c_{55}}{\delta_{XW}} w_w$$
$$- \frac{y_v \Delta x c_{33}}{\delta_{ZF}} w_F - \frac{y_v \Delta x c_{33}}{\delta_{ZR}} w_R - y_v \left[\frac{\Delta_z c_{55}}{\delta_{ZF} + \delta_{ZR}} \left(\frac{\delta_{XE} - \delta_{Xe}}{\delta_{XE}} - \frac{\delta_{XW} - \delta_{Xw}}{\delta_{XW}} \right) \right] (u_F u_R)$$
$$- \frac{y_v \Delta z c_{55}}{\delta_{ZEFE} + \delta_{ZERE}} . \frac{\delta_{Xe}}{\delta_{XE}} (u_{FE} - u_{RE}) + \frac{y_v \Delta z c_{55}}{\delta_{ZWFW} + \delta_{ZWRW}} . \frac{\delta_{Xw}}{\delta_{XW}} (u_{FW} - u_{RW})$$

$$-\frac{y_v \Delta x c_{31}}{(\delta_{XE}+\delta_{XW})}\left(\frac{\delta_{ZF}-\delta_{Zf}}{\delta_{ZF}}-\frac{\delta_{ZR}-\delta_{Zr}}{\delta_{ZR}}\right)(u_E-u_W)$$

$$-\frac{y_v \Delta x c_{31}}{\delta_{XFEF}+\delta_{XFWF}}.\frac{\delta_{Zf}}{\delta_{ZF}}(u_{FE}-u_{FW})+\frac{y_v \Delta x c_{31}}{\delta_{XRER}+\delta_{XRWR}}.\frac{\delta_{Zr}}{\delta_{ZR}}(u_{FE}-u_{FW})$$

$$=y_v \Delta A K_{3P} \qquad (A.59)$$

The following notations are used to express the coefficients of the unknown displacements u and w.

$$P_2 = y_v\left[\Delta z c_{55}\left(\frac{1}{\delta_{XE}}+\frac{1}{\delta_{XW}}\right)+\Delta x c_{33}\left(\frac{1}{\delta_{ZF}}+\frac{1}{\delta_{ZR}}\right)\right] \qquad (A.60)$$

$$E_2 = \frac{y_v \Delta z c_{55}}{\delta_{XE}} \qquad (A.61)$$

$$W_2 = \frac{y_v \Delta z c_{55}}{\delta_{XW}} \qquad (A.62)$$

$$F_2 = \frac{y_v \Delta x c_{33}}{\delta_{ZF}} \qquad (A.63)$$

$$R_2 = \frac{y_v \Delta x c_{33}}{\delta_{ZR}} \qquad (A.64)$$

$$B_7 = y_v\left[\frac{\Delta_z c_{55}}{\delta_{ZF}+\delta_{ZR}}\left(\frac{\delta_{XE}-\delta_{Xe}}{\delta_{XE}}-\frac{\delta_{XW}-\delta_{Xw}}{\delta_{XW}}\right)\right] \qquad (A.65)$$

$$B_8 = \frac{y_v \Delta z c_{55}}{\delta_{ZEFE}+\delta_{ZERE}}.\frac{\delta_{Xe}}{\delta_{XE}} \qquad (A.66)$$

$$B_9 = \frac{y_v \Delta z c_{55}}{\delta_{ZWFW}+\delta_{ZWRW}}.\frac{\delta_{Xw}}{\delta_{XW}} \qquad (A.67)$$

$$B_{10} = \frac{y_v \Delta x c_{31}}{(\delta_{XE}+\delta_{XW})}\left(\frac{\delta_{ZF}-\delta_{Zf}}{\delta_{ZF}}-\frac{\delta_{ZR}-\delta_{Zr}}{\delta_{ZR}}\right) \qquad (A.68)$$

$$B_{11} = \frac{y_v \Delta x c_{31}}{\delta_{XFEF}+\delta_{XFWF}}.\frac{\delta_{Zf}}{\delta_{ZF}} \qquad (A.69)$$

$$B_{12} = \frac{y_v \Delta x c_{31}}{\delta_{XRER} + \delta_{XRWR}} . \frac{\delta_{Zr}}{\delta_{ZR}} \qquad (A.70)$$

After substituting (A.60) to (A.70) into equation (A.59) one obtains:

$$m_P \frac{d^2 w_P}{dt^2} + P_2 w_P - E_2 w_E - W_2 w_W - F_2 w_F - R_1 w_R - B_7(u_F - u_R) - B_8(u_{FE} - u_{RE}) + B_9(u_{FW} - u_{RW}) - B_{10}(u_E - u_W) - B_{11}(u_{FE} - u_{FW}) + B_{12}(u_{RE} - u_{RW}) = F_{zP} \qquad (A.71)$$

In (A.71) m_P is the total mass contained inside of the finite volume and F_{zP} is the total concentrated force applied in the z axis. Equation (A.71) is the semi-discrete motion equation of the w displacement in the z direction.

In [9, 10] the semi-discrete motion equations were transformed into static equations. In order to obtain the static equations, one needs to set to zero the acceleration terms in equations (A.58) and (A.71). These equations become:

$$P_1 u_P - E_1 u_E - W_1 u_W - F_1 u_F - R_1 u_R - B_1(w_F - w_R) - B_2(w_{FE} - w_{RE}) + B_3(w_{FW} - w_{RW}) - B_4(w_E - w_W) - B_5(w_{FE} - w_{FW}) + B_6(w_{RE} - w_{RW}) = F_{xP} \qquad (A.72)$$

$$P_2 w_P - E_2 w_E - W_2 w_W - F_2 w_F - R_1 w_R - B_7(u_F - u_R) - B_8(u_{FE} - u_{RE}) + B_9(u_{FW} - u_{RW}) - B_{10}(u_E - u_W) - B_{11}(u_{FE} - u_{FW}) + B_{12}(u_{RE} - u_{RW}) = F_{zP} \qquad (A.73)$$

Equations (A.72) and (A.73) are 2D static equilibrium equations. By adding proper boundary conditions, one can use (A.72) and (A.73) to obtain the static equilibrium of a piezoelectric-metal beam.

Appendix B

Material properties

B.1 Copper.

Mass density

$$\rho = 8700 \quad \left[\frac{kg}{m^3}\right] \tag{B.1}$$

Young's modulus

$$Y = 110e^9 \quad [Pa] \tag{B.2}$$

Poisson's ratio

$$v = 0.35 \tag{B.3}$$

Stiffness matrix

$$c = \begin{bmatrix} 1.254.10^{11} & 4.387.10^{10} & 4.387.10^{10} & 0 & 0 & 0 \\ 4.387.10^{10} & 1.254.10^{11} & 4.387.10^{10} & 0 & 0 & 0 \\ 4.387.10^{10} & 4.387.10^{10} & 1.254.10^{11} & 0 & 0 & 0 \\ 0 & 0 & 0 & 4.074.10^{10} & 0 & 0 \\ 0 & 0 & 0 & 0 & 4.074.10^{10} & 0 \\ 0 & 0 & 0 & 0 & 0 & 4.074.10^{10} \end{bmatrix} \left[\frac{N}{m^2}\right] \tag{B.4}$$

B.2 Lead Zirconate Titanate.

Mass density

$$\rho = 7500 \quad \left[\frac{kg}{m^3}\right] \tag{B.5}$$

Stiffness matrix

$$c^E = \begin{bmatrix} 1.27205.10^{11} & 8.02122.10^{10} & 8.46702.10^{10} & 0 & 0 & 0 \\ 8.02122.10^{10} & 1.27205.10^{11} & 8.46702.10^{10} & 0 & 0 & 0 \\ 8.46702.10^{10} & 8.46702.10^{10} & 1.17436.10^{11} & 0 & 0 & 0 \\ 0 & 0 & 0 & 2.29885.10^{10} & 0 & 0 \\ 0 & 0 & 0 & 0 & 2.29885.10^{10} & 0 \\ 0 & 0 & 0 & 0 & 0 & 2.34742.10^{10} \end{bmatrix}$$

$$\left[\frac{N}{m^2}\right] \tag{B.6}$$

Electro-mechanical coupling matrix

$$e = \begin{bmatrix} 0 & 0 & 0 & 0 & 17.0345 & 0 \\ 0 & 0 & 0 & 17.0345 & 0 & 0 \\ -6.62281 & -6.62281 & 23.2403 & 0 & 0 & 0 \end{bmatrix} \left[\frac{C}{m^2}\right] \tag{B.7}$$

Vita

Ivan Arturo Renteria Marquez was born in Ciudad Juárez, Chihuahua. He graduated from Colegio de Bachilleres plantel número 7, Ciudad Juárez, Chihuahua, in the spring of 2005 and he entered the Mechatronic engineering program at Tecnológico de Monterrey with an academic scholarship. During the bachelor's degree program he was in a seven month internship with CAPCOM, after that, he was in a year internship with Robert Bosch. In the spring of 2011 he graduated with distinction. In the spring of 2012 he entered the PhD fast track program of the University of Texas at El Paso. In the fall of 2015 he obtained his Master of Science degree with specialty in Electrical engineering. During 2012 to 2016 he has been research assistant, teacher assistant and lecturer.

Permanent address: Wallington
El Paso, Texas, 79902

This dissertation was typed by Ivan Arturo Renteria Marquez.